HYDROGEN-BONDED LIQUID CRYSTALS FROM FLUOROPHENOLS AND ALKOXYSTILBAZOLES

by

Joanna Pik-Wan Wong

Submitted in conformity with the requirements for the degree of

MSc in Chemistry by Research

The University of York

December 2009

Abstract

Hydrogen-bonded complexes between 4-alkoxy-4'-stilbazoles and phenols with different degrees of fluorine substitution were prepared. In contrast to the components, the complexes were observed to exhibit nematic and smectic A phases by polarised optical microscopy, and nematic tendency was found to decrease with increasing alkoxy chain length. A correlation between mesophase stability and the fluorine substitution positions for a given number of fluorine substituents in the phenol was also observed. The mesomorphism of the fluorophenol complexes prepared are compared with similar complexes formed between stilbazoles and 2-, 3- and 4-cyanophenol, as well as between stilbazoles and 3- and 4-nitrophenol.

Nine X-ray crystallographic structures of the 4-octyoxy-4'-stilbazole complexed with fluorophenols were also obtained. Eight of the complexes crystallised in the $P\overline{1}$ space group, with a back-to-back dimer motif, while the complex of 4-fluorophenol crystallised in the Pbca space group and formed head-to-tail, zig-zagged chains. A linear relationship between the N⋯H separation and the pK_a value of the corresponding fluorophenol was discovered. Comparisons are made with the analogous halogen-bonded 4-(*N,N*-dimethylamino)pyridine and iodofluorobenzene complexes, in addition to with the crystal packing of the pure fluorophenols.

Acknowledgements

I would like to thank my supervisor, Professor Dr. Duncan W. Bruce, for his guidance, advice and patience in helping me complete this work. I am also grateful to Dr. Isabel Saez for her support and advice.

I am also indebted to my fellow group members, Carsten Präsang, Valery Kozhevnikov, Amedeo Santoro, Navpreet K. Sethi, Saleesh N. S. Kumar, Matthew Spencer and Steve Wainwright, for both their help and friendship.

I would also like to thank my first cousins, Siew Choo Tan and Hugh Steward, for listening and being my home away from home; as well as my parents, brother and sister, for their support and understanding.

Table of Contents

List of Tables

List of Figures

List of Schemes

Abbreviations

ΔH	Enthalpy
ΔS	Entropy
B	Crystal Smectic B Phase
CCD	Charge Coupled Device
Cr	Crystalline Solid
DMAP	4-(*N*,*N*-Dimethylamino)pyridine
DMF	Dimethyformamide
DSC	Differential Scanning Calorimetry
DSM	Dynamic Scattering Mode
E	Crystal Smectic E Phase
FTIR	Fourier Transformed Infrared
G	Crystal Smectic G Phase
H	Crystal Smectic H Phase
HOMO	Highest Occupied Molecular Orbital
Iso	Isotropic Liquid
J	Crystal Smectic J Phase
K	Crystal Smectic K Phase
LCPs	Liquid Crystalline Polymers
LUMO	Lowest Unoccupied Molecular Orbital
N	Nematic Phase
NMR	Nuclear Magnetic Resonance
RCA	Radio Corporation of America
SmA	Smectic A Phase
SmB	Hexatic Smectic B Phase
SmC	Smectic C Phase
SmF	Hexatic Smectic F Phase
SmI	Hexatic Smectic I Phase
thf	Tetrahydrofuran
vdW	Van der Waals
XRD	X-ray Diffraction

CHAPTER 1

INTRODUCTION

1.1 Liquid Crystals: A Brief History

Matter is generally thought of to exist in one of the three basic states of solid, liquid and gas. However, in 1888 an Austrian botanist, Friedrich Reinitzer found that the compound cholesteryl benzoate (Figure 1.1) had two distinct melting points.[1] As he increased the temperature of the solid, the crystal melted into a turbid liquid at 145.5 °C. Further increasing the temperature caused the substance to change again into a clear, transparent liquid at 178.5 °C. He also observed upon cooling the clear liquid a brief appearance of a pale blue colour at the transition temperature, and a blue-violet colour just before crystallisation.
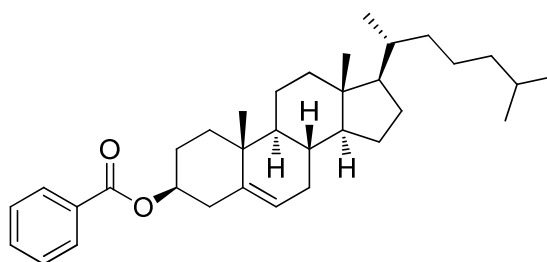
Figure 1.1: Molecular structure of cholesteryl benzoate

Reinitzer approached the German physicist and crystallographer Otto Lehmann, who examined the material under his polarising optical microscope equipped with a heating stage and reported that the turbid liquid had characteristics of both a crystal and a liquid. He eventually came to the conclusion that the turbid liquid was a new state of matter and named the new material *liquid crystals*, for their properties being between a crystalline solid and a liquid.[2]

In 1922, Georges Friedel came up with a classification scheme for the structure and properties of liquid crystals, dividing them into three phases, the nematic, smectic and cholesteric phases.[3] These phases are all also known as mesophases, 'meso' meaning intermediate. Gray published the first major book on liquid crystals in 1962, and two

years later Heilmeier, then working in the RCA laboratories, invented the first dynamic scattering mode (DSM) liquid crystal display.[4]

1.2   Introduction

Thus, liquid crystals are substances that exhibit a state of matter that has some properties of both a conventional liquid and of a solid crystal. In crystalline solids, the molecules are in fixed positions and packed close together, arranged in highly ordered geometric patterns or lattices with repeating unit cells extending in all three spatial dimensions. Molecules in the liquid phase on the other hand, are still packed quite close together but do not have fixed positions and are free to move around, giving fluidity.[2] This normal liquid is also known as an isotropic liquid as, unlike in liquid crystals, its properties are not directionally dependent. In the liquid crystalline phase the molecular arrangement falls in between that of a crystal solid and an isotropic liquid as depicted in Figure 1.2 below.
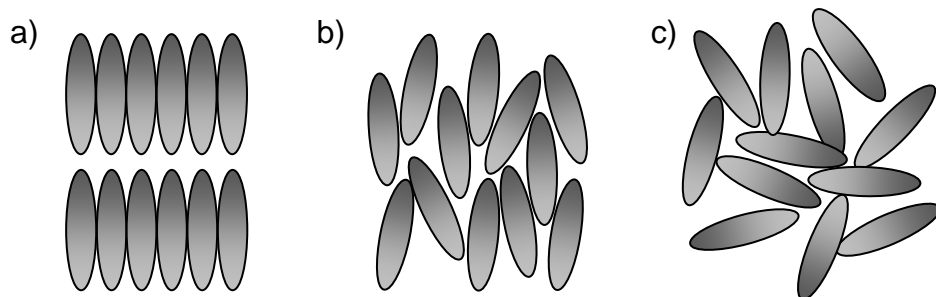
Figure 1.2: The molecular arrangement in the a) crystalline solid, b) liquid crystalline and c) isotropic liquid phases.

Liquid-crystalline materials can generally be catagorised as shown in Figure 1.3. Transitions into the liquid crystalline phase can be brought about by the action of heat or of a solvent. In the former case, the materials are known as *thermotropic* liquid crystals, while the latter case refers to *lyotropic* liquid crystals.[2] Lyotropic liquid crystals will not be discussed further.
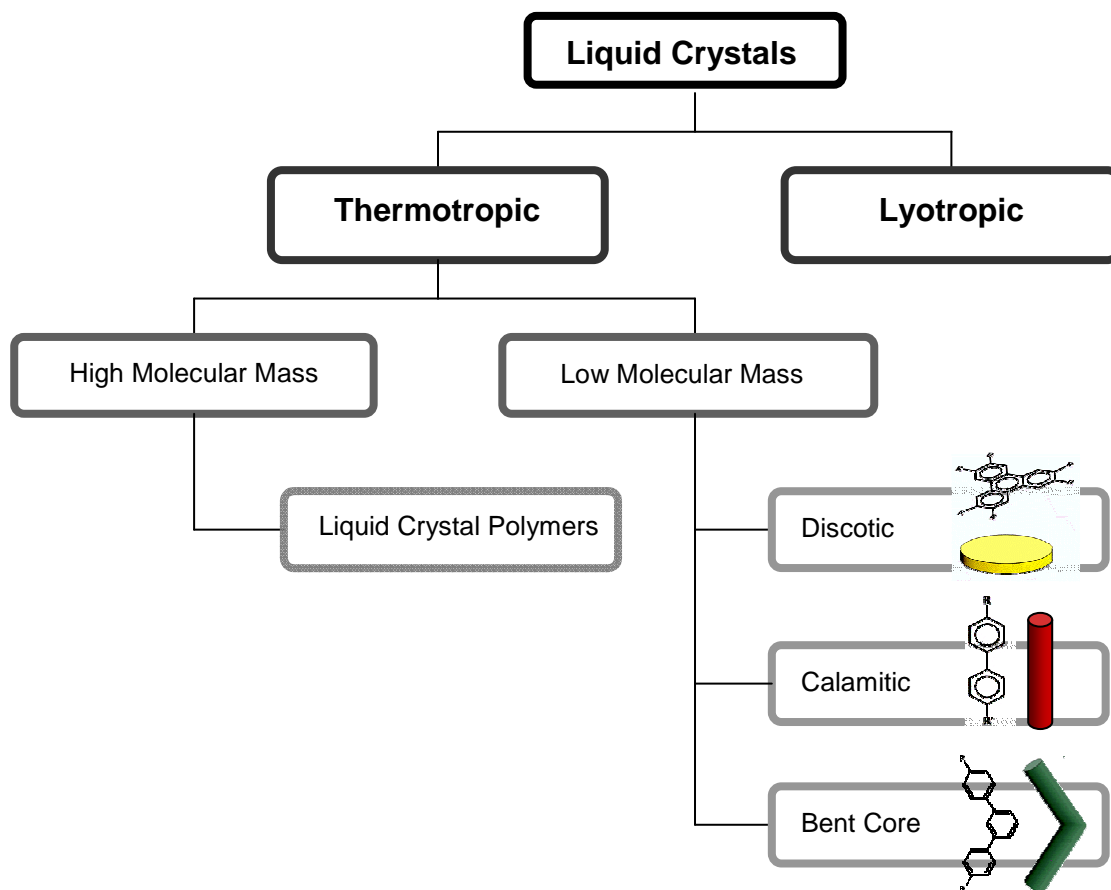
Figure 1.3: A general classification of liquid crystals.

1.2.1 Thermotropic Liquid Crystals

Thermotropic liquid crystals can be of high or low molecular mass. High molecular mass liquid crystals are also known as liquid crystal polymers (LCPs)[1] and combine the properties of polymers and liquid crystals. LCPs are usually made up of flexible chains with a mesogenic group incorporated into the backbone of the polymer (main-chain LCPs) or attached as a side group to a flexible main-chain or spacer group (side-chain LCPs), as shown in Figure 1.4. The mesophases formed by LCPs are the same as those formed by low molecular mass liquid crystals, and depend on the backbone, mesogens and spacers used in the polymer.
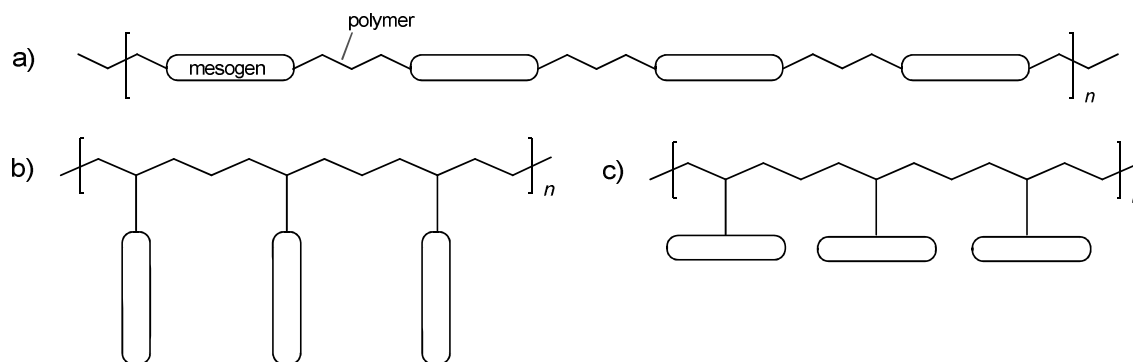
Figure 1.4: a) A main-chain liquid crystal polymer; b) and c) side-chain liquid crystal polymers.

Low molecular mass thermotropic liquid crystals are generally made up of molecules that have one molecular axis which is quite different in dimension to the other two, such as molecules which are rod-shaped (one axis is longer than the other two) and disc-like (one axis is shorter than the other two).[2] This shape anisotropy allows for orientational and positional order, so that even if the molecular positions are random, their orientation can be aligned in a regular pattern. It is this direction-dependent character in a material that allows for mesogenic behaviour. More recently, it has been shown that bent-core molecules can show liquid crystalline phases as they have sufficient overall anisotropy to organise into layers.[5] This project concentrates on thermotropic calamitic (rod-shaped) liquid crystals.

1.2.1.1 Liquid Crystal Phases Formed by Rod-like Molecules

The structure in an ordered crystal can be described by a molecule's orientational order and positional order. Orientational order represents a measure of the tendency of the molecules to align their symmetry axes parallel to a dimensionless spatial vector or director, **n**, on a long-range basis.[1,6] Positional order exists when there is a translational symmetry or a tendency for the centres of mass to spend more time in layers than between layers as they diffuse throughout the sample,[2,6] constraining them to occupy certain sites in a lattice. The molecules also need to be fairly rigid over some portion of their length to be able to maintain anisotropy and produce dispersion forces that favour alignment and stabilise the intermediate liquid crystalline order.[8]

The Nematic Phase (N)

The nematic phase is the simplest of the mesophases, in that the molecules only have one-dimensional orientational order. The molecules generally align their long axes parallel to the director, **n** (Figure 1.5), and there is no positional order.[9]
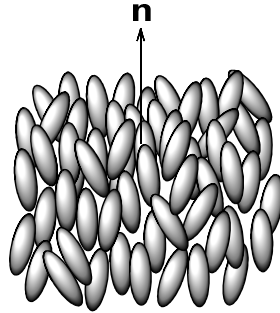
Figure 1.5: Arrangement of the molecules in the nematic phase.

The degree of orientational order in the phase is quantified by the scalar order parameter, *S*:

$$S = \frac{1}{2} < 3\cos^2\theta - 1 >$$

where θ is the angle between an individual molecular long axis and the director, and the brackets indicate an averaged quantity over a collection of molecules.[9] The molecules are free to diffuse throughout the sample, making this phase an anisotropic fluid.[6]

The Smectic A Phase (SmA)

There exist a large family of liquid crystal mesophase characterised by partial translational ordering, known collectively as *smectic phases*.

Like in the nematic phase, the smectic A phase also has one-dimensional orientational order, but in addition, possesses a molecular time-averaged distribution or density function that can be represented by a sinusoidal wave, indicating a loosely layered structure.[6] These non-rigid layers give the phase a degree of positional order (Figure 1.6).
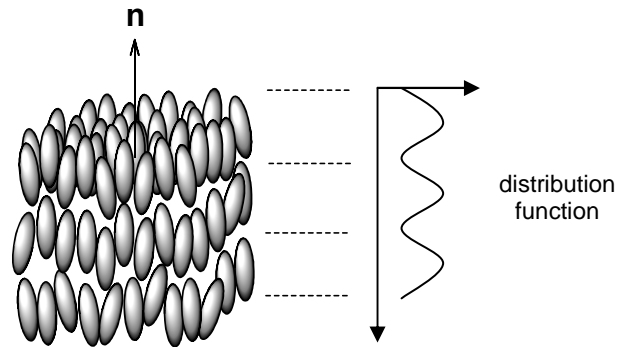
Figure 1.6: Arrangement of the molecules in the smectic A phase.

The Smectic C Phase (SmC)

The smectic C phase is very similar to the smectic A phase, except that the molecular long axes are tilted at an angle, θ, to the layer normal. Figure 1.7 depicts this arrangement as well as the molecular distribution function that corresponds to the loose layers. As the molecules are still free to diffuse between layers, both this phase and the SmA phase are fluid.[10]
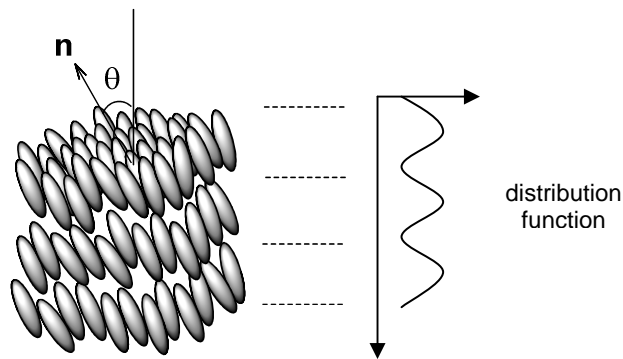
Figure 1.7: Arrangement of the molecules in the smectic C phase.

The Hexatic Smectic Phases

In the hexatic smectic phases, there is hexagonal order (Figure 1.8). Within the layers, this ordering is, however, not long-range and defects occur which can destroy it. Positional correlations between layers are negligible.[11]

6
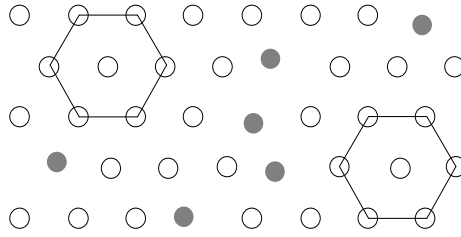
Figure 1.8: A layer view of the molecular ordering in a hexatic smectic phase. The filled dots represent defects or molecules which break the long range order of the structure.

There are three hexatic smectic phases: the SmB, SmF and SmI. The SmB derives from the SmA, where the director, **n**, is perpendicular to the layers, while the SmF and SmI derive from the SmC phase, in which the director is tilted at an angle, θ, to the layer normal. The molecules in the SmF phase tilt toward the edge of the hexagonal array, while in the SmI phase molecules are tilted toward the vertex of the layer hexagons (Figure 1.9).[9]
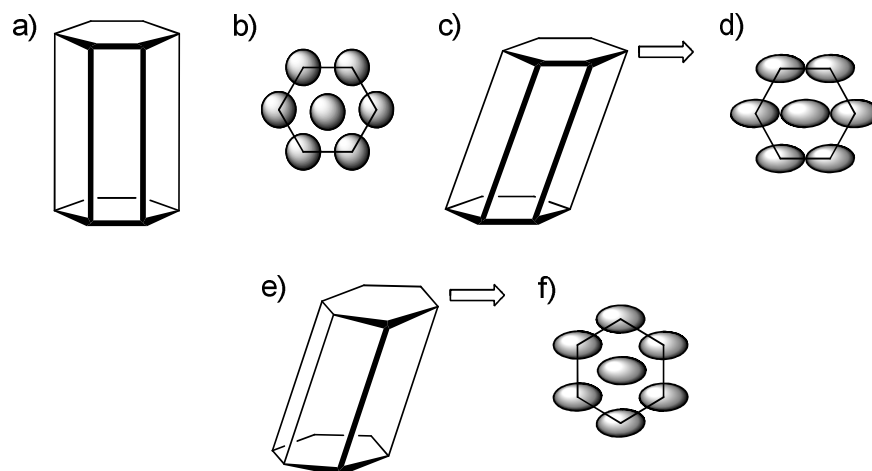
Figure 1.9: a) The SmB phase lattice. b) A top view of the SmB layer. The molecular long axes are perpendicular to the layer and thus look like circles from above. c) and e) The SmF and SmI phase lattice respectively. d) and f) A top view of the SmF and SmI layers respectively. The axis of the ellipse indicates the direction in which the molecules tilt with respect to the hexagon axes.

The Crystal Smectic Phases

The crystal smectic phases are more ordered than the hexatic smectics as they have long-ranged positional order. However, as interlayer forces are weak, there is little orientational order throughout the material.[10] There are six basic crystal smectic phases: B, G, J, E, H, and K. The B, G and J phases, which derive from the SmB, SmF and SmI

phases respectively. These phases differ from true crystal phases by exhibiting concerted molecular rotation about their long axes. As in the SmB phase, the molecules in the B phase orient in a direction perpendicular to the layer, while the G and J phases have the director tilted toward the edge and vertex of the hexagon axes, respectively.[6]

In the E, H and K phases, freedom of rotation is lost and instead the molecules arrange themselves in a herringbone pattern within the layers, as shown in Figure 1.10. The E phase has orthorhombic symmetry and is derived from the B phase, while the H and K phases are more ordered versions of the G and J respectively.[6,9]
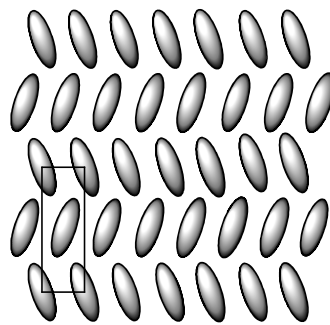
Figure 1.10: View of the herringbone packing within the layers in the E phase.

Table 1.1 below, taken from Collings and Hird's book,[2] summarises the layer smectics and crystal layered phases discussed.

Table 1.1: The grouping of liquid-crystalline and crystal layered phases according to some of their properties.[2]

Non-tilted Phases	Tilted Phases	In-plane Order	Molecular Rotation
Smectic A	Smectic C	None	Unhindered
Hexatic Smectic B	Hexatic Smectic F, I	Bond Order	Unhindered
Crystal Smectic B	Crystal Smectic G, J	Positional Order	Unhindered
Crystal Smectic E	Crystal Smectic H, K	Positional Order	Hindered

1.3 Liquid Crystals and Non-covalent Intermolecular Interactions

Non-covalent intermolecular interactions greatly influence the molecular arrangement and packing produced in a material, and, while there is no necessary translation of crystal packing behaviour into the arrangement in the mesophase of a compound, it is not impossible that some of the motifs observed in the solid state may also influence the arrangement in the mesophase. The work in this research project however, takes on the more supramolecular chemistry definition in combining non-covalent intermolecular interactions and liquid crystals. Here, the non-covalent intermolecular bond is utilised to design and synthesise new mesogens by way of molecular assemblies. There is a wide variety of non-covalent interactions from which to choose from, from strengths of hundreds of kJ mol^{-1} to bond energies less than 5 kJ mol^{-1}. Table 1.2 lists a few of these interactions and their binding energies.[12] This project makes use of the hydrogen-bond to create new liquid-crystalline materials.

Table 1.2: Some examples of non-covalent interactions used in supramolecular chemistry and their binding energies.

Intermolecular Interaction	Binding energy/ kJ mol^{-1}
Ion-ion	100 – 350
Ion-dipole	50 – 200
Dipole-dipole	5 – 50
Hydrogen bonding	10 – 120
π–π stacking	5 – 80
Van der Waals	< 8

1.3.1 The Hydrogen Bond

The hydrogen bond is an intermolecular interaction which occurs between the hydrogen atom of a molecular group, X–H (where X is an electronegative atom and gives the X–H bond a dipole moment), with a Y-atom of another molecular group which has a free lone pair of electrons. Thus the X–H group is the hydrogen bond donor, while the lone electron pair donor group is the hydrogen bond acceptor, and the hydrogen bond formed can be represented as a dotted line as in X–H⋯Y.[12] Both atoms X and Y are conventionally thought of as F, O, N or Cl. Hydrogen bonds are directional and mostly linear or almost linear, depending on the surrounding forces.[13]

The strength of the hydrogen bond can vary between 10 to 50 kJmol^{-1} for weak hydrogen bonds, while strong hydrogen bonds (such as in the ion HF_2^-) can have bond energies greater than 100 kJ mol^{-1}. Weak hydrogen bonds have bond lengths which are slightly less than the sum of the van der Waals radii, with the H atom located nearer its parent atom. Strong hydrogen bonds on the other hand, are significantly shorter than the sum of the van der Waals radii with the H atom roughly centred between X and Y in X–H···Y.[14] Ionic hydrogen bonds are the strongest of the three with binding energies between 20 to 145 kJ mol^{-1}. There are two different ionic hydrogen bonds; the cationic version, BH$^+$···B', where the hydrogen donor ion, BH$^+$, is usually a protonated base, and its anionic counterpart, A$^-$···HA', in which A$^-$ is usually a deprotonated acid.[15] Though small and weak in comparison to covalent bonds, in high numbers the hydrogen bond can make a big difference to the properties of a material, such as in the high boiling point of water, the folding of proteins, and the double helical structure of DNA.

1.3.2   Hydrogen Bonded Liquid Crystals: A Brief History

The original hydrogen bonded liquid crystals were the dimeric aromatic carboxylic acids,[16-20] for example, the hydrogen bonding between two 4-alkoxybenzoic acids [19,21,22] The newly extended calamitic molecule induced nematic and smectic C phases (Figure 1.11).[2] A few years later, Fischer and Salway both reported observing anomalous melting behaviours for some monosaccharides with long alkyl chains.[19,23,24] It was only in 1938 that a paper was published attributing Fischer's observations to liquid crystallinity from hydrogen bonded amphiphilic carbohydrates.[25]
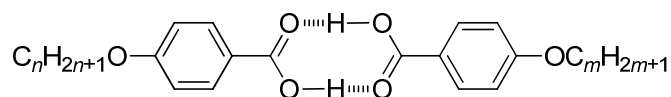
Figure 1.11: Hydrogen bonded dimer between 4-alkoxybenzoic acids

Interest in hydrogen bonded liquid crystal materials then grew again after the work of Kato and Fréchet,[26] and of Lehn and coworkers,[27] both in 1989. Kato and Fréchet reported the first liquid-crystalline, hydrogen-bonded complex formed between two distinct and non-mesogenic components. The single hydrogen bond formed between the

carboxylic group on 4-butoxybenzoic acid with the pyridine nitrogen on *trans*-4-[(4-ethoxybenzoyl)oxy]-4'-stilbazole (Figure 1.12), resulted in a new mesogen. On heating, a smectic phase was observed between 136–160 °C and subsequently a nematic phase which cleared at 238 °C.
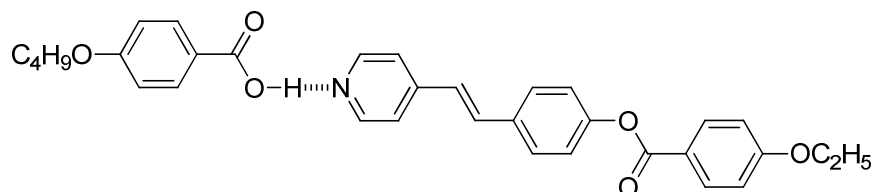
Figure 1.12: The hydrogen-bonded, liquid-crystalline complex reported by Kato and Fréchet.[26]

The complex was prepared by slowly evaporating the solvent from an equimolar mixture of the two components dissolved in pyridine. FTIR spectroscopy measurements showed that the band of the acid dimer of 4-butoxybenzoic acid at 1681 cm^{-1} was replaced by a band at 1704 cm^{-1} attributed to the new hydrogen-bonded complex.[25]

Lehn and co-workers reported triply hydrogen-bonded complexes between 2,6-diamino-pyridine and uracil, each of which had two terminal alkyl chains (Figure 1.13).[27] The supramolecular complexes were then shown by X-ray diffraction to self assemble into columnar hexagonal liquid crystalline phases.
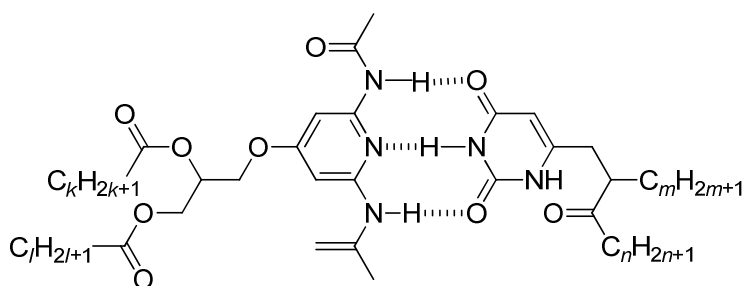
Figure 1.13: The triply hydrogen bonded 2,6-diamino-pyridine and uracil complex.

These early studies showed the great possibilities and importance of the use of hydrogen bonding in the design of both liquid crystals and soft materials in general.

1.3.3   Single Hydrogen Bonds

Most liquid crystals containing single hydrogen bonds have employed pyridyl and carboxyl moieties.[5,19] In these, hydrogen bonding extends the rigid-rod segment of the new calamitic mesogen formed, and the resulting complex behaves as a one-component liquid crystal compound; the two components of the acceptor and donor complex may or may not be mesomorphic. In both cases, however, and primarily for non-mesomorphic molecules, hydrogen bonding provides the molecule with sufficient anisotropy for the formation of liquid crystalline phases.[5,18] The extended mesogens produced have been found to show general structural-mesophase relationships which are very similar to their covalently bonded relatives.

In a later publication, Kato *et al.* reported almost-room-temperature nematic and smectic complexes of 4-alkyloxy- or 4-alkylbenzoic acids (n = 6–8, 10) with 4-octyl- or 4-undecylpyridine (Figure 1.14(a) and (b)).[28] The resulting complexes also had broad nematic ranges, leading to the use of mixtures of the nematogenic complexes obtained in electro-optic experiments. The authors also found that clearing temperatures were depressed and smectic phases induced by adding a lateral fluoro or chloro substituent, as shown in Figure 1.14(c), just as in covalently bonded calamitic molecules.[18]
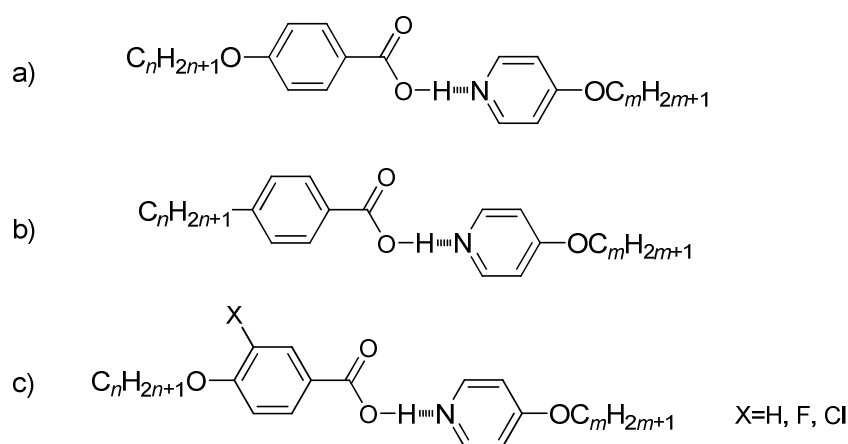
Figure 1.14: Hydrogen-bonded liquid-crystalline complexes of 4-alkyloxy- or 4-alkylbenzoic acids.

The effect of terminal substitution on mesomorphism was studied by Price *et al.* using complexes of 4-cyano- or 4-nitrostilbazole with various *para*-substituted benzoic acids (Figure 1.15). The complexes were observed to be mostly nematogenic with high clearing temperatures.[19,29] The cyano group was found to be slightly better at stabilising

liquid crystallinity than the nitro group when comparing the two series, while the phenyl complexes exhibited enantiotropic, 60 °C phase ranges to clear at 222 °C.
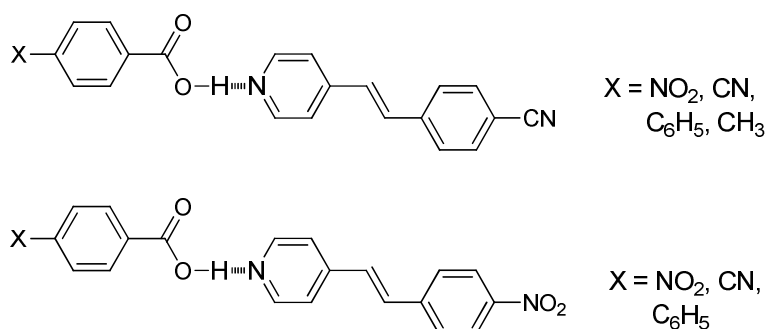
Figure 1.15: Hydrogen bonded liquid crystalline complexes of 4-cyano- and 4-nitrostilbazole.

Complexation utilising 4-alkoxy-4'-stilbazoles and 4-alkoxy-3'-stilbazoles with 3- or 4-decyloxybenzoic acid moieties, allowed for the production of hydrogen-bonded complexes bent to varying degrees (Figure 1.16).[30] The modifications to the molecular shape were found to result in changes to the molecular packing and mesomorphism, with the more angled structures exhibiting lower transition temperatures.[18,19] A wider range of liquid-crystalline phases were also observed for the skewed molecules then as for their more linear counterparts.
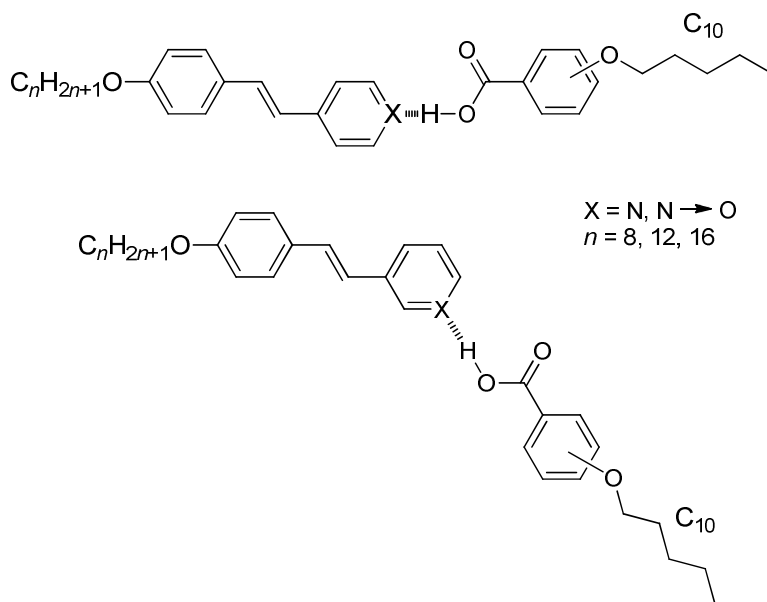
Figure 1.16: The structures of bent hydrogen bonded liquid crystalline complexes.

Cholesterol-based, hydrogen-bonded complexes were also found to be liquid crystalline (Figure 1.17).[19,31] The self-assembled complex of 3-cholesteryloxycarbonylpropanoic acid, 4-(4-alkoxybenzoyloxy)-4'-stilbazoles and *N*-(4-pyridylmethylidene)anilines were observed to exhibit smectic A, smectic C, nematic phases, as well as unidentified smectic phases. N-[4-(3-cholesteryloxycarbonylpropionyloxy)benzylidene]-4-alkoxy-anilines were synthesized as covalently bonded analogues for comparison and found to both melt and clear at temperatures higher than the corresponding hydrogen-bonded complexes.[31]
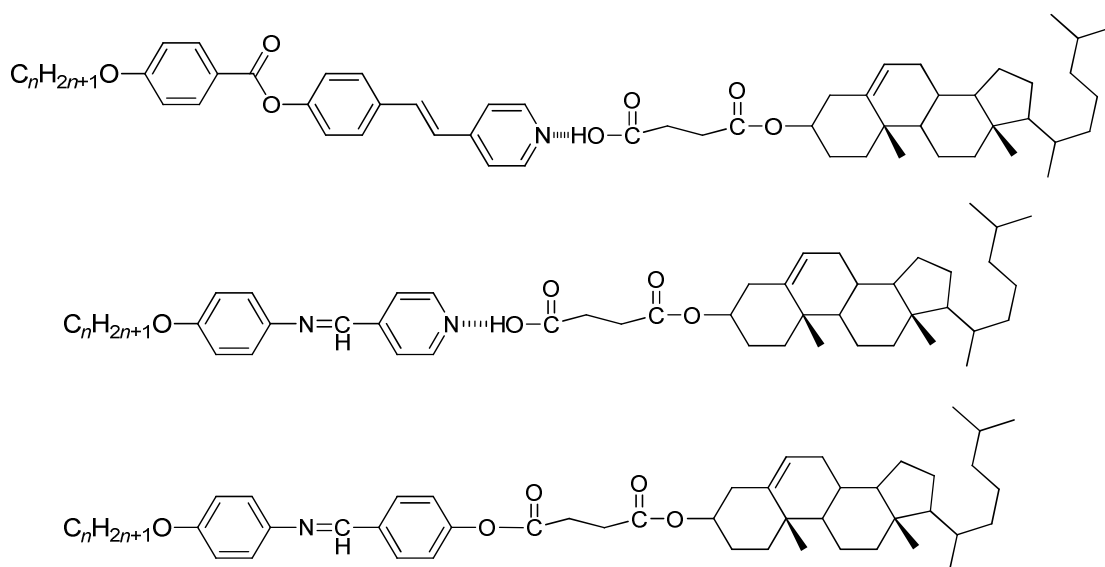
Figure 1.17: Some cholesterol based hydrogen-bonded, liquid-crystalline complexes.

There has been a smattering of reports in literature that digress from the usual pyridyl-carboxyl system. One among them employs 6-dodecyloxyisoquinoline in replacement of a pyridine moiety as the hydrogen bond acceptor to be complexed with an alkoxybenzoic acid (Figure 1.18).[19,32] The resulting complexes with the stronger base exhibited smectic A phases. On the other hand, the carboxylic acid donor was also successfully substituted for phenols, which are weaker acids. 4-Alkoxy-4'-stilbazoles were complexed with nitrophenols to give nematic and smectic A mesogens.[33]
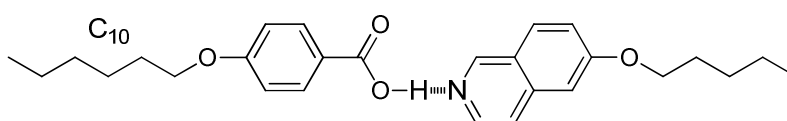
Figure 1.18: Hydrogen-bonded liquid crystal formed between 6-dodecyloxyisoquinoline and 4-decyloxy-4'-benzoic acid.

1.3.4 Multiple Hydrogen Bonds

As earlier mentioned, Lehn and co-workers reported the earliest multiply hydrogen-bonded liquid crystals between diaminopyridine and uracil. The components complexed through three hydrogen bonds and then went on to self assemble into columnar liquid crystals.[18,19] The complex in Figure 1.19 was found to behave similarly. Two hydrogen bonds between the amide and carboxylic groups gave rise to dimers which then stacked into columnar structures stabilised by interdimeric hydrogen bonding.[34]
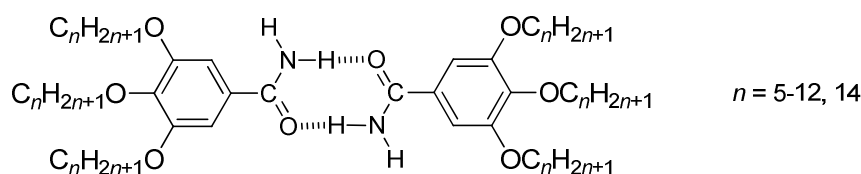
Figure 1.19: Hydrogen bonded dimeric complexes.

Another example of multiple hydrogen bonding is the compound 6,7-bis(alkyloxy)-2,3-dihydrophthalazine-1,4-dione synthesized by Suarez and co-workers.[19,35] The molecule self assembled into a trimeric disc-like structure connected by six hydrogen bonds, as shown in Figure 1.20. The discs then stacked, forming columns of the aromatic rings, which arranged into hexagonal and rectangular columnar mesophases, depending on the chain length.[35]
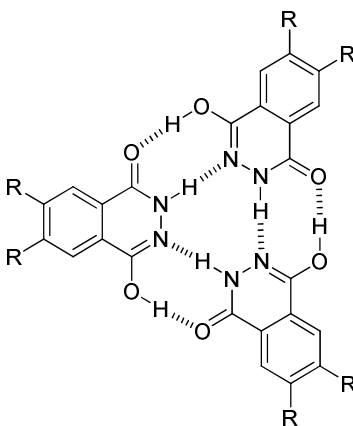
Figure 1.20: Trimeric disc-like structure connected by six hydrogen bonds.

Interestingly, 2,6-diacylaminopyridines and 4-alkoxybenzoic acids were found to interact and form an unusual T-shaped molecule, seen in Figure 1.21, joined by two hydrogen bonds. Mosaic textures were observed as monotropic phases for all homologues.[19,36]

Figure 1.21: T-shaped hydrogen bonded liquid crystalline complex.

1.4 Electronic Spectroscopy Studies

Price *et al.* reported variable-temperature electronic spectroscopy studies on the golden-yellow, hydrogen-bonded complex of 4-decyloxy-4'-stilbazole and 2,4-dinitrophenol, whose components, stilbazole and 2,4-dinitrophenol, were cream coloured (λ_{max}(thf) 326 nm) and pale yellow in colour (λ_{max}(thf) 295, sh 340 nm), respectively.[37] The colour change on complexation is indicative of the shift in absorption maxima which the nitrogen atom in the stilbazole and oxygen atom in the phenol undergo.

The complex was made up into a concentrated solution in tetrahydrofuran, of which a drop was placed between two microscope coverslips and heated to evaporate off the solvent. Spectra of the sample were recorded every 0.33 or 1 °C while heating at 1 or 4 °C min^{-1}.

Figure 1.22: The electronic spectra of the hydrogen-bonded complex from 90 to 118 °C.[37]

The spectra obtained (Figure 1.22) at lower temperature showed two peaks at 348 nm (**A**) and 400 nm (**C**) corresponding to the stilbazole and phenol in the neutral, hydrogen-bonded species. At higher temperature, through the SmA phase, two new peaks at 368 nm (**B**) and 426 nm (**D**) appeared, indicating proton transfer occurred to give the ionic hydrogen-bonded species that persisted beyond clearing (Figure 1.23). Thus, rupture of the hydrogen bond does not drive the clearing of the complex.
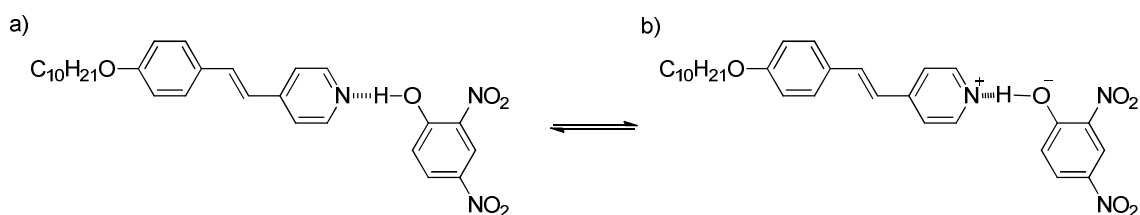
Figure 1.23: Proton transfer between (a) the normal, neutral state of hydrogen bonding and (b) the ionic hydrogen-bond state.[37]

1.5   The Halogen Bond as an Analogue of the Hydrogen Bond

Similar to the hydrogen bond, the halogen bond is also an electron donor–electron acceptor relationship. The halogen bond can be defined as the directional interaction between a halogen atom, X, and an electronegative atom, A, and is usually represented by the dotted line in D–X⋯A.[38] Halogen bonds also show energetic and geometric trends comparable to those of the hydrogen bond, and have short contact distances that are markedly shorter than the sum of the van der Waals radii.[39] X-Ray crystallographic studies have shown that the electron density around the halogen concerned is not spherical but polarised such that it is anisotropically distributed. This polarisation of the

17

electron density increases in the order of Cl < Br < I, and is also amplified by bonding to electron withdrawing groups such as perfluorocarbons or perfluoroarenes.[40]

Thus, as the halogen bond also represents a non-covalent interaction, Nguyen *et al.* who had previously worked with hydrogen-bonded liquid crystals, reported the first halogen-bonded mesogens from non-mesomorphic components.[41] The complexes between 4-alkoxy-4'-stilbazole and pentafluoroiodobenzene (Figure 1.24) exhibited nematic and smectic A phases, stable up to 84 °C.

$n = 4, 6, 8, 10, 12$
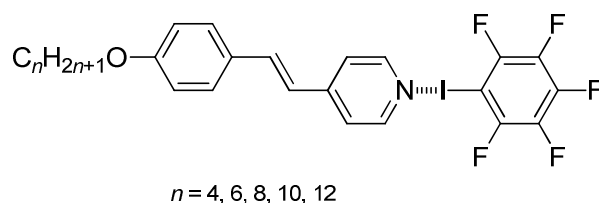
Figure 1.24: Structure of the halogen-bonded complex between 4-alkoxy-4'-stilbazole and pentafluoroiodobenzene.[41]

A systematic study of halogen-bonded complexes of varying electron density on the halogen bond donor of iodobenzene, by Präsang *et al.*,[42] found that the length of the halogen bond in the crystal decreased with increasing fluorine substitution on the iodobenzene (Figure 1.25). This is because a higher degree of fluorination on the iodobenzene withdraws electron density for a more electron poor iodine centre, and thus a stronger halogen bond is produced.
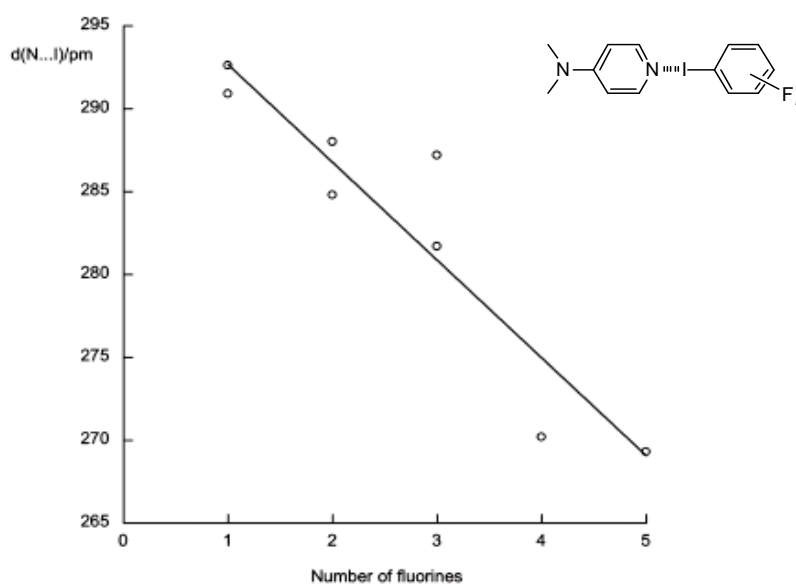
Figure 1.25: Plot of the N···I distance as a function of the number of fluorines attached to the iodobenzene ring.[42]

1.6 Project Aims

In light of the discovery of the relationship between halogen bond length and the number of fluorine substitution, it is of interest to see if a parallel correlation holds for the relationship between the hydrogen bond length and the degree of fluorine substitution. Thus, the aim of this project is to prepare and study a systematic range of hydrogen-bonded complexes between 4-alkoxy-4'-stilbazoles and a range of fluorinated phenols. Single crystal studies for a particular stilbazole will allow study of the hydrogen bond length, while polarised optical microscopy and DSC will allow their liquid crystalline properties to be evaluated.

$$C_nH_{2n+1}O \quad \text{-stilbazole-} \quad N\text{-----}H\text{-}O \quad F_m$$
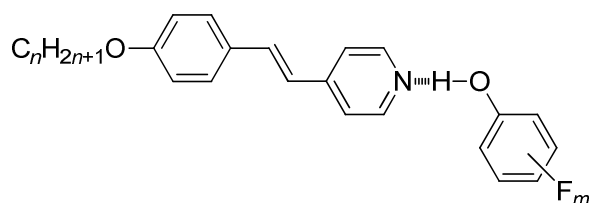
where n = 4, 8, 12
m = 1-5

References:

1. S. Singh and D. A. Dunmur, *Liquid Crystals: Fundamentals,* World Scientific Publishing, Danvers, 2002.
2. P. J. Collings and M. Hird, *Introduction to Liquid Crystals Chemistry and Physics,* Taylor and Francis, London, 1998
3. G. H. Heilmeier and L. A. Zanoni, *Appl. Phys. Lett.,* 1968, **13(3)**, 91.
4. J. A. Castellano, *Liquid Gold: The Story of Liquid Crystal Displays and the Creation of an Industry,* World Scientific Publishing, Singapore, 2005.
5. H. Takezoe and Y. Takanishi, *Jpn. J. Apl. Phys.,* 2006, **45(2A)**, 597.
6. S. Kumar, *Liquid crystals: Experimental Study of Physical Properties and Phase Transitions,* Cambridge University Press, Cambridge, 2001
7. A. J. Leadbetter, *Critical Reports on Applied Chemistry*, 1987, **22**, 1, Wiley, Chichester.
8. D. W. Bruce, *Struct. Bonding*, 2008, **126,** 161, Springer-Verlag, Berlin, Heidelberg.
9. I. Dierking, *Textures of Liquid Crystals,* Wiley-VCH, Weinheim, 2003.
10. S. Chandrasekhar, *Liquid Crystals 2nd Ed.,* Cambridge University Press, Cambridge, 1992.
11. R. J. Bushby, O. R. Lozman, *Curr. Opin. Colloid and Interfac. Sci.*, 2002, **7,** 343.
12. Y. Maréchal, *The Hydrogen Bond and the Water Molecule*, Elsevier, Oxford, 2007.
13. I. Olovsson and P. G. Jonsson, *The Hydrogen Bond: Recent Developments in Theory and Experiment.,* Eds: P. Schuster, G. Zamdel and C. Sandorfy, North Holland, Amsterdam, 1976.
14. J. Emsley, *Chem. Soc. Rev.,* 1980, **9**, 91.
15. M. Meot-Ner, *Chem. Rev.,* 2005, **105**, 213.
16. A.C. de Kock, *Z. Phys. Chem.,* 1904, **48**, 129; D. Vorländer, *Ber. Dtsch. Chem. Ges.,* 1908, **41**, 2033; A.E. Bradfield and B. Jones, *J. Chem. Soc.,* 1929, 2660; C. Weygand and R.Z. Gabler, *Z. Phys. Chem.,* 1940, **B46**, 270; M. Gaubert, *C.R. Acad. Sci.,* 1919, **168**, 277.
17. T. Kato, *Struct. Bonding,* Springer Verlag Berlin Heidelberg, 2000, **96**, 95.
18. T. Kato, *Handbook of Liquid Crystals,* Eds: D. Demus, J. Goodby, G.W. Gray, H.W. Spiess and V. Vill, Wiley-VCH: Weinheim, 1998, Vol. 2B, Chapter XVII.
19. C.M. Paleos and D. Tsiourvas, *Liq. Cryst.,* 2001, **28(8)**, 1127.
20. G.W. Gray, *Molecular Structure and the Properties of Liquid Crystals,* London, Academic Press, 1962.
21. G.W. Gray and B. Jones, *J. Chem. Soc.,* 1953, 4179.
22. G.W. Gray and B. Jones, *J. Chem. Soc.,* 1954, 1467.
23. E. Fischer and B. Helferich, *Justus Liebigs Ann. Chem.,* 1911, **383**, 68.
24. A.H. Salway, *J. Chem. Soc.,* 1913, 1022C.
25. C.R. Noller and W.C. Rockwell, *J. Am. Chem. Soc.,* 1938, **60**, 2076.
26. T. Kato, and J.M.J. Fréchet, *J. Am. Chem. Soc.,* 1989, **111**, 8533.
27. M.J. Brienne, J. Galard, J.M. Lehn and I. Stibor, *J. Chem. Soc., Chem. Commun.,* 1989.
28. T. Kato, M. Fukumasa and J. M. J. Fréchet, *Chem. Mater.,* 1995, **7**, 368.
29. D. J. Price, H. Adams, and D. W. Bruce, *Mol. Cryst. Liq. Cryst.*, 1996, 289, 127.
30. H. C. Lin and Y. S. Lin, *Liq. Cryst.,* 1998, **24**, 315.
31. Y. Tian, X. Xu, Y. Ahao, X. Tang and T. Li, *Liq. Cryst.,* 1997, **22**, 87.
32. H. C. Lin, C. W. Ko, K. Guo and T. W. Cheng, *Liq. Cryst.,* 1999, **26**, 613.

33. D. J. Price, K. Willis, K. Richardson, T. Ungar and D. W. Bruce, *J. Mater. Chem.,* 1997, **7**, 883.
34. U. Beginn and G. Lattermann, *Mol. Cryst. Liq. Cryst.,* 1994, **241**, 215.
35. M. Suarez, J. M. Lehn, S. C. Zimmerman, A. Skoulios and B. Heinrich, *J. Am. Chem. Soc.,* 1998, **120**, 9526.
36. T. Kato, Y. Kubota, M. Nakano and T. Uryu, *Chem. Lett.,* 1995, 1127.
37. D. J. Price, T. Richardson and D. W. Bruce, *J. Chem. Soc., Chem. Commun.,* 1995, 1911.
38. M. Fourmigué, *Curr. Opin. Solid State Mater. Sci.*, 2009, **13**, 36.
39. P. Metrangolo, F. Meyer, T. Pilati, G. Resnati, and G. Terraneo, *Angew. Chem. Int. Ed.,* 2008, **47**, 6114.
40. G. R. Desiraju and R. Parthasarathy*, J. Am. Chem. Soc.,* 1989, **111 (23)**, 8725.
41. H. L. Nguyuen, P. N. Horton, M. B. Hursthouse, A. C. Legon and D. W. Bruce, *J. Am. Chem. Soc.,* 2004, **126**, 16.
42. C. Präsang, A. C. Whitwood, and D. W. Bruce, *Cryst. Growth Des.,* 2009, **9(12)**, 5319.

CHAPTER 2

RESULTS AND DISCUSSION

2.1   Synthesis

2.1.1   Synthesis of the 4-Alkoxystilbazoles

A summary of the general synthetic route used to prepare the stilbazoles is shown in Scheme 2.1.
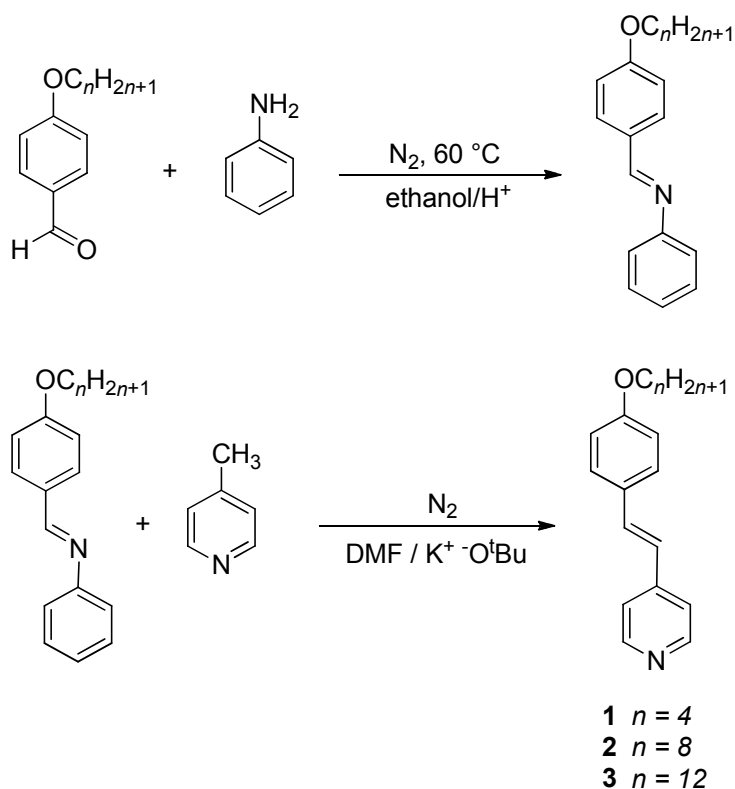
Scheme 2.1: Synthetic route for the component 4-alkoxy-4'-stilbazole

The imines were first prepared by reacting the appropriate alkoxybenzaldehyde with aniline in ethanol catalysed by a few drops of acetic acid to give the product as colourless, shiny flakes in very good yield.[1]

The Siegrist method was then chosen to convert the benzylideneaniline to the stilbazole for its high selectivity in favour of the *trans*-isomer of the product and good yield.[2] Once cooled, the solution was neutralised with hydrochloric acid, the yellow solid then collected and then washed with water. The product was crystallised from hexane to give a pale beige powder.

The hydrogen NMR spectrum of the 4-octyloxy-4'-stilbazole is shown in two sections in Figures 2.1 and 2.2. In the former spectrum, the straight, alkoxy-chain carbons appear as four peaks in the lower field region and the integration values give the ratio 2:2:10:3, while the peak that appears at 1.51 ppm is due to residual water in the solvent. The triplet at 3.92 ppm represents H_g and is shifted to lower field as it is a methylene hydrogen bound to an oxygen atom attached to an aromatic ring. [3]
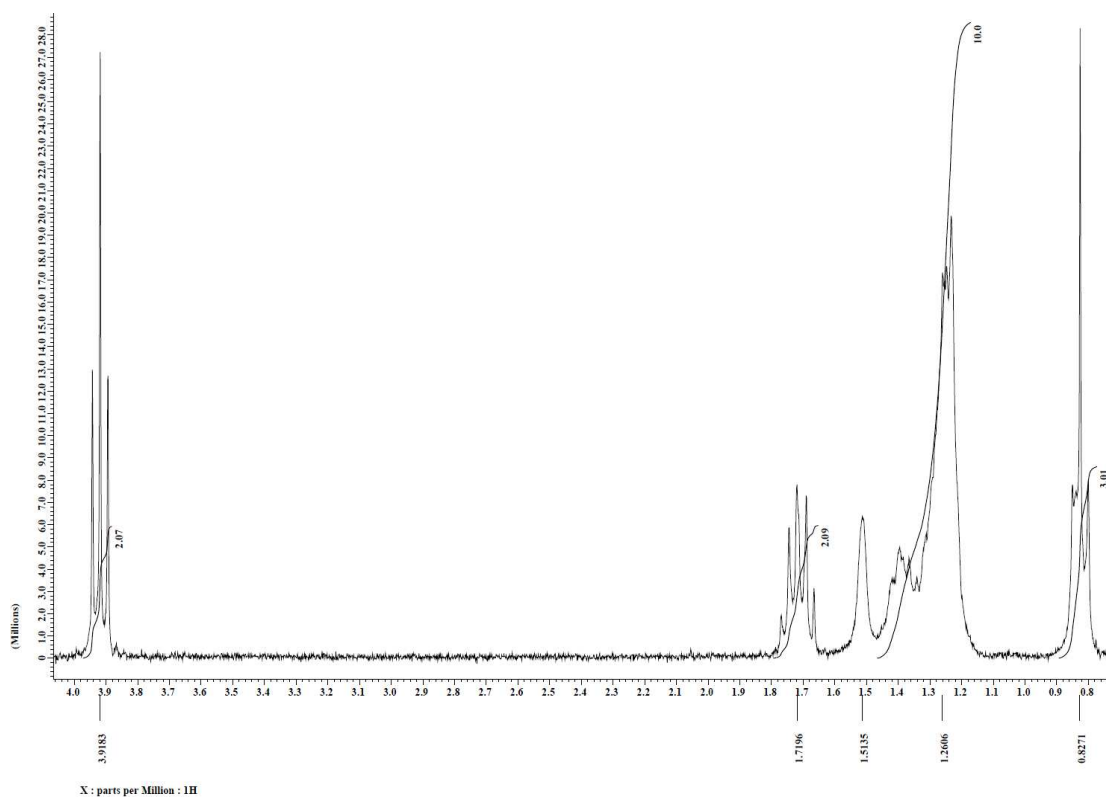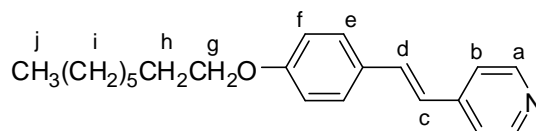
Figure 2.1: Aliphatic portion of the ^{1}H NMR Spectrum of 4-octyloxy-4'-stilbazole.

The two vinylic hydrogens, H_c and H_d, are observed as an AB quartet at 6.84 and 7.22 ppm (J = 16.5 Hz), respectively, while the two sets of chemically equivalent, but magnetically inequivalent AA'XX' protons appear as four multiplets in the range 6.7–8.5 ppm (Figure 2.2).[4] Modulated coupling constants for AA'XX' signals were measured between the two most intense signals within the multiplet. As the H_a protons are the closest to the pyridine nitrogen, they would be the most deshielded and lowest field (8.45 ppm). These would be followed by the H_f protons which are three bonds away from the electronegative oxygen atom, and then the H_b protons, separated from the less electronegative nitrogen atom by three bonds as well. This assignment is confirmed by the coupling constant values, where J_a and J_b = 6.3 Hz, and J_e and J_f = 8.7 Hz. As H_a and H_b make up one AA'XX' system, and H_e and H_f another, the coupling constants within a system should be equivalent.[5]
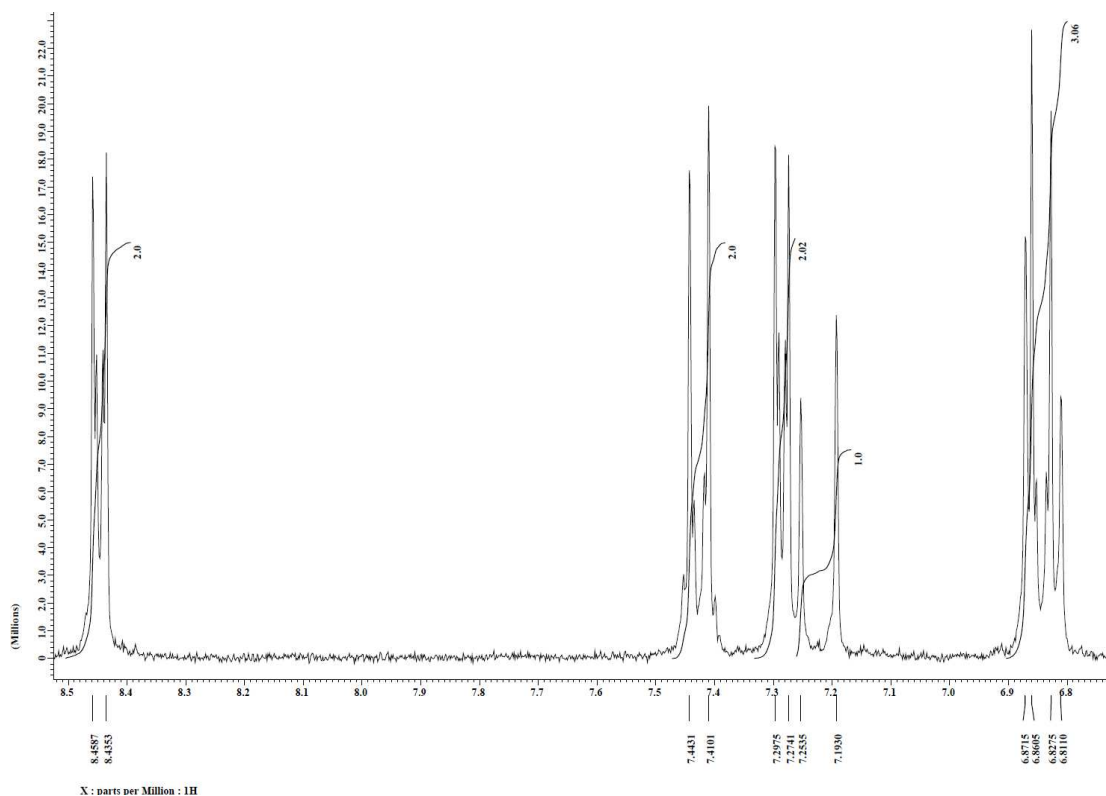
Figure 2.2: Aromatic portion of the ^{1}H NMR spectrum of 4-octyloxy-4'-stilbazole.

2.1.2   Stilbazole-Fluorophenol Complex Formation

The hydrogen-bonded complexes to be studied were prepared by separately dissolving the appropriate stilbazole and fluorophenol and then combining the two solutions with stirring at room temperature for 1½ hours. Pentane was used as the solvent for complexation for the 4-butoxy-4'-stilbazole and 4-octyloxy-4'-stilbazole homologues, while hexane was found to work better for the 4-dodecyloxy-4'-stilbazole complexes. Crystals of the product complex were then grown from the saturated solution at room temperature or dilute solution at 4 °C. A majority of the complexes crystallised as bunches of needles growing from a single nucleation point, while some grew as plates and others blocks. The crystals obtained were then collected by decantation and washed with a small amount of solvent.

The crystals of the pentafluorophenol complexes were a light yellow in colour. However, the colour reduced in intensity with reducing number fluorine substituents, so that crystals of the monofluorinated complexes were colourless. This colour change indicates the increasing strength of the hydrogen bond formed with increasing fluorine substitution. A stronger hydrogen bond is a shorter bond between the pyridine nitrogen and phenol hydrogen. The hydrogen atom can only more closely approach the pyridine when more loosely held by the acid, *i.e.* in a stronger acid, where proton dissociation is greater. In turn, the strength of the acid depends on the stability of the conjugate base, which increases when the electron density at oxygen is reduced.[6] A higher degree of fluorine substitution withdraws electron density through conjugation to stabilise the phenate ion (Figure 2.3).
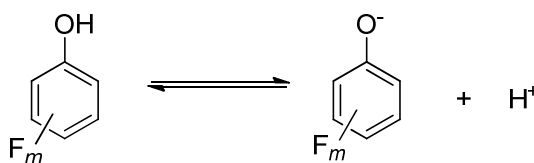
Figure 2.3: Acid dissociation equilibrium of the fluorophenol

As the strength of the hydrogen bond increases, a great positive charge develops on the pyridine nitrogen, which in turn stabilises the LUMO (Figure 2.4). This has the effect of reducing the HOMO-LUMO gap and so red shifting the absorption maximum.[7] This leads to a great tail of the absorption into the visible part of the spectrum causing the

yellow colouration; clearly this will intensify with increasing hydrogen atom transfer to nitrogen.[3]
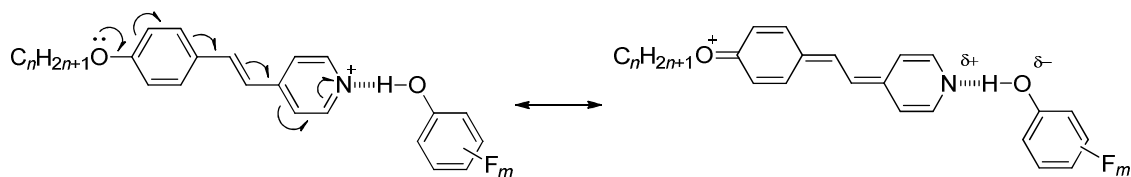
Figure 2.4: Resonance structures of the hydrogen bonded complex. The left and right structures can be considered as representing the HOMO and LUMO of the stilbazole, respectively.

The complexes formed are numbered according to the representations shown in Scheme 2.2. The synthesized butoxy-, octyloxy- and dodecyloxy-stilbazoles are indicated by the numbers **1**, **2** and **3**, respectively, while the purchased fluorophenols are numbered from **4** to **8**. In the naming system applied hereafter, the stilbazole involved is indicated first, followed by a hyphen and the notation for the fluorophenol; thus, the complex formed between 4-octyloxy-4'-stilbazole and 2,4,5-trifluorophenol is **2-6c**.
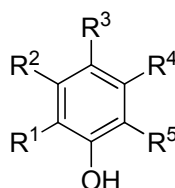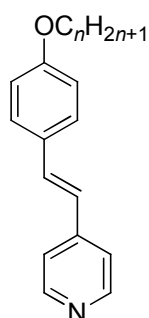
1: $n = 4$
2: $n = 8$
3: $n = 12$

4a: $R^1 = F$
4b: $R^2 = F$
4c: $R^3 = F$
5a: $R^1 = R^2 = F$
5b: $R^1 = R^3 = F$
5c: $R^1 = R^4 = F$
5d: $R^1 = R^5 = F$
5e: $R^2 = R^3 = F$
5f: $R^2 = R^4 = F$

6a: $R^1 = R^2 = R^3 = F$
6b: $R^1 = R^2 = R^5 = F$
6c: $R^1 = R^3 = R^4 = F$
6d: $R^1 = R^3 = R^5 = F$
6e: $R^2 = R^3 = R^4 = F$
7: $R^1 = R^2 = R^4 = R^5 = F$
8: $R^1 = R^2 = R^3 = R^4 = R^5 = F$

Scheme 2.2: The three different stilbazoles used in combination with different fluorinated phenols; all R^x substituents are hydrogen where not indicated as fluorine.

2.2   Mesomorphic and Thermal Behaviour Studies

2.2.1   Results

2.2.1.1   Starting Materials

The liquid crystalline properties of the stilbazoles have been reported by Bruce *et. al.* in 1988.[8] The thermal properties of **1**, **2** and **3**, which are of interest in this project, are summarised in Table 2.1. All of the fluorophenols used were non-mesomorphic.

Table 2.1: Thermal data for the stilbazole, taken from reference 8.

Derivative	Transition	$T/°C$
1	Cr – Iso	95.5
	(Iso – E)	(90.5)
2	Cr – E	75.2
	E – Iso	88.9
3	Cr – Cr'	84.4
	Cr' – E	85.4
	E – Iso	87.9

2.2.1.2   Mesomorphic and Thermal Behaviour of the Complexes

The mesomorphic properties of the complexes prepared were studied by polarised optical microscopy and differential scanning calorimetry. The transition temperatures and thermodynamic data obtained for the complexes are summarised in Table 2.2 to 2.4 respectively, while Figures 2.5, 2.7 and 2.9 give graphical representations of the data for each series. In the figures, monotropic nematic phases are shown without their associated melting points for clarity.

Table 2.2: Thermal Data for the 4-Butoxy-4'-stilbazole Fluorophenol Complexes.

Compound	Transition§	T/°C	ΔH/kJ mol⁻¹	ΔS/J mol⁻¹ K⁻¹
1-8	Cr – Cr₁	61.4	7.6	73
	Cr₁ – N	88.5	26.3	22
	N – Iso	91.0	-	-
1-7	Cr – Cr₁	55.0 – 58.0	7.9	24
	Cr₁ – N	82.0	10.1	28
	N – Iso	87.2	0.1	0.4
1-6a	Cr – Iso	89.1	39.2	109
	(N – Iso)	(88.1)	-	-
1-6b	Cr – Iso	89.7	35.8	99
	(N – Iso)	(87.0)	-	-
1-6c	Cr – Iso	106 - 109	30.6	80
	(N – Iso)	(97.5)	-	-
1-6d	Cr – Cr₁	†	0.3	0.9
	Cr₁ – Iso	91.5	29.5	81
	(N – Iso)	(82.6)	(0.5)	-
1-6e	Cr – Cr₁	66.0	0.7	2
	Cr₁ – Iso	76.5	31.2	90
	(N – Iso)	(73.5)	-	-
1-5a	Cr – Cr₁	48.0	10.1	31
	Cr₁ – N	74.5	20.7	59
	N – Iso	80.9	0.5	1
1-5b	Cr – Cr₁	†	0.3	1
	Cr₁ – Iso	87.0–93.0	28.0	77
1-5c	Cr – Cr₁	†	0.3	0.8
	Cr₁ – Cr₂	†	0.5	1
	Cr₂ – N	91.9	24.0	66
	N – Iso	95.9	0.7	2
1-5d	Cr – Iso	89.8	30.6	85
1-5e	Cr – Cr₁	†	4.2	12
	Cr₁ – Iso	63.5–72.5 (broad)	35.0	101
	(N – Iso)	(69.7)	-	-
1-5f	Cr – Iso	82.0–84.5 (broad)	40.1	113
	(N – Iso)	(79.7)	(0.6)	-
1-4a	Cr – Cr₁	†	0.6	2
	Cr₁ – Cr₂	†	2.1	6
	Cr₂ – Iso	101 (very broad)	20.2	54
1-4b	Cr – Cr₁	†	0.1	0.5
	Cr₁ – Iso	62.3	4.2	12
1-4c	Cr – Iso	101.0	37.7	101

† Not observed by microscopy

§ Here and in subsequent tables, monotropic transition temperatures are shown as heating events so that the temperatures are reliable thermodynamically.

Thermal Behaviour of the 4-Butoxy-4'-stilbazole Complexes
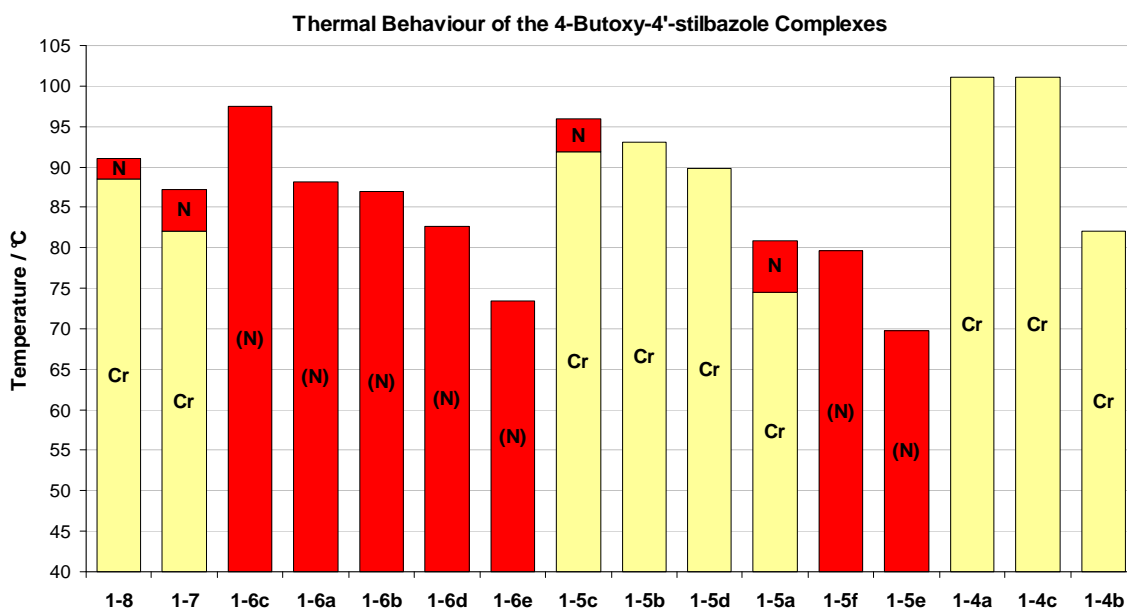
Figure 2.5: Graphical representation of the liquid crystalline behaviour of the 4-butoxy-4'-stilbazole complexes.

The complexes of 4-butoxy-4'-stilbazole were nematic where liquid crystallinity was observed. Under the microscope, the nematic phase was observed to be very homeotropic. Displacing the cover slip on the sample produced the four-brush schlieren texture and colourful shimmers[9] as shown in Figure 2.6(a) and (b). The occurrence of the nematic phase observed in this series was not surprising as the short, four carbon alkoxy chain length is unlikely to stabilise lamellar packing.[10] It is also important to note that the crystals were observed to melt cleanly without biphasic behaviour, indicating that the sample was pure.[11]

(a)   (b)
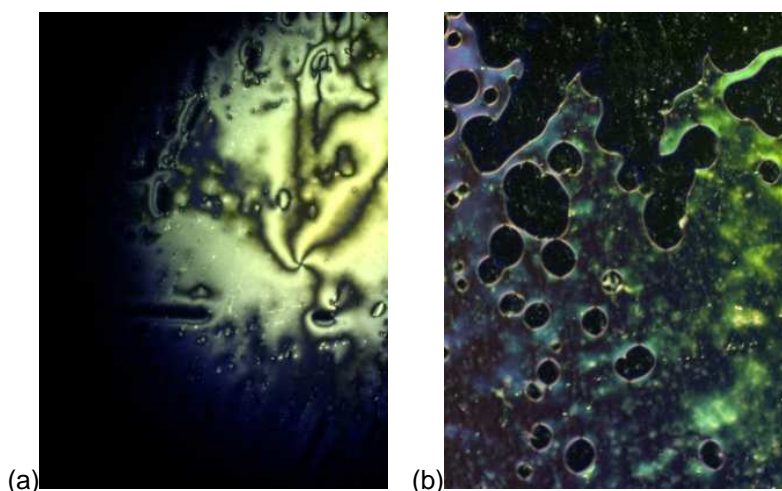
Figure 2.6: Photomicrograph of the nematic phase of **1-8** depicting (a) the schlieren texture and (b) the colourful, shimmery texture observed on displacing the coverslip.

Figure 2.5 is a graphical representation of the thermal data observed by microscopy. The complexes are grouped according to their degree of fluorination and are arranged in order of decreasing clearing temperature within these groups. Complexes **1-8** and **1-7** showed an enantiotropic nematic phase between 88.5–91.0 °C and 82.0–87.2 °C respectively. The trifluorophenol complexes were all monotropic, and of these the 2,4,5-substituted fluorophenol complex, **1-6c**, had the highest clearing temperature at 97.5 °C. The difluorophenol complexes exhibited a mixture of enantiotropic, monotropic and non-mesomorphic behaviour with complex **1-5c** clearing at the highest temperature, exhibiting an enantiotropic nematic phase between 91.9 °C and 95.9 °C. The monosubstituted fluorophenol complexes were all non-liquid crystalline.

Table 2.3: Thermal Data for the 4-Octyloxy-4'-stilbazole Complexes.

Compound	Transition	$T/°C$	ΔH/kJ mol^{-1}	ΔS/J mol^{-1} K^{-1}
2-8	Cr – N	87.5	40.2	112
	N – Iso	91.5	0.3	1
2-7	Cr – Cr$_1$	†	5.2	15
	Cr$_1$ – Cr$_2$	†	3.7	11
	Cr$_2$ – N	90.4		
	N – Iso	90.6	40.8	112
2-6a	Cr – Cr$_1$	†	18.1	54
	Cr$_1$ – SmA	65.1	19.8	59
	SmA – N	86.9	0.6	2
	N – Iso	92.7	1.2	3
2-6b	Cr – SmA	65.3	35.3	105
	SmA – N	86.7	0.5	1
	N – Iso	92.3	0.7	2
2-6c	Cr – Cr$_1$	†	12.9	38
	Cr – SmA	90.6	26.6	73
	SmA – N	95.6	0.8	2
	N – Iso	99.3	1.2	3
2-6d	Cr – SmA	60.1	36.3	109
	SmA – N	88.5	1.8	5
	N – Iso	89.7	1.7	5
2-6e	Cr – N	75.5	45.1	129
	N – Iso	81.1	0.7	2
2-5a	Cr – SmA	73.5	41.4	119
	SmA – N	78.9	0.2	0.7
	N – Iso	86.4	0.8	2.28
2-5b	Cr – Iso	94.7	14.2	39
2-5c	Cr – Cr$_1$	76.9	30.9	89
	Cr$_1$ – SmA	92.0	10.5	29
	SmA – N	96.0	1.3	4
	N – Iso	99.3	1.0	3
2-5d	Cr – SmA	61.5	38.9	115
	SmA – Iso	91.0	5.0	14

2-5e	Cr – N	61.2	41.6	124
	N – Iso	76.7	0.7	2
2-5f	Cr – Iso	93.0	52.7	144
	(N – Iso)	(81.1)	(0.7)	(2)
2-4a	*	65.5	24.3	72
	Cr – Iso	95.2	13.8	37
2-4b	Cr – Cr_1	†	0.1	0.4
	Cr_1 – Cr_2	†	1.9	6
	Cr_2 – Iso	76.5	44.7	128
	(N – Iso)	(78.9)	-	-
	(SmA – N)	(64.2)	-	-
	(E – SmA)	(48.0)	-	-
2-4c	Cr – Iso	89.5	43.2	119

† Not observed by microscopy

* Described in text
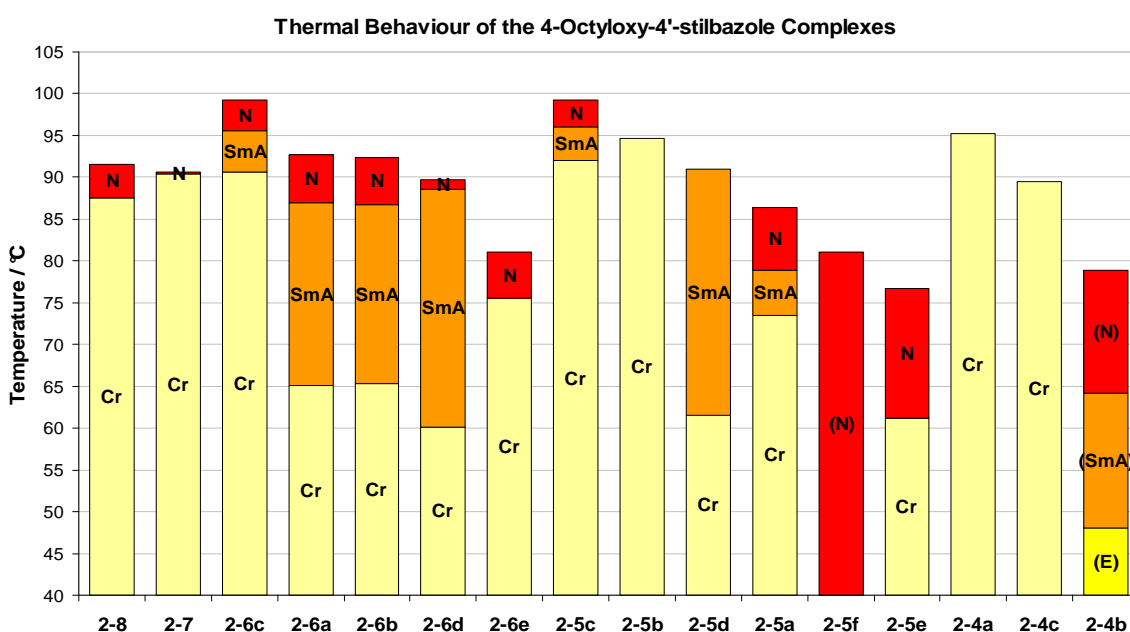
Figure 2.7: Graphical representation of the liquid crystalline behaviour of the 4-octyloxy-4'-stilbazole complexes.

Increasing the terminal chain length to eight carbons brought about an increase in the number of homologues that were mesomorphic (Figure 2.7). As the molecule is now long enough for lamellar packing, the smectic A phase was observed in quite a few of the complexes.[9] On cooling, the schlieren texture of the nematic phase was observed followed by bright spots and on a fluid dark background (Figure 2.8(a) and (b)). As the complex is very homeotropic the transition from the nematic to smectic A phase is subtle; a majority of the bright spots are observed to disappear in a wave-like movement across the sample (Figure 2.8(c)). Thus, the SmA phase was also characterised using 5 µm cells coated with nylon homogenously align the molecules.[9]

31

The crystals of complex **2-4a** were observed to undergo a softening at 65.5 °C before melting at 95.2 °C. A mosaic texture which grew with feathered ends, characteristic of the crystal smectic E phase (Figure 2.8(d)), was also observed for complex **2-4b**.
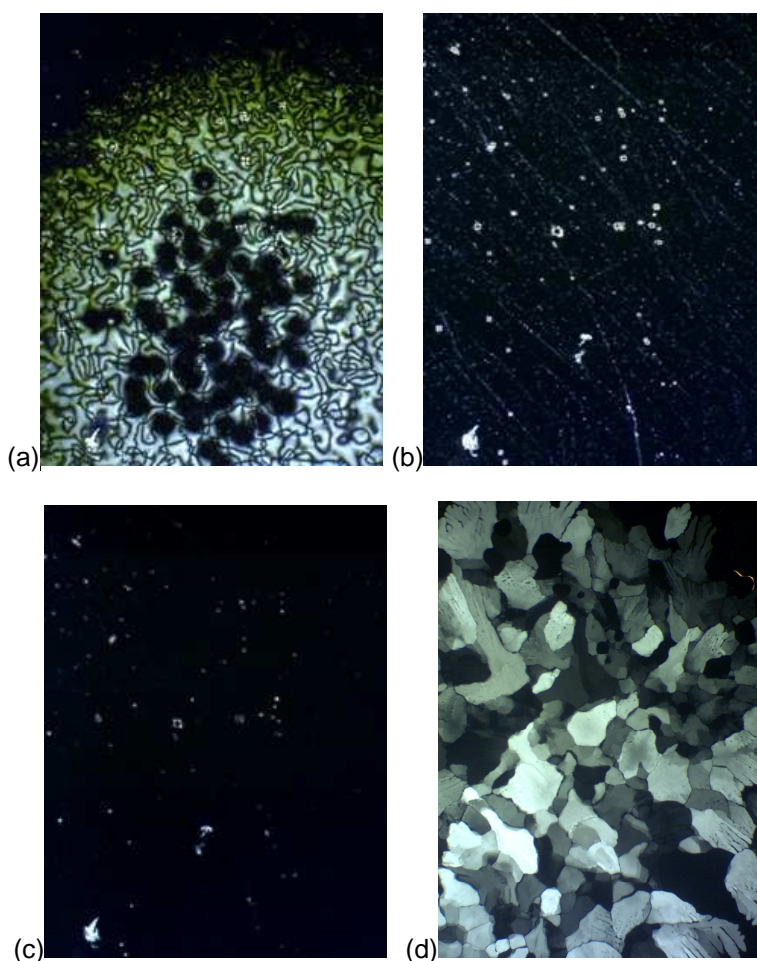
Figure 2.8: Optical photomicrographs of (a) schlieren texture of the N phase on cooling from the isotropic liquid, (b) and (c) subtle change in texture on transition from the N phase to the SmA phase on cooling, and (d) the mosaic texture of the crystal smectic E phase.

As in the previous series, the complexes with pentafluorophenol and 2,3,5,6-tetrafluorophenol showed an enantiotropic nematic phase, this time between 87.5–91.5°C and 90.4–90.6°C respectively. On the other hand, the trifluorinated derivatives have all become enantiotropic, as the longer alkyl chain length diminishes crystal phase stability to lower the melting point.[9] The difluorophenol derivatives are still a mixture of enantiotropic, monotropic and non-mesomorphic complexes while the mono-fluorinated derivatives remain non-mesomorphic with the exception of **2-4b**, which exhibits monotropic E, SmA and N phases. It is important to note that when the complexes are arranged in decreasing clearing temperature (within a group of a given

number of fluorine substituents), the same order is observed as for those complexes with **1**; indicating the influence of substituent position on the transition temperature.

Table 2.4: Thermal Data for the 4-Dodecyloxy-4'-stilbazole Complexes.

Compound	Transition	T/°C	ΔH/kJ mol^{-1}	ΔS/J mol^{-1} K^{-1}
3-8	Cr – Iso	97.8 (broad)	50.9	138
	(N – Iso)	(92.9)	-	-
	(SmA – N)	(92.0)	-	-
3-7	Cr – Iso	95.5	48.1	131
	(SmA – Iso)	(92.9)	-	-
3-6a	Cr – SmA	78.7	53.9	153
	SmA – Iso	98.7	5.0	13
3-6b	Cr – SmA	79.0	55.5	158
	SmA – Iso	98.5	5.1	14
3-6c	Cr – Cr$_1$	†	1.2	4
	Cr$_1$ – Cr$_2$	†	0.4	1
	*	87.0–89.5	31.3	87
	SmA – Iso	103.5	6.2	16
3-6d	Cr – Cr$_1$	†	0.5	1
	Cr$_1$ – SmA	83.1	42.7	120
	SmA – Iso	96.5	5.2	14
3-6e	Cr – Iso	86.0	63.9	179
	(N – Iso)	(82.7)	-	-
	(SmA –N)	(79.4)	-	-
3-5a	Cr – Cr$_1$	†	0.2	0.6
	Cr$_1$ – SmA	85.8	58.8	164
	SmA – Iso	92.2	5.5	15
3-5b	Cr – Cr$_1$	†	25.2	74
	Cr$_1$ – Cr$_2$	†	27.9	80
	Cr$_2$ – SmA	92.0	9.7	27
	SmA – Iso	98.8	7.3	20
	(E – SmA)	(93.2)	9.9	27
3-5c	Cr – SmA	90.8	49.5	137
	SmA – Iso	103.0	6.0	16
3-5d	Cr – SmA	79.8	55.4	157
	SmA – Iso	98.5	7.0	19
3-5e	Cr – SmA	65.0–67.4	55.1	162
	SmA – Iso	77.9	3.3	10
3-5f	Cr – Iso	100.0	75.0	202
	(N – Iso)	(82.3)	-	-
	(SmA – N)	(78.5)	-	-
3-4a	Cr – E	81.0	48.7	137
	E – SmA	94.5	9.3	25
	SmA – Iso	99.3	9.0	24
3-4b	Cr – Iso	88.0	70.1	194
	(SmA – Iso)	(85.0)	-	-

3-4c	Cr – Iso	94.3	64.5	176
	(SmA – Iso)	(78.2)	-	-

† not observed by microscopy

* described in text
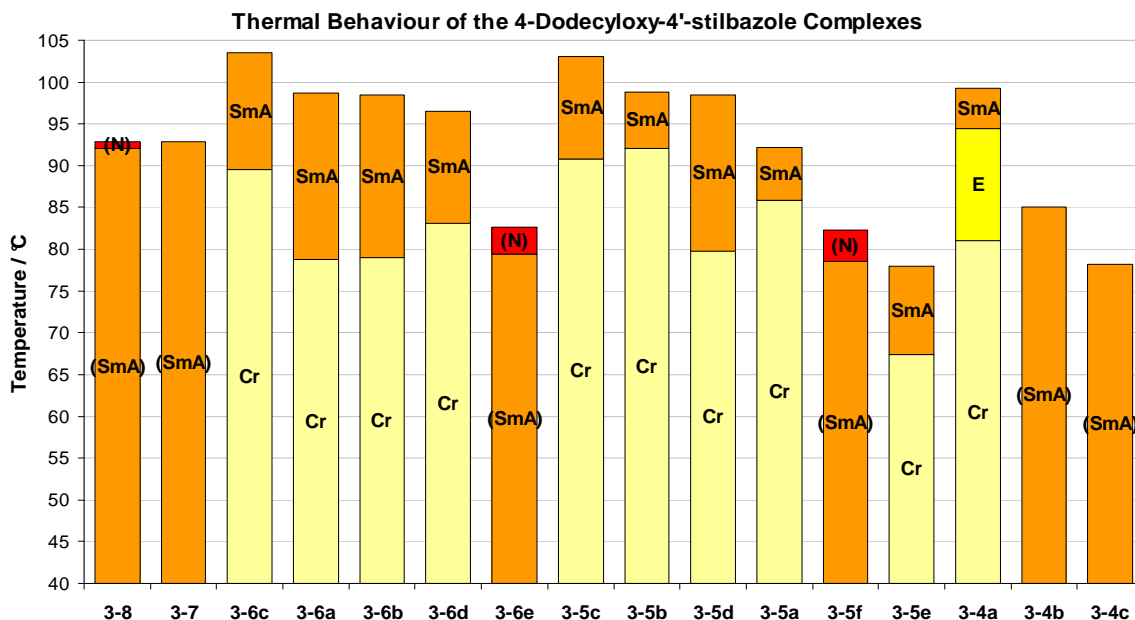
Figure 2.9: Graphical representation of the liquid crystalline behaviour of the 4-dodecyloxy-4'-stilbazole homologous series.

In the series of complexes with **3**, all derivatives are now mesomorphic (Figure 2.9) due to the increased balance between molecular rigidity and flexibility.[12] The complexes also all exhibit the smectic A phase as the long alkoxy chain favours lamellar packing,[9] and any nematic character is only observed as a monotropic phase in this series. As before, the smectic A phase is homeotropic and observed as a few bright spots on a dark, fluid background but in some complexes is seen as a focal conic texture[7] (Figure 2.10(a)).

In the temperature range of 87.0–89.5 °C, complex **3-6c** was observed to melt in two stages before forming a SmA phase. Observations by microscopy support the view that at 87 °C, the hydrogen bond breaks to give the liquid phenol plus the solid stilbazole and then, as the temperature is raised, the stilbazole melts. With both components in the fluid phase, the hydrogen bond re-forms and the complex shows a SmA phase. This is explained as follows. Up to 87 °C, the crystalline phase of the hydrogen-bonded complex is the stable state. Above this temperature, it is thermodynamically preferable for the two components to exist as the solid form of the stilbazole and the free phenol

until the stilbazole melts, at which point the two components hydrogen bond once more, revealing the mesophase. This view is further supported by literature precedent, where the same pattern of behaviour is found in complexes between *p*-toluic acid and 4-cyanostilbazole.[13]

A monotropic E phase which can not be represented in the graph was also observed for compound **3-5b,** the mosaic texture observed is shown in Figure 2.10(b).

(a)   (b)
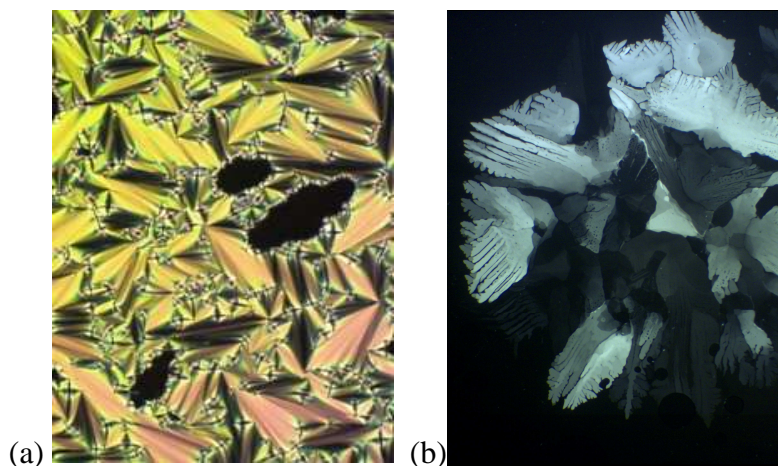
Figure 2.10: (a) The focal conic texture of the SmA phase observed and (b) the mosaic texture of the E phase.

As depicted in Figure 2.9, complex **3-8** and **3-7** are monotropic, clearing at 92.0 and 92.9 °C respectively. Complexes with three fluorine substituents saw an increase of about 6 °C in clearing from their respective analogues in the previous series, while those with two fluorine substituents showed an average increase of 4°C in clearing from increased van der Waals attractions. The stability of the mesophase as a function of fluorine substitution pattern was again preserved when organised in decreasing clearing temperature, with exception to the monofluorinated complexes. The monofluorinated complexes melted in the order of **x-4a = x-4c > x-4b** (where **x** represents the stilbazole) when **x = 1** or **2**. However, when **x = 3**, the clearing order became **3-4a > 3-4b >3-4c.**

2.2.2 Discussion

Generally, the hydrogen-bonded complexes prepared were observed to clear at increasing temperatures with increasing alkoxy chain length. The 4-butoxy-4'-stilbazole complexes were mostly nematogenic, the 4-octyloxy-4'-stilbazole complexes exhibited both the nematic and smectic A phase, while the majority of the 4-dodecyloxy-4'-stilbazole complexes displayed only the smectic A phase. The change in thermal behaviour as a function of alkoxy chain length for the complexes of **5c** is discussed as an example. Figure 2.11 is a graphical representation of these data.
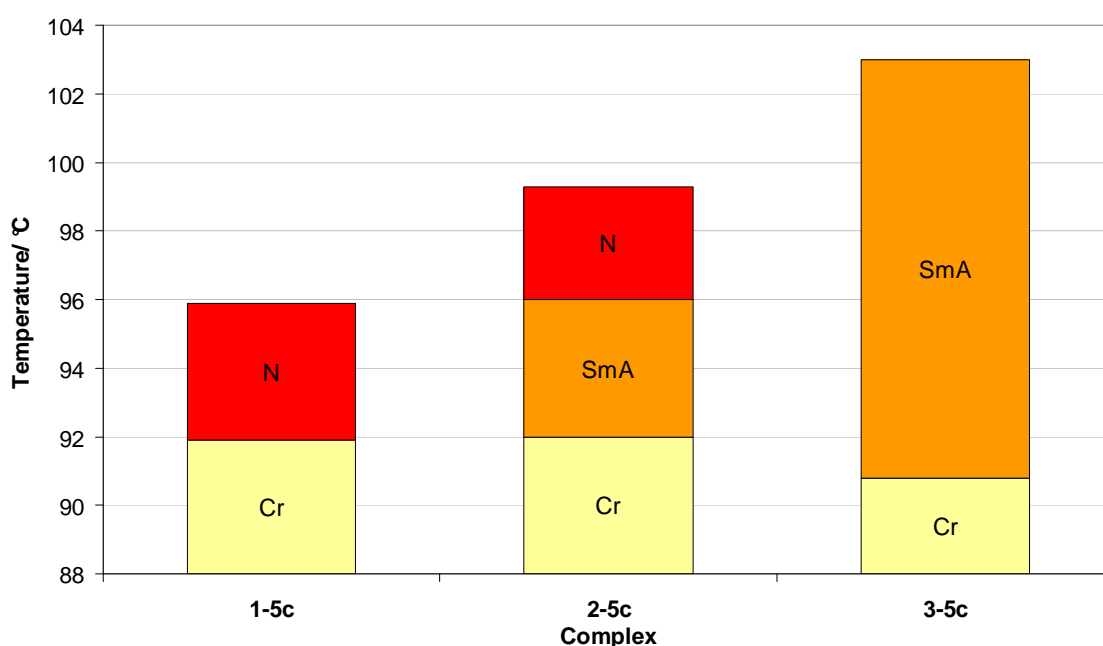
Figure 2.11: Graphical representation of the liquid crystalline behaviour of the 2,5-difluorophenol complex homologous series.

Thus, Figure 2.11 shows an obvious increase in clearing temperature as the chain length of the stilbazole increases. Complex **1-5c** clears at 95.9 °C, while complex **2-5c** clears 4 °C higher at 99.3 °C, with complex **3-5c** clearing at 103.0 °C. The increase in terminal chain length increases the molecular length and in turn the intermolecular van der Waals forces stabilising the phase. To overcome these forces for clearing, more energy must be provided to the system and so the clearing temperature of the complex is increased.[9,12]

Also observed is an increase in smectic A tendency with increasing alkoxy chain length, which eventually eliminates the nematic phase in complex **3-5c**. This is because longer terminal chains extend the molecular length and lateral interaction with one another. The greater lateral attractions promote lamellar packing and consequently the smectic phase is observed.[9,12]

Moving from left to right across the graph in Figure 2.11 sees the melting point of the complex almost invariant at about 92.0 °C. The lowering in the melting transition temperature with increasing terminal chain length is due to the diminishing crystal phase stability. Longer terminal chains have greater molecular flexibility, which disrupts the crystal packing and thus lowers the melting point of **3-5c**.[9,12]

Figure 2.12 combines the graphical representations of the liquid crystalline behaviour of the three homologous series on the same scale for comparison. In the complexes with 4-butoxy-4'-stilbazole, none of the monosubstituted fluorophenol complexes was found to be liquid crystalline, while when complexed with 4-octyloxy-4'-stilbazole only the **2-4b** homologue exhibited mesomorphism. All three mono-substituted fluorophenol complexes were only observed to be liquid crystalline together when the alkoxy chain length was twelve carbons long. Thus, the three are only comparable when complexed with the 4-dodecyloxy-4'-stilbazole, where they cleared in the order: **3-4c** < **3-4b** < **3-4a**.
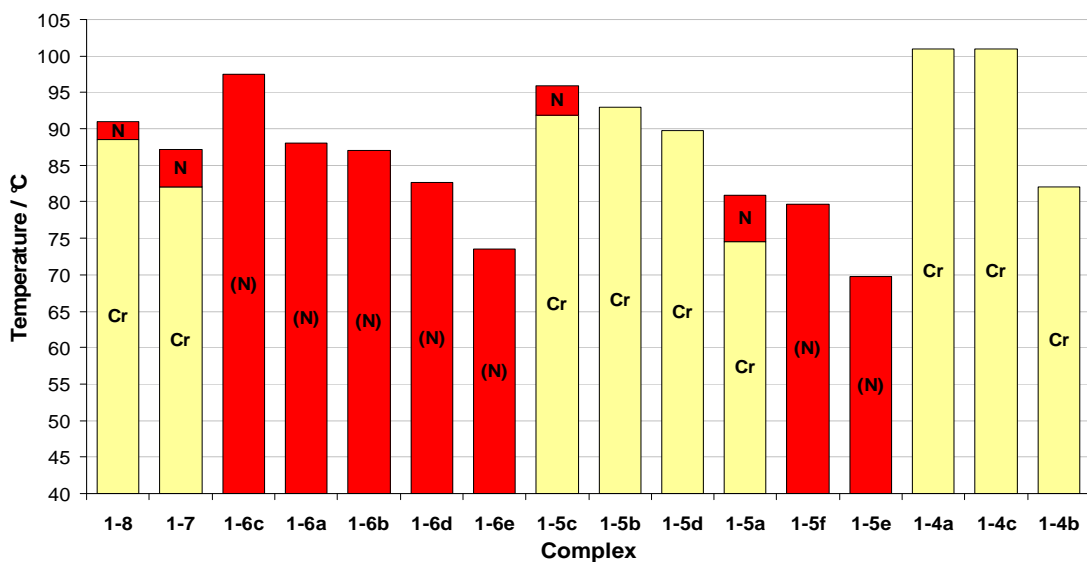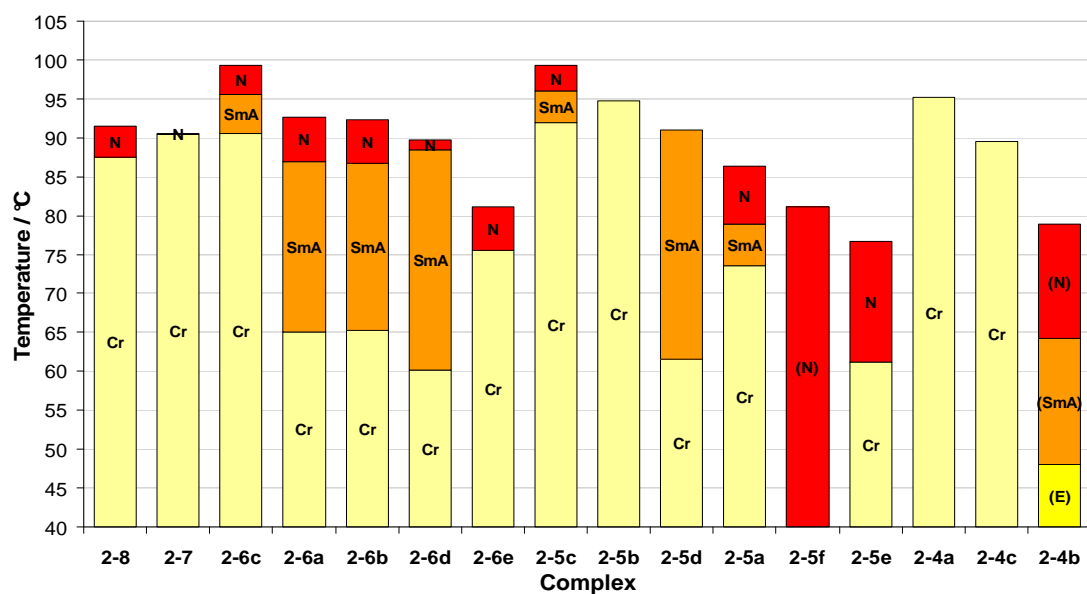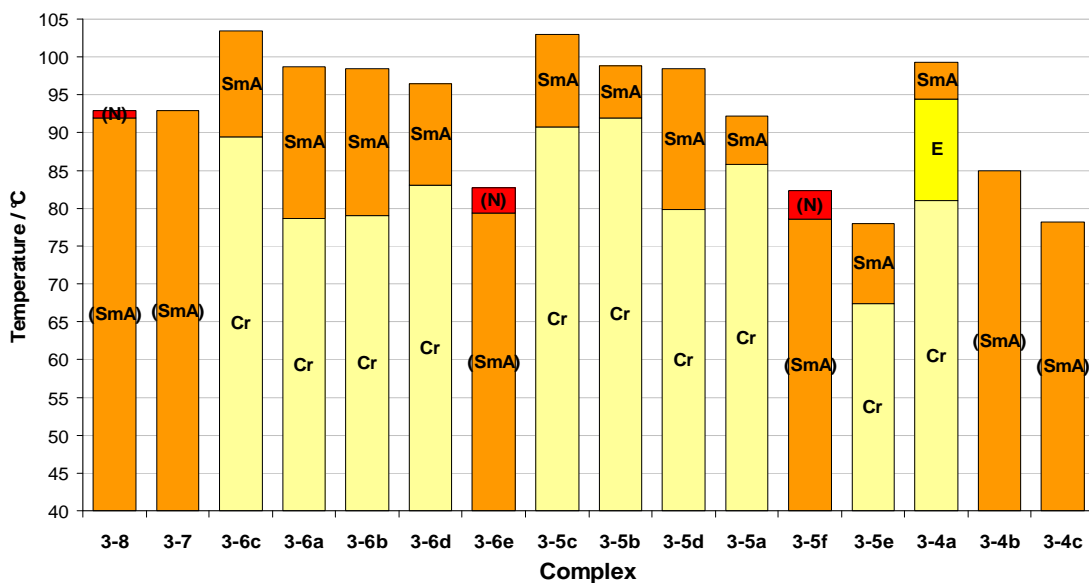
Figure 2.12: Graphical representation of the liquid crystalline behaviour of the (a) complexes of **1**, (b) complexes of **2** and (c) complexes of **3**.

Of the three, complex **3-4a** clears 14.3 °C higher than complex **3-4b** and 21.1 °C higher than complex **3-4c**, both differences being sizeable values. This is in contrast to the behaviour of the 2-cyanophenol with 4-alkoxy-4'-stilbazole complexes which showed greatly reduced mesophase stability in comparison to the analogous 3- and 4-cyanophenol complexes, due to reduced molecular anisotropy.[11] The reason for the **3-4a** complex being the highest clearing may be explained by the ability of the fluorine atom *ortho* to the hydroxyl group to interact with a proton adjacent to the pyridine nitrogen, as illustrated in Figure 2.13 (a). This is not seen in the single crystal X-ray diffraction crystal structures, but is possibly present when the complex melts due to the breakdown of other interactions in the crystal phase. In forming this intramolecular hydrogen bond, the complex is further stabilised (or intermolecular forces of attraction and molecular packing are least disrupted, depending on which way one looks at it) and the overall rod-like shape of the molecule is preserved, in turn stabilising the liquid crystalline phase and improving lateral intermolecular forces of attraction which uphold liquid crystal transition temperatures.[9]
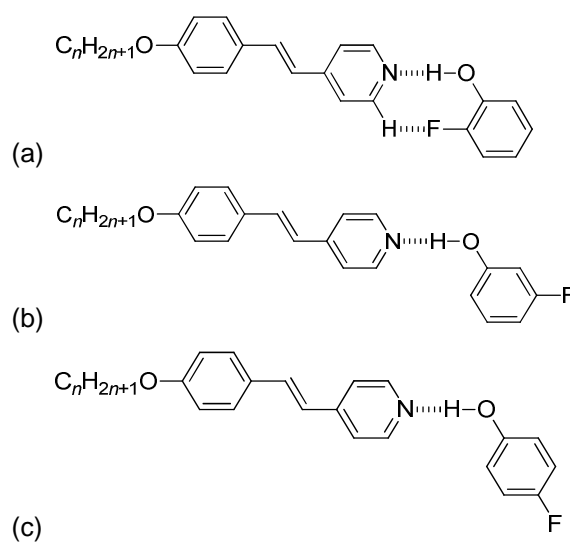
Figure 2.13: (a) Interaction of the *ortho*-fluorine with a proton on the pyridine ring. (b) Stilbazole complexed with 3-fluorophenol. (c) Stilbazole complexed with 4-fluorophenol.

In complex **3-4b**, the fluorine substituent is *meta* to the hydroxyl group, as pictured in Figure 2.13(b), and serves to increase the molecular length-to-breadth ratio slightly while maintaining the molecule's rod-shape and structural anisotropy.[14,15] This too, favours liquid-crystalline phase stability, though to a lesser extent than with the fluorine atom being in the *ortho*-position. In the *para*-position the fluoro substituent protrudes and is off the molecule axis (Figure 2.13(c)). This reduces molecular anisotropy and lateral intermolecular interactions, leading to lower liquid crystalline phase stability.[15]

Thus the complexes clearing in the order of **3-4c** < **3-4b** < **3-4a** can reasonably be justified.

This view is further supported by earlier work[11] in which 2-cyanophenol complexes with alkoxystilbazoles were prepared and examined for their liquid crystal properties. In this case, only complexes with long alkoxy chains (C_{12}, C_{13}) showed a (monotropic) SmA phase (*ca* 65 °C) and a planar structure with intramolecular hydrogen bonding would be precluded on steric grounds and so a less favourable structure is likely (Figure 2.14).
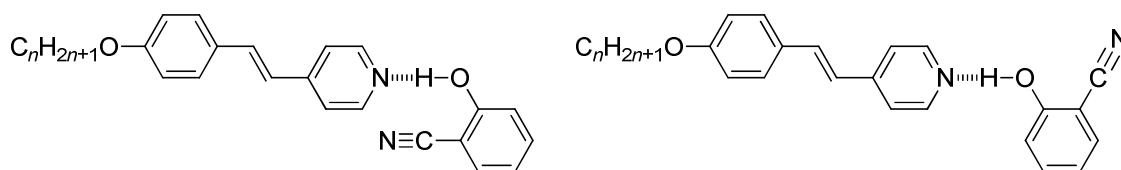
Figure 2.14: Conformers of the 2-cyanophenol and alkoxystilbazole complex.[11]

As aforementioned, the remaining complexes were found to show the same progression in decreasing temperature, regardless of alkoxy chain length, when arranged in decreasing clearing temperature within groups with the same number of fluoro subtituents. This points importantly to a consistent effect of the fluorophenols on the liquid-crystalline properties.

For the disubstituted fluorophenol complexes, while the order is upheld in all three homologous series, the complexes are only all liquid crystalline with 4-dodecyloxy-4'-stilbazole (Figure 2.12). This order in increasing clearing is **x-5e** < **x-5f** < **x-5a** < **x-5d** < **x-5b** < **x-5c**, where **x** represents the stilbazole. Among these, the four highest clearing complexes are those with one of the two fluoro substituents in position-2, which allows for interaction with a proton on the pyridine ring, agreeing with the results for the monofluorinated complexes of **3** above. Thus, due to the additional stability, all complexes with a position-2 fluoro substituent clear at higher temperatures then their counterparts which do not have a fluorine substituent in position-2. Completely removing any *ortho*-fluorine in the complex (complexes of **5e** and **5f**) saw the clearing fall by about 20 °C. Complexes with **5c** were the highest clearing in the group, which is consistent with the above argument, as the complex can be seen as a combination of complexes **4a** and **4b** (refer to Figure 2.15), putting together the stability of the position-2 fluorine and the increase in molecular length of the position-3 fluorine to

give among the highest clearing points among the whole homologous series of complexes.
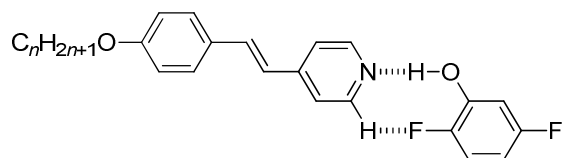
Figure 2.15: Structure of the complexes of **5c**.

The same trend is observed for the complexes of the trifluorinated phenols which clear in the order of **x-6e** < **x-6d** < **x-6b** < **x-6a** < **x-6c**, where **x** is the stilbazole (Figure 2.12). Again, the complexes with higher clearing points possessed a position-2 fluoro substituent, while the absence of fluorine in this position caused the clearing to fall by about 20°C. The **x-6c** complex is stabilised by intramolecular fluorine-hydrogen interactions (Figure 2.16) and has increased molecular length due to the position-4 and -5 fluorines, conferring it the highest clearing temperature.[14]
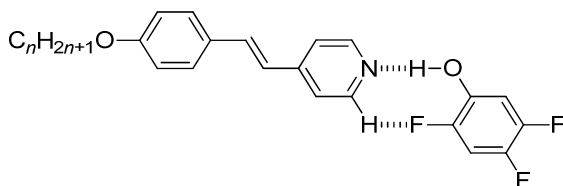
Figure 2.16: Structure of the complexes of **6c**.

Also, the fact that there is no relation between the clearing temperature and the fluorination in the complexes supports the premise that clearing is not driven by the breaking of the hydrogen-bond, rather the hydrogen-bonded complex molecule remains intact even into the isotropic phase. This is derived from the plot of clearing temperature versus pK_a in Figure 2.17, where there is no correlation between the two variables.

The pK_a values used for this plot are the calculated pK_a values of the corresponding fluorophenol, reported by Han and Tao.[16] While the report also included experimental values, the data set was not complete, and so the calculated values were chosen over the experimental values. The pK_a value is an indication of the strength of the hydrogen bond formed; a shorter hydrogen bond results from a more stable conjugate base which comes from a stronger acid, and the stronger the acid the lower its pK_a value. Hence, if

the clearing process was driven by the rupture of the hydrogen bond, complexes with low pK_a values would clear at higher temperatures. As this correlation is not found in the plot in Figure 2.17, it follows that the clearing of the complexes is not driven by the rupture of the hydrogen bond.
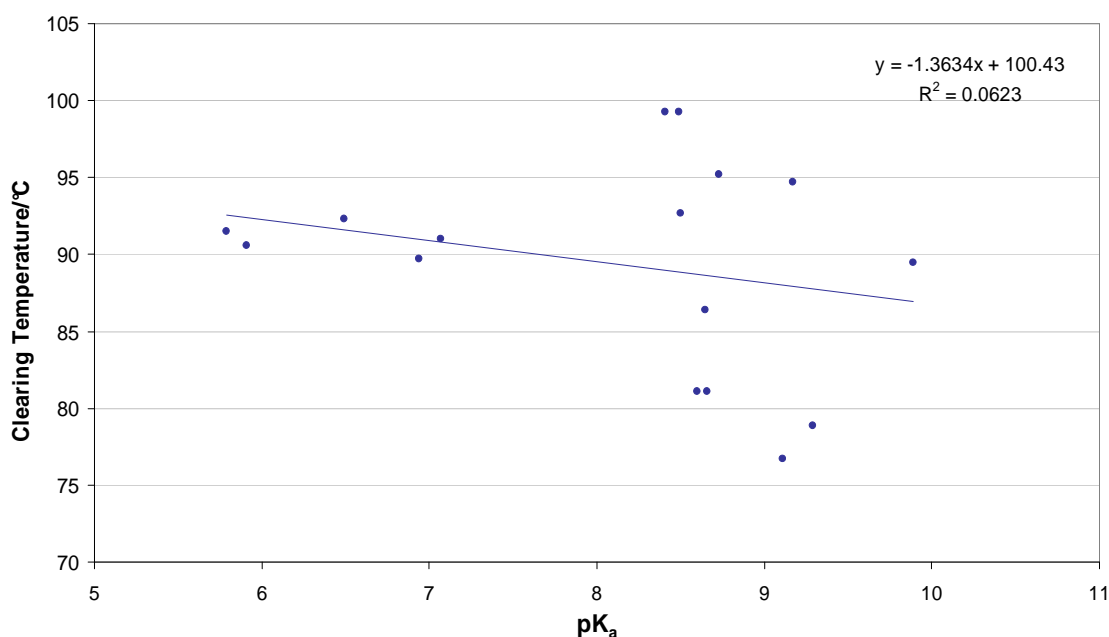
Figure 2.17: Plot of the clearing temperatures of the complexes of **2** against the pK_a of the corresponding fluorophenol.

This is also supported by variable-temperature electronic spectroscopy studies conducted by Price *et al*. on the hydrogen-bonded complex formed between 4-decyl-oxy-4'-stilbazole and 2,4-dinitrophenol, discussed earlier.[17] Deviation in the spectrum from normal isosbestic behaviour was attributed to the dissociation of the hydrogen-bonded complex. This deviation was only seen above 121 °C, 4 °C higher than the clearing point of the complex, further substantiating that the rupture of the hydrogen bond does not drive isotropisation.[17]

Willis *et al.*, Bruce *et al.* and Price *et al.* all reported hydrogen-bonded alkoxystilbazole-nitrophenol and alkoxystilbazole-cyanophenol complexes (Figure 2.18) analogous to those synthesised in this project.[11,17,18] The transition temperatures of the complexes are given in Table 2.5.

$C_nH_{2n+1}O$ —[structure]— $N\cdots H-O$ ... NC

9 $n = 8$
10 $n = 12$

$C_nH_{2n+1}O$ —[structure]— $N\cdots H-O$ ... NO_2

11 $n = 4$
12 $n = 8$
13 $n = 12$

$C_nH_{2n+1}O$ —[structure]— $N\cdots H-O$ ... CN

14 $n = 4$
15 $n = 8$
16 $n = 12$

$C_nH_{2n+1}O$ —[structure]— $N\cdots H-O$ ... NO_2

17 $n = 4$
18 $n = 8$
19 $n = 12$

$C_nH_{2n+1}O$ —[structure]— $N\cdots H-O$ ... CN

20 $n = 4$
21 $n = 8$
22 $n = 12$
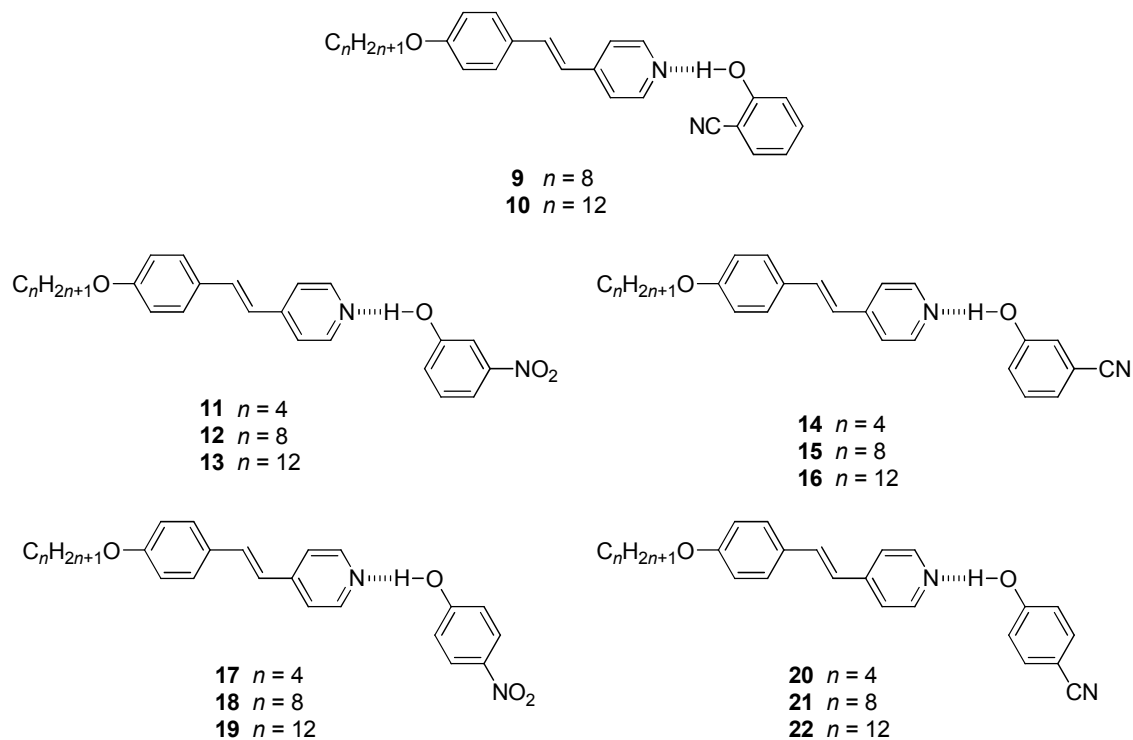
Figure 2.18: The structures of the hydrogen-bonded cyanophenol and nitrophenol complexes reported in references 11, 17 and 18.

Table 2.5: The transition temperatures of the hydrogen-bonded complexes.[11,17,19]

Complex	Transition	T/℃	Complex	Transition	T/℃
9	Cr – Iso	103	**17**	Cr – Iso	100
10	Cr – Iso	92		(N – Iso)	79
	(SmA – Iso)	(63)	**18**	Cr – Iso	99
11	Cr – N	66		(N – Iso)	80
	(Cr' – N)	(60)	**19**	Cr – SmA	80
	N – Iso	89		SmA – Iso	91
12	Cr – N	75	**20**	Cr – Iso	94
	(Cr' – N)	(74)		(N – Iso)	(67)
	N – Iso	90	**21**	Cr – Iso	95
13	Cr – SmA	80		(N – Iso)	(71)
	(Cr' – SmA)	(66)	**22**	Cr – Iso	91
	SmA – Iso	92		(SmA – Iso)	(67)
14	Cr – N	67			
	N – Iso	80			
15	Cr – Iso	75			
16	Cr – N	65			
	N – Iso	80			

Complexes **9** and **10** are both *ortho*-substituted and are comparable to complexes **2-4a** and **3-4a**, respectively. Figure 2.19 is a graphical comparison of the transition temperatures of the said complexes.

43
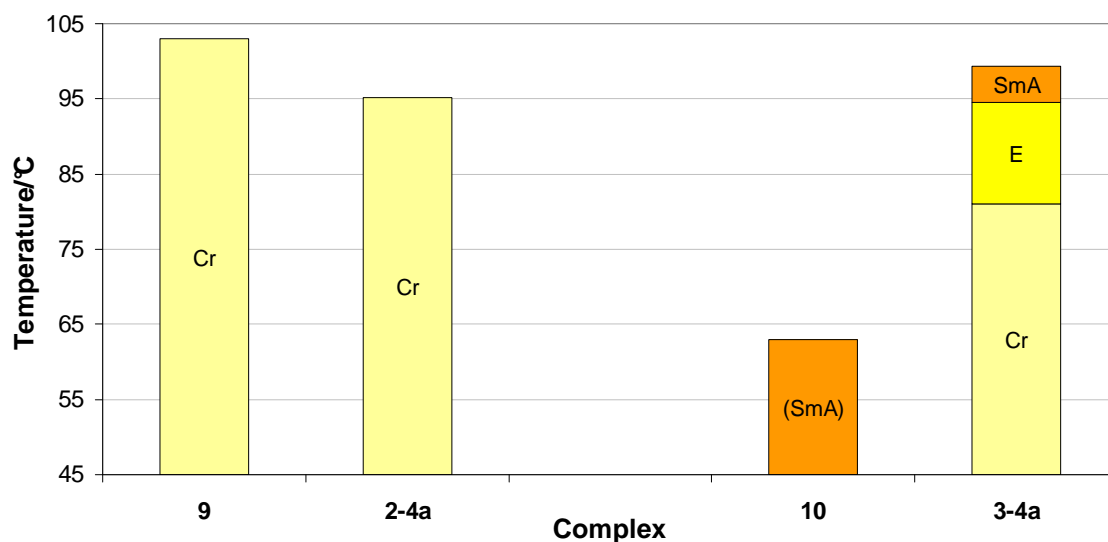
Figure 2.19: A graphical comparison of the transition temperatures of complexes **9** and **10** with **2-4a** and **3-4a**.

Both complexes **9** and **2-4a** are non-mesomorphic compounds, melting directly to the isotropic liquid phase at 103 °C and 95.2 °C, respectively. Increasing the alkyl chain length to ten carbons induces liquid crystallinity in both the cyano- and fluoro-substituted complexes. As mentioned above, the *ortho*-fluorine in position-2 probably forms an intermolecular hydrogen bond to an *ortho*-hydrogen on the pyridine ring, making the molecule more compact and stable. The overall rod shape of the molecule is then preserved, improving the lateral intermolecular forces of attraction and allowing the liquid crystalline phase to be stable up to higher temperatures.[11] On the other hand, the cyano substituent is not tied down *via* intramolecular hydrogen bonding, and can form either of the conformers shown in Figure 2.20. The conformer on the right has a molecular shape which is less conducive to liquid crystallinity as the cyano substitutent protrudes off the molecular axis. This would disrupt packing in the liquid crystalline phase and hence lower the clearing point of complex **9**.[12]
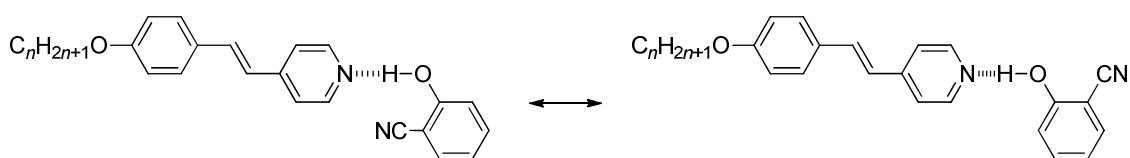
Figure 2.20: Conformers of complex **9**.

The plots in Figure 2.21 compare the clearing temperatures of the 3-substituted complexes (Figure 2.21(a) and the 4-substituted complexes (Figure 2.21(b), respectively. In both plots, the nitro-substituted complexes are thermally the most stable, and of the two substitution positions, the 3-nitro complexes showed greater stability. The clearing points of the cyano- and fluoro-substituted complexes showed no discernable trend.
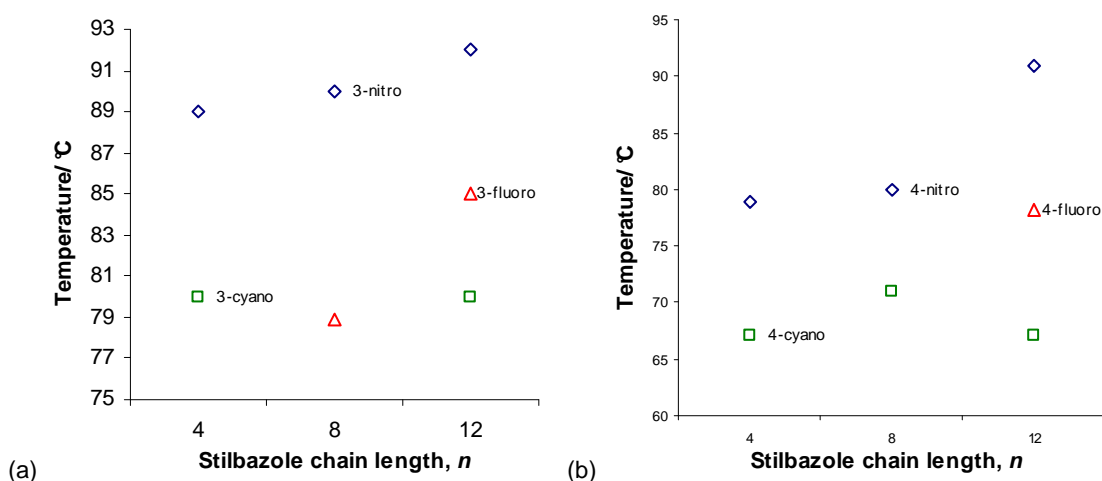
Figure 2.21: Plot of the clearing points of the (a) 3-substituted complexes and (b) 4-substituted complexes versus stilbazole chain length.

While all the 3-substituted complexes probably form antiparallel dimers,[14,18] to give better thermal stability than their para-substituted counterparts,[14] the nitro-substituted dimer gave rise to the best mesophase stability (Figure 2.22). As the nitro substituent is a larger terminal group, it increases the overall molecular size and polarizability, making the complex more stable.[9,11,14] Correspondingly, the 3-nitro substituted complexes cleared at higher temperatures than the 3-cyano and 3-fluoro complexes.
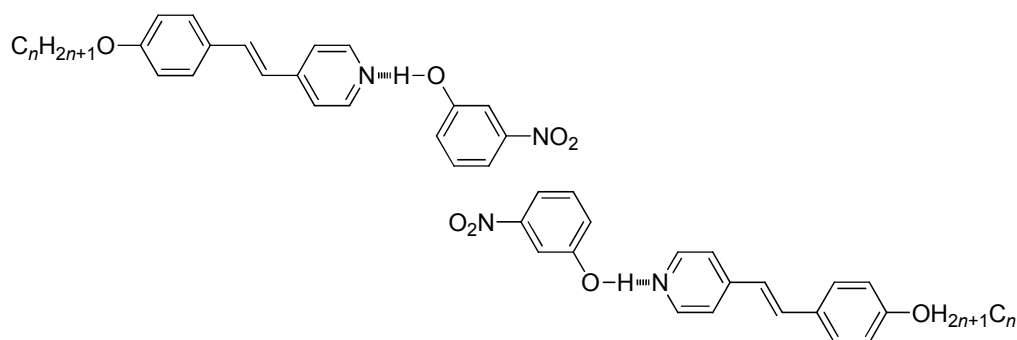
Figure 2.22: The antiparallel dimers of the nitrophenol and alkoxystilbazole complex taken from reference 11.

References:

1. D.M. Huck, H.L. Nguyen, B. Donnio and D.W. Bruce, *Liq. Cryst.,* 2004, **31**, 503.
2. H. Meier, *Angew. Chem. Int. Ed. Engl.,* 1992, **31**, 1399.
3. D. L. Pavia, G. M. Lampman, and G. S. Kriz, *Introduction to Spectroscopy,* Brooks and Cole, USA, 2000.
4. H. Günther, *Angew. Chem. Int. Ed. Engl.,* 1972, **11(10)**, 861.
5. P. Beagley, E. J. Starr, J. Bacsa, J. R. Moss and A. T. Hutton, *J. Org. Chem.,* 2002, **645**, 206.
6. J. McMurry, *Fundamentals of Organic Chemistry, 5th Ed.,* Thompson, Brookes and Cole, Pacific Grove, 2003.
7. H.L. Nguyen, P.N. Horton, M.B. Hursthouse, A.C. Legon and D.W. Bruce, *J. Am. Chem. Soc.,* 2004, **126**, 16.
8. D.W. Bruce, D.A. Dunmur, E. Lalinde, P.M. Maitlis and P. Styring; *Liq. Cryst,* 1988, **3**, 385.
9. P.J. Collings and M. Hird, *Introduction to Liquid Crystals Chemistry and Physics,* Taylor & Francis, Great Britain, 1997.
10. S. Singh and D.A. Dunmur, *Liquid Crystals: Fundamentals,* World Scientific Publishing, Danvers, 2002.
11. K. Willis, D.J. Price, H. Adams, G. Ungar and D.W. Bruce, *J. Mater. Chem.,* 1995, **5(12)**, 2195.
12. S. Kumar, *Liquid Crystals: Experimental Study of Physical Properties and Phase Transitions,* Cambridge University Press, Cambridge, 2001.
13. D. J. Price, H. Adams and D. W. Bruce, *Mol. Cryst., Liq. Cryst.*, 1996, **289**, 127.
14. D. J. Price, K. Willis, T. Richardson, G. Ungar and D. W. Bruce, *J. Mater. Chem.,* 1997, **7(6)**, 883.
15. M. Hird, *Chem. Soc. Rev.,* 2007, **36**, 2070.
16. J. Han and F. M. Tao, *J. Phys. Chem. A,* 2006, **257**, 110.
17. D. J. Price, T. Richardson and D. W. Bruce, *J. Chem. Soc., Chem. Commun.,* 1995, 1911.
18. D. W. Bruce and D. J. Price, *Adv. Mater. Opt. Electron.,* 1994, **4**, 273.
19. D. J. Price, *PhD Thesis,* University of Sheffield, 1995.

CHAPTER 3

SINGLE CRYSTAL X-RAY DIFFRACTION STUDIES

3.1   Preamble – Crystal Structure Determination

The first step in crystal structure determination by X-ray crystallography involves selecting a crystal suitable for analysis. The crystal chosen must be a single crystal in order for it to scatter the X-ray beams into a clear diffraction pattern. The selected single crystal is then mounted on a goniometer head using a minimum amount of an amorphous glue. The goniometer holds the crystal in the X-ray beam and can rotate to provide analysis of the crystal from many precise different angles and orientations.[1]

The single crystal will diffract an X-ray beam; the reflections from this are recorded on a detector as spots.[1] A single, fixed diffracted X-ray beam gives only a few reflections or spots, and so to obtain more spots or data, the crystal is rotated in the X-ray beam. This however, can get messy, as there are a great many angles to record from, and so for a systematic analysis the crystal is rotated about the direction of a unit cell axis. The individual reflections are then assigned *hkl* indices.[2] In this project, a camera equipped with a charge coupled device (CCD) area sensor was used in XRD analysis to detect and record the reflection patterns obtained from diffraction. The CCD detector is exactly like that used in digital cameras; it contains a rectangular array of capacitors onto which photons from light strike and produce a charge. The charge is then converted in to electrical pulses which can then be stored in memory. As a higher photon flux produces a higher charge in the capacitor, the electrical pulses generated by the CCD detector are proportional to the intensity of the reflected light.[3] Thus, from this process, a list of reflections, each with *hkl* indices and a measured intensity is obtained.

The data collected are affected by various factors for which correction is needed. Among the corrections which must be made are for functions of geometry of the equipment, for polarised reflection radiation, for changes in the intensity of the incident X-ray beam and scattering power of the crystal due to decomposition, and for the change in path length of the X-ray through different orientations.[2] As the data include repeated and symmetry-equivalent measurements, merging and averaging calculations

are applied to scale down the data set. All this can be done in a few minutes by computer to give a list of reflections as h, k, l, F^2_o, and $\sigma(F^2_o)$.

To solve the structure, one needs to work backwards from the diffraction data to determine the electron density distribution of the unit cell, using the following equation:[2]

$$\rho(xyz) = \frac{1}{V} \sum_{h,k,l} |F(hkl)| \cdot \exp[i\phi(hkl)] \cdot \exp[-2\pi i(hx + ky + lz)]$$

However, the phases of the reflections, which are required of the above equation, are not known. There are two common methods used to determine the phase, the Patterson Synthesis and the Direct Method.[2] In brief, the Patterson synthesis is a map of vectors produced from the Fourier transform of the F^2_o, with all phases set as zero. The vectors mark positions between two atoms, and a peak in the Patterson map indicates where atoms are positioned in relation to each other. Heavy atoms result in more defined peaks, which stand out against the general level making them easier to locate.

The Direct Method, on the other hand, involves selecting the strongest reflections which would contribute most to the electron density of the diffraction pattern (the Fourier transform),[1] and then by an educated trial-and-error method, different trial phases are attempted to find the values that best fit. These values are then used with the observed amplitudes to calculate Fourier transforms. The resulting electron density map is then checked for recognisable molecular features.[1,2]

Typically, the structure solution obtained at this stage is only partial, and so to find more atoms, the observed structure is compared to the model structure. Firstly, the calculated amplitude and phase values ($|F_c|$ and ϕ_c) are obtained from the electron density of the model structure, using the forward Fourier transform equation. The $|F_c|$ and ϕ_c values are then compared to the observed amplitudes, $|F_o|$, using the residual factor, $wR2$, in which each reflection has its own weight, w.[2]

$$wR2 = \sqrt{\frac{\sum w(F^2_o - F^2_c)^2}{\sum w(F^2_o)^2}}$$

The calculated parameters are then corrected and the reverse Fourier transform of the new $|F_c|$ and ϕ_c values results in a new electron density model structure that gives the position of more atoms. Thus this process uses the observed experimental values to correct the errors in the calculated values from the model, providing an improved model. This process can then be repeated until there are no further improvements in the calculated parameters. This procedure is known as bootstrapping.[2]

The corrected model structure must next be refined so that its diffraction pattern agrees with the observed diffraction pattern. This is to improve the quality and reduce the quantity of the observed X-ray scattering data (which is usually in excess, or 'over-determined'), so that a reliable structure can be derived. A computer usually carries out the bulk of work for this stage due to the numerous calculations and repetitions that needed. Refinement gives the final electron density map of the X-ray diffraction observed, including the unit cell space group, the positions of the atoms in the unit cell and their displacement parameters (due to the atom's thermal vibrations).[1,2] From these, other geometrical results are derived, such as bond lengths and angles, torsion angles, planarity and intermolecular interactions. Finally, all these can then be displayed as pictures of the molecules and their packing in the crystal structure.

All of the .cif files and tables of bond lengths and bond angles of the obtained crystal structures in this project are included on a CD, which forms part of this thesis.

3.2   Results

Single crystals of the 4-octyloxy-4'-stilbazole complexed with the nine different fluorinated phenols were obtained from pentane at ambient temperature or 4°C, and the structure determined by single crystal x-ray diffraction. All single crystals obtained were found to have crystallized into the $P\overline{1}$ space group with exception to that of the **2-1c** complex, which crystallized in the Pbca crystal space group. The crystallographic data collected are tabulated in Table 2.5. All short contacts were defined as shorter than the sum of the Van der Waals radii minus 0.1Å ([<$\sum$ vdW – 0.1] Å).

Table 3.1: Crystallographic data of the complexes

	2-7	2-6b	2-6e
Empirical formula	$C_{27}H_{29}F_4NO_2$	$C_{27}H_{30}F_3NO_2$	$C_{27}H_{30}F_3NO_2$
Formula weight/g mol^{-1}	475.51	457.52	457.52
T/K	110(2)	110(2)	110(2)
λ/Å	0.71073	0.71073	0.71073
Crystal system	Triclinic	Triclinic	Triclinic
Space group	P-1	P-1	P-1
Unit cell dimensions/Å	a = 5.6936(15)	a = 6.1720(3)	a = 10.4066(6)
	b = 12.539(3)	b = 11.3711(5)	b = 14.3652(8)
	c = 16.714(4)	c = 16.6214(7)	c = 15.9121(8)
Unit Cell Angles/°	α = 99.854(5)	α = 89.5710(10)	α = 87.7860(10)
	β = 95.866(5)	β = 89.5410(10)	β = 85.4180(10)
	γ = 92.065(5)	γ = 81.6710(10)	γ = 87.0740(10)
Volume/ Å^3	1167.7(5)	1154.17(9)	2366.6(2)
Z	2	2	4
ρ_{calc}/Mg m^{-3}	1.352	1.317	1.284
Absorption coefficient/mm^{-1}	0.106	0.098	0.096
$F(000)$	500	484	968
Crystal	Yellow blocks	Light yellow needles	Light yellow needles
Crystal size/mm^3	0.24 x 0.09 x 0.04	0.46 x 0.32 x 0.06	0.29 x 0.21 x 0.12
θ range for data collection	1.65 to 25.04	1.81 to 29.99	1.88 to 28.35
Index ranges	$-6 \leq h \leq 6, -14 \leq k \leq 14, -19 \leq l \leq 19$	$-8 \leq h \leq 8, -15 \leq k \leq 15, -23 \leq l \leq 23$	$-13 \leq h \leq 13, -19 \leq k \leq 19, -21 \leq l \leq 21$
Reflections collected	7248	17480	24719
Independent reflections	4042 [R_{int} = 0.0408]	6580 [R_{int} = 0.0156]	11685 [R_{int} = 0.0213]
Completeness to θ = 27.48°/%	97.8	98.0	98.9
Absorption correction	Semi-empirical from equivalents	Semi-empirical from equivalents	Semi-empirical from equivalents
Max. and min. transmission	0.996 and 0.427	0.994 and 0.873	0.9886 and 0.9727
Refinement method	Full-matrix least-squares on F^2	Full-matrix least-squares on F^2	Full-matrix least-squares on F^2
Data / restraints / parameters	4042 / 0 / 312	6580 / 0 / 303	11685 / 0 / 605
Goodness-of-fit on F^2	0.951	1.036	1.018
Final R indices [$F^2 > 2\sigma(F^2)$]	R_1 = 0.0482, wR_2 = 0.1047	R_1 = 0.0422, wR_2 = 0.1194	R_1 = 0.0434, wR_2 = 0.1110
R indices (all data)	R_1 = 0.1066, wR_2 = 0.1249	R_1 = 0.0473, wR_2 = 0.1256	R_1 = 0.0648, wR_2 = 0.1245
Largest diff. peak and hole/e Å^{-3}	0.209 and -0.257	0.484 and -0.255	0.315 and -0.202

	2-5a	**2-5d**	**2-5f**
Empirical formula	$C_{27}H_{31}F_2NO_2$	$C_{27}H_{31}F_2NO_2$	$C_{27}H_{31}F_2NO_2$
Formula weight/g mol^{-1}	439.53	439.53	439.53
T/K	110(2)	110(2)	110(2)
λ/Å	0.71073	0.71073	0.71073
Crystal system	Triclinic	Triclinic	Triclinic
Space group	P-1	P-1	P-1
Unit cell dimensions/Å	$a = 7.7812(9)$	$a = 7.7808(10)$	$a = 7.7371(4)$
	$b = 9.7838(11)$	$b = 9.6495(11)$	$b = 9.7508(5)$
	$c = 15.2278(17)$	$c = 15.3919(19)$	$c = 15.4363(8)$
Unit Cell Angles/°	$\alpha = 87.505(2)$	$\alpha = 92.913(3)$	$\alpha = 92.6130(10)$
	$\beta = 89.314(2)$	$\beta = 90.091(3)$	$\beta = 90.0900(10)$
	$\gamma = 88.837(2)$	$\gamma = 90.415(3)$	$\gamma = 91.7080(10)$
Volume/ Å^3	1157.9(2)	1154.1(2)	1162.83(10)
Z	2	2	2
ρ_{calc}/Mg m^{-3}	1.261	1.265	1.255
Absorption coefficient/mm^{-1}	0.089	0.090	0.089
$F(000)$	468	468	468
Crystal	Pale yellow needles	Pale yellow needles	Pale yellow needles
Crystal size/mm^3	0.52 x 0.14 x 0.13	0.40 x 0.09 x 0.07	0.50 x 0.27 x 0.10
θ range for data collection	2.08 to 28.34	2.11 to 25.07	2.09 to 28.32
Index ranges	$-10 \leq h \leq 10, -13 \leq k \leq 13, -20 \leq l \leq 20$	$-9 \leq h \leq 8, -10 \leq k \leq 11, -18 \leq l \leq 18$	$-10 \leq h \leq 10, -12 \leq k \leq 11, -20 \leq l \leq 20$
Reflections collected	11974	6529	9300
Independent reflections	5695 [$R_{int} = 0.0172$]	4062 [$R_{int} = 0.0165$]	5510 [$R_{int} = 0.0153$]
Completeness to θ = 27.48°/%	98.6	99.2	95.3
Absorption correction	Semi-empirical from equivalents	Semi-empirical from equivalents	Semi-empirical from equivalents
Max. and min. transmission	0.988 and 0.824	0.994 and 0.595	0.991 and 0.881
Refinement method	Full-matrix least-squares on F^2	Full-matrix least-squares on F^2	Full-matrix least-squares on F^2
Data / restraints / parameters	5695 / 0 / 313	4062 / 0 / 294	5510 / 0 / 294
Goodness-of-fit on F^2	1.023	1.034	1.051
Final R indices [$F^2 > 2\sigma(F^2)$]	$R_1 = 0.0448, wR_2 = 0.1154$	$R_1 = 0.0439, wR_2 = 0.0953$	$R_1 = 0.0442, wR_2 = 0.1141$
R indices (all data)	$R_1 = 0.0546, wR_2 = 0.1235$	$R_1 = 0.0632, wR_2 = 0.1067$	$R_1 = 0.0537, wR_2 = 0.1218$
Largest diff. peak and hole/e Å^{-3}	0.314 and -0.239	0.181 and -0.187	0.283 and -0.215

	2-4a	2-4b	2-4c
Empirical formula	$C_{27}H_{32}FNO_2$	$C_{27}H_{32}FNO_2$	$C_{27}H_{32}FNO_2$
Formula weight/g mol^{-1}	421.54	421.54	421.54
T/K	110(2)	110(2)	110(2)
λ/Å	0.71073	0.71073	0.71073
Crystal system	Triclinic	Triclinic	Orthorhombic
Space group	P-1	P-1	Pbca
Unit cell dimensions/Å	*a* = 7.8382(11)	*a* = 7.6690(9)	*a* = 14.4911(7)
	b = 9.5985(13)	*b* = 9.8547(11)	*b* = 6.1494(3)
	c = 15.231(2)	*c* = 15.2857(17)	*c* = 51.527(3)
Unit Cell Angles/°	*α* = 88.188(3)	*α* = 86.725(2)	*α* = 90
	β = 89.391(3)	*β* = 89.923(2)	*β* = 90
	γ = 87.520(3)	*γ* = 88.706(2)	*γ* = 90
Volume/ Å^3	1144.2(3)	1153.0(2)	4591.7(4)
Z	2	2	8
ρ_{calc}/Mg m^{-3}	1.223	1.214	1.220
Absorption coefficient/mm^{-1}	0.082	0.081	0.081
F(000)	452	452	1808
Crystal	Colourless needles	Colourless needles	Colourless plates
Crystal size/mm^3	0.36 x 0.11 x 0.07	0.79 x 0.13 x 0.09	0.37 x 0.18 x 0.08
θ range for data collection	2.12 to 28.32	2.07 to 30.00	1.58 to 28.34
Index ranges	$-10 \leq h \leq 10, -12 \leq k \leq 12, -20 \leq l \leq 20$	$-10 \leq h \leq 10, -13 \leq k \leq 13, -21 \leq l \leq 21$	$-19 \leq h \leq 19, -8 \leq k \leq 8, -68 \leq l \leq 68$
Reflections collected	11875	12925	59278
Independent reflections	5625 [R_{int} = 0.0190]	6442 [R_{int} = 0.0195]	5723 [R_{int} = 0.0536]
Completeness to θ = 27.48°/%	98.7	95.8	99.8
Absorption correction	Semi-empirical from equivalents	Semi-empirical from equivalents	Semi-empirical from equivalents
Max. and min. transmission	0.994 and 0.918	0.993 and 0.764	0.994 and 0.911
Refinement method	Full-matrix least-squares on F^2	Full-matrix least-squares on F^2	Full-matrix least-squares on F^2
Data / restraints / parameters	5625 / 0 / 285	6442 / 0 / 295	5723 / 0 / 285
Goodness-of-fit on F^2	1.035	1.003	1.095
Final *R* indices [$F^2 > 2\sigma(F^2)$]	R_1 = 0.0422, wR_2 = 0.1077	R_1 = 0.0435, wR_2 = 0.1192	R_1 = 0.0497, wR_2 = 0.1145
R indices (all data)	R_1 = 0.0590, wR_2 = 0.1178	R_1 = 0.0614, wR_2 = 0.1338	R_1 = 0.0615, wR_2 = 0.1223
Largest diff. peak and hole/e Å^{-3}	0.331 and -0.233	0.305 and -0.221	0.305 and -0.209

3.2.1 Description of the Crystal Structures of Complexes 2-7 and 2-6b

The first two complexes are almost identical in their crystal structure and packing. Additionally, both **2-7** and **2-6b** have unit cell dimensions and angles that are very similar (refer to Table 3.1) and have for that reason been grouped together in the following discussion.

3.2.1.1 Complex 2-7

The single crystal structure of **2-7** showed the crystal to be in the $P\bar{1}$ space group. The fluorophenol and stilbazole units are hydrogen bonded in a 1:1 ratio with an N···H distance of 1.507 Å, 57.1% of the sum of the van der Waals radii of nitrogen and hydrogen (Figure 3.1). Within a single hydrogen-bonded molecule, the three aromatic rings lie more or less co-planar (refer to Figure 3.2 for side-on view). This is probably partly possible because the N···H–O angle bends slightly at 165.11°, thus accommodating co-planarity. The angle between the planes of the two aromatic rings in the stilbazole ligand is 6.73°, while the angle between the planes of the pyridine and fluorophenol rings is 6.03°. There are also intramolecular short contacts between F1 and H9 (2.360 Å, 92.2% sum of vdW radii), F1 and C9 (3.021 Å, 95.3% sum of vdW radii), H1 and C9 (2.546 Å, 91.3% sum of vdW radii), and H1 and C8 (2.431 Å, 87.1% sum of vdW radii) which support the hydrogen bonded complex formed (Figure 3.1). Also interestingly noted is the unsymmetrical nature of the O–H bond with the hydrogen bond shown by H1···C9 ≠ H1···C8.
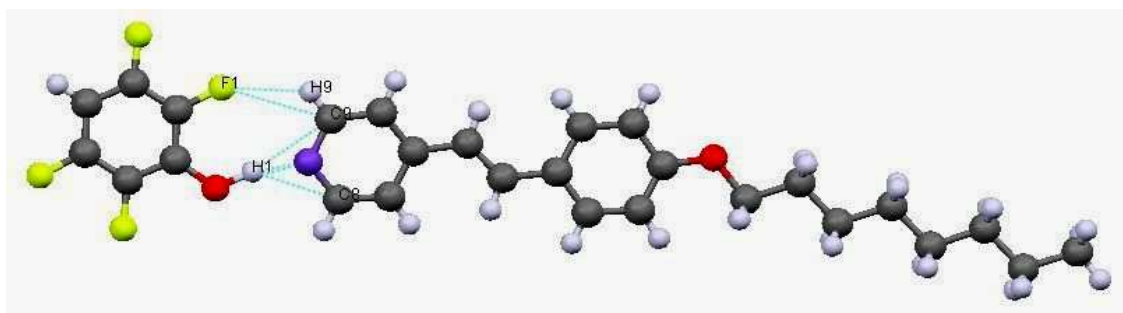
Figure 3.1: Crystal structure of a single hydrogen-bonded molecule of **2-7**, showing the intramolecular short contacts between the fluorophenol and the stilbazole.

Two molecules of the complex then dimerize with the phenols aligned back-to-back and are connected by two short contacts between F3 and H4 (2.396 Å, 81.5% sum of vdW radii). As seen in the dimer pair in Figure 3.2, the two molecules are antiparallel and co-planar, forming an almost flat, one dimensional dimer.

(a)

(b)
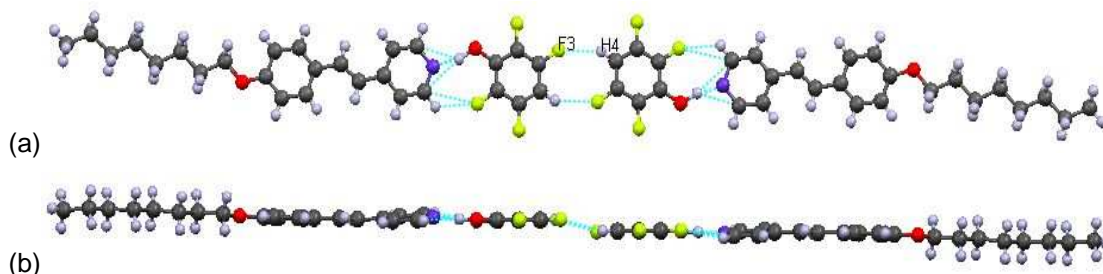
Figure 3.2: A dimer of complex **2-7**. (a) The dimers form via back-to-back interactions between the fluorophenols. (b) The dimer is almost co-planar when view at a 90° rotation of (a) through the *x*-axis.

These dimers then arrange side-by-side in a slipped fashion so that two fluorophenol rings lie next to the two aromatic rings in the stilbazole of a neighbouring dimer. This packing forms a flat, one-dimensional ribbon-like layer, supported by intermolecular short contacts between F4 and two hydrogen atoms (H7 and H13) at 2.454 Å (95.9% sum of vdW radii) and 2.408 Å (94.1% sum of vdW radii) respectively, as depicted in Figure 3.3.
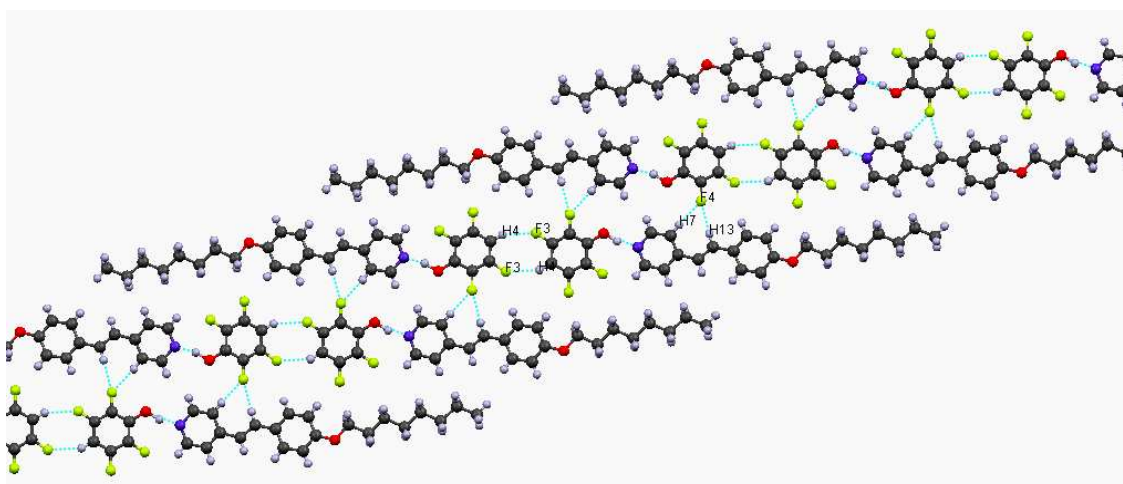
Figure 3.3: Dimers of the complex molecule arrange side-by-side, linked by four F–H short contact interactions to form a flat, one dimensional layer.

The long ribbon-like layers stack up into a slipped ladder in the direction perpendicular to the layer plane, as shown in Figure 3.4(a) below. No short contact interactions are present in between layers and the ring overlap in stacking is slight as shown in Figure 3.4(b).

(a)

(b)
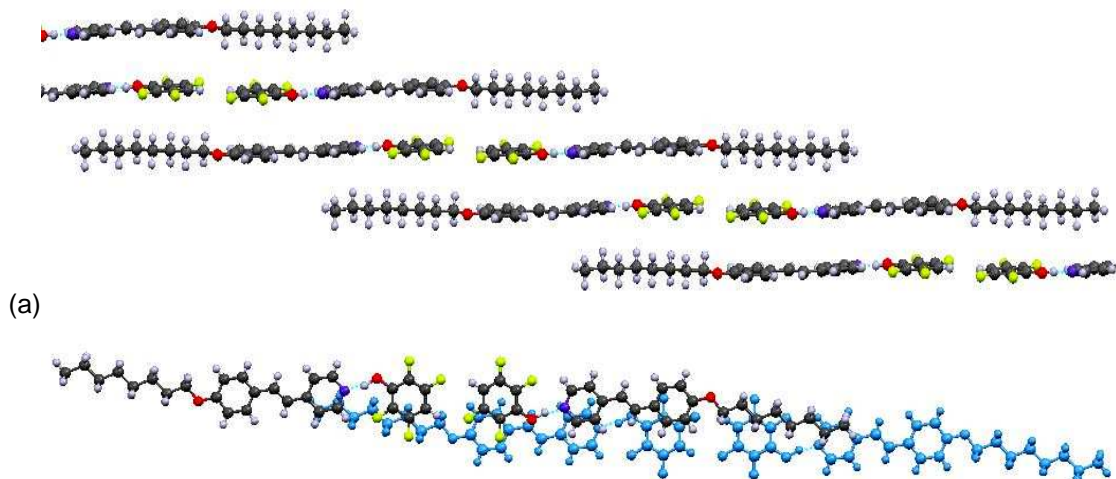
Figure 3.4: (a) Slipped ladder stacking of layers of **2-7**. Only one dimerized pair is shown per layer for clarity. (b) Stacking of two dimers, the dimer in blue is below the other dimer in the figure. The aromatic rings in the dimer only slightly overlap with each other in stacking up into layers.

3.2.1.2   Complex 2-6b

The crystal structure of **2-6b** (Figure 3.5) reveals complex molecules very similar to those of **2-7**. The newly extended molecule is very nearly planar (refer to Figure 3.7(a)) with the angle between planes of the two aromatic rings in the stilbazole unit being only 3.05°. The fluorophenol ring is also a mere 1.75° out of plane with the pyridine ring. The hydrogen bond length, $d_{N \cdots H}$ is appreciably longer than that in complex **2-7**, at 1.729 Å, 65.5% of the sum of the van der Waals radii, and the N⋯H–O angle deviates even further from linearity than **2-7** at 158.01 °. There are only two intramolecular short contacts present within the complex supporting the hydrogen bond, which are between H1 and C7 (2.406 Å, 86.2% sum of vdW radii), and O1 and C7 (3.031 Å, 94.1% sum of vdW radii). These again show an unsymmetrical hydrogen-bonded interaction.
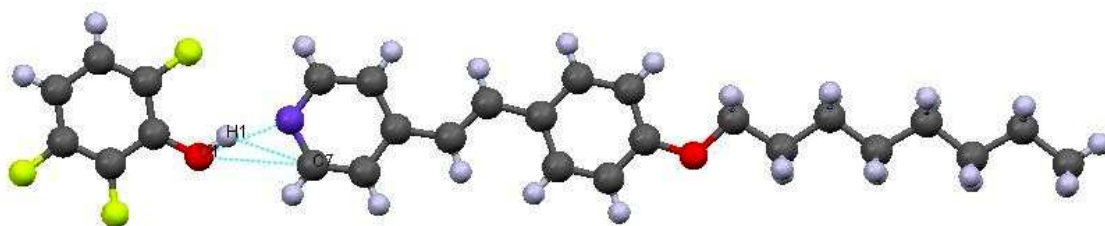
Figure 3.5: A single hydrogen-bonded molecule of **2-6b** and the intramolecular short contacts interactions.

The crystal packing of **2-6b** is essentially identical to that of **2-7** (Figures 3.6 and 3.7) with exception to the short contacts linking the molecules within a layer. As the short contacts for this discussion have been defined as less than the sum of the van der Waals radii minus 0.1 Å ($< (\sum$ vdW radii $- 0.1$ Å), there are no hydrogen-fluorine short contact interactions linking the back-to-back dimers seen in Figure 3.6. However, this motif is clearly present and, more importantly, appears to drive the structure packing. The distances between the two F2 and H4 atom pairs bridging the two complexes within the dimer are 2.597 Å, 101.4% of the sum of the vdW radii. The dimers, as shown, are interlinked between F1 and H12 (2.354 Å, 92.0% sum of vdW radii) and between H5 and O2 (2.618 Å, 100.3% sum of vdW radii) within a layer.
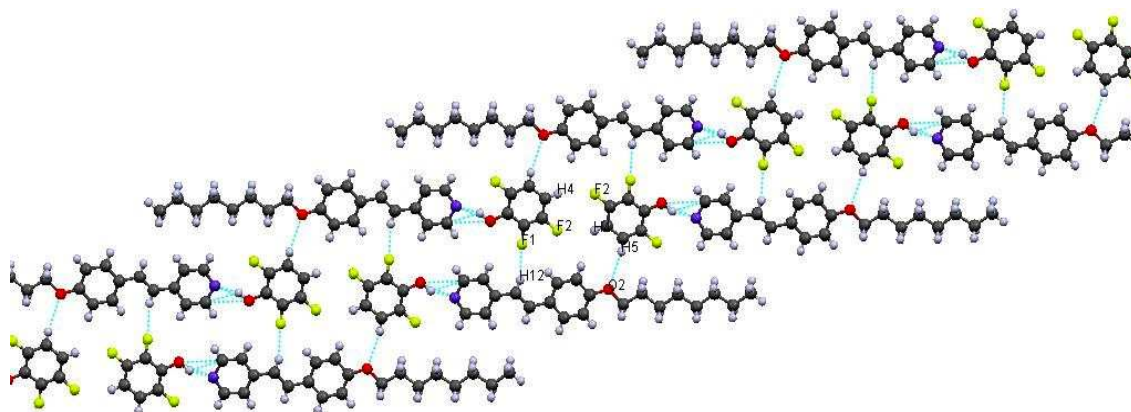
Figure 3.6: Dimers of back-to-back complex molecules line up side-by-side, linked by two O2–H5 and two F1–H12 short contact interactions to form a flat, one dimensional layer.

The other difference between this crystal structure and that previously described is that in the **2-6b** complex the ring overlap in the stacking of layers is greater, as depicted in Figure 3.7(b).

56

(a)

(b)
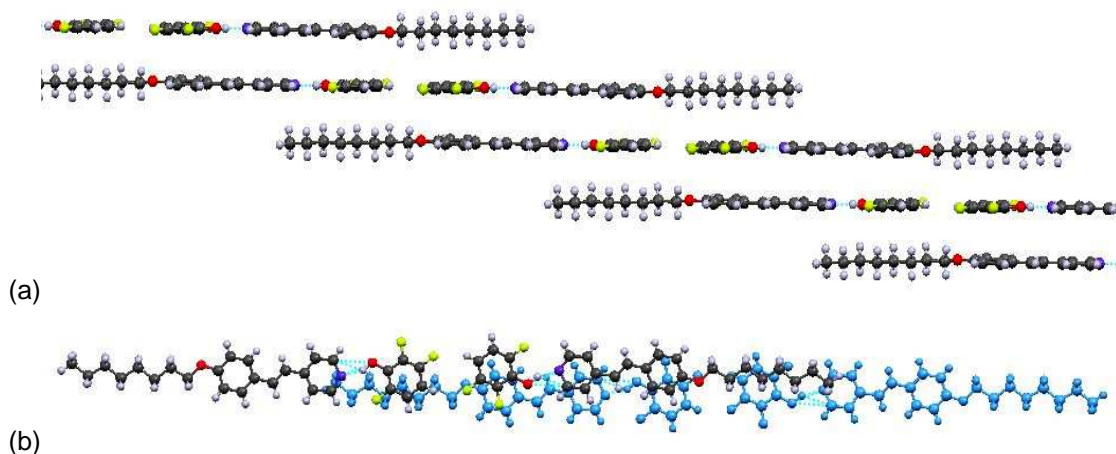
**Figure 3.7**: (a) Slipped ladder stacking of layers of **2-3b**. Only one back-to-back pair is shown per layer for clarity. (b) Stacking of two dimers, viewed along the axis of the stacking direction. The dimer in blue is below the other dimer in the figure. The aromatic rings in the dimer overlap slightly with each other in stacking up into layers.

3.2.2 Description of the Crystal Structure of Complex 2-6e

Complex **2-6e** stands alone in its crystal structure and packing with unit cell dimensions and angles that are different from the other complex single crystals obtained (Table 3.1). While still in the $P\bar{1}$ space group, the fluorophenol ring in complex **2-6e** is no longer co-planar with the stilbazole rings but is instead twisted 58.37° out of plane from the pyridine ring. In turn, the angle between the planes of the aromatic rings of the stilbazole is now increased to 9.13°. The N···H–O bond is nearly linear at an angle of 177.08°, while the hydrogen bond length here is 1.685 Å or 63.8% of the sum of the van der Waals radii value. There are two intramolecular short contacts between H1 and the two carbons on each side of the hydrogen bonded nitrogen (C7 and C11) 2.648 Å (94.9% sum of vdW radii) and 2.642 Å (94.7% sum of vdW radii) in length respectively (Figure 3.8) and now show an almost symmetric interaction.
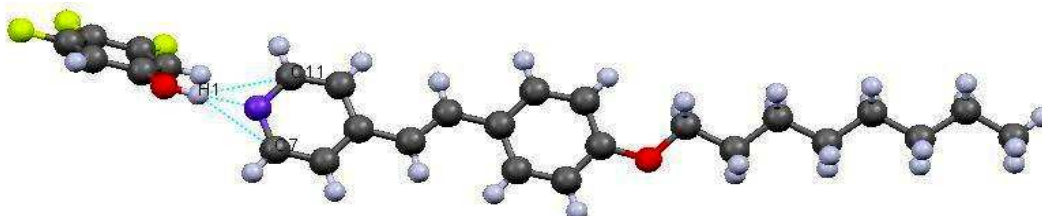
Figure 3.8: A single hydrogen-bonded molecule of **2-6e** and its intramolecular short contact interactions.

In contrast to the earlier two complexes, dimers of complex **2-6e** form through the stacking two fluorophenol rings which interact through two weak π–π short contact interactions at C1 and C3, both 3.243 Å in length and 95.4% of the sum of the vdW radii (Figure 3.9(a)). The fluorophenols are not strictly parallel but are instead slipped so that only C3 and C1 in one fluorophenol ring lies directly above C1 and C3 respectively in the lower fluorophenol ring (Figure 3.9(b)). Dimerisation is also further supported by two intermolecular F1···H11 short contacts (2.547 Å, 99.5% sum of vdW radii) between the fluorophenol and stilbazole units of two different complexes, seen in Figure 3.9(a).

(a)

(b)
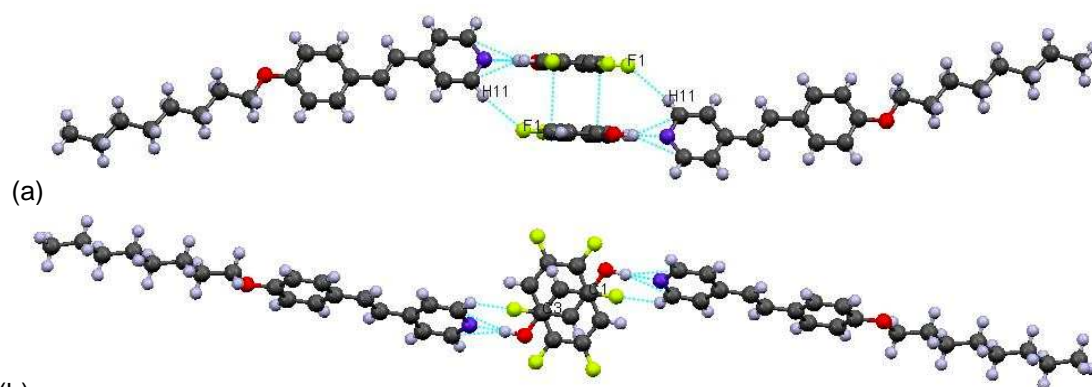
Figure 3.9: The dimer (Dimer A) formed between two **2-6e** molecules: (a) weak π–π stacking interactions of the fluorophenol rings supported by short contacts between F1 and H11; (b) the dimer in (a) is rotated 90° through the horizontal *x*-axis to show how the fluorophenol rings do not fully overlap in stacking.

The dimers then line up side-by-side in a stepped fashion to form a flat 'segment' as shown in Figure 3.10(a), with all stilbazole rings almost co-planar or flat. Two dimer pairs are linked by two short contacts between O1 and H7, 2.531 Å in length, 97.0% of the sum of the vdW radii. Two 'segments' then fit together through an interdigitation of the the stilbazole alkoxy chains (Figure 3.10(b)), while still keeping all stilbazole aromatic rings in plane. This extends the layer into an infinite sheet in the *xy*-plane.

(a)

(b)
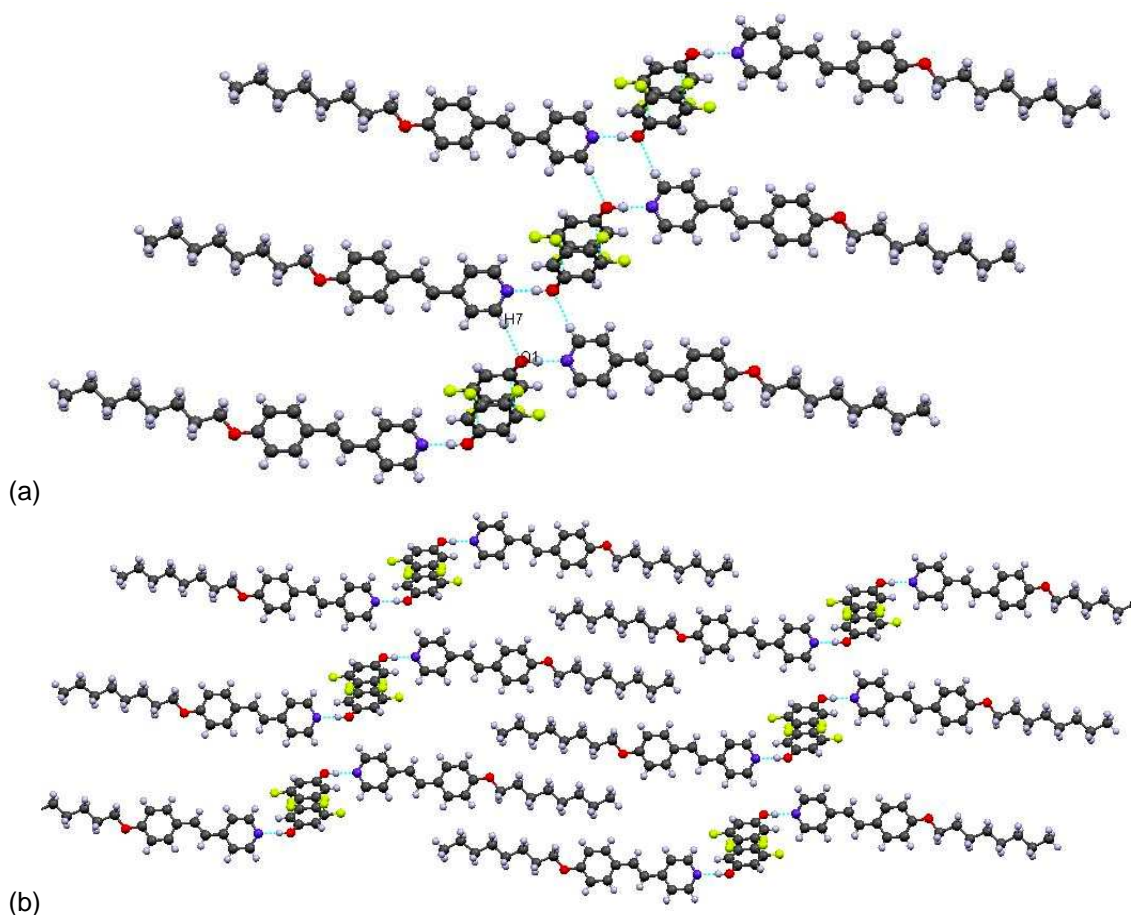
Figure 3.10: Gradual expansion of **2-6e** crystal structure within a layer. (a) A 'segment' consisting of dimers lining up in the *y*-direction. (b) Interdigitation of two 'segments' in which alkoxy chains interlock. Interdigitated complex molecules on the left and right of the figure have been omitted for clarity.

Complex **2-6e** has a second dimer pair, Dimer B, which is almost identical to its first, except that the face-to-face flourophenols are further apart (Figure 3.11(a)). The two weak π–π short contact interactions are between C28 and C30 (3.453 Å, 101.6% sum of vdW radii). There are also two F4···H34 short contacts (2.519 Å, 98.4% sum of vdW radii) supporting dimerisation. As before, the fluorophenols also overlap in a slipped manner (Figure 3.11(b)) and arrange into a sheet through interdigitation (Figure 3.10).

(a)
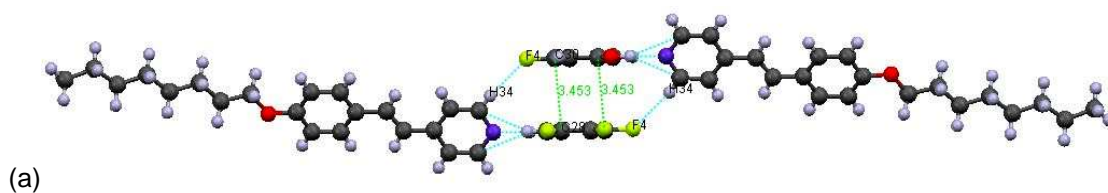
(b)

Figure 3.11: The second dimer (Dimer B) formed between two **2-6e** molecules: (a) weak π–π stacking interactions of the fluorophenol rings supported by short contacts between F4 and H34; (b) the dimer in (a) is rotated 90° through the horizontal *x*-axis to show how the fluorophenol rings do not fully overlap in stacking.

The two different sheets, made up of Dimer A and Dimer B, respectively, then stack up alternately, with the upward stacking direction cutting approximately perpendicular through the stilbazole ring planes. The two different layers interact *via* weak π–π short contacts at C14···C28 (3.342 Å, 98.3% sum of vdW radii) and C7···C41 (3.301 Å, 97.1% sum of vdW radii) as shown in Figure 3.12.
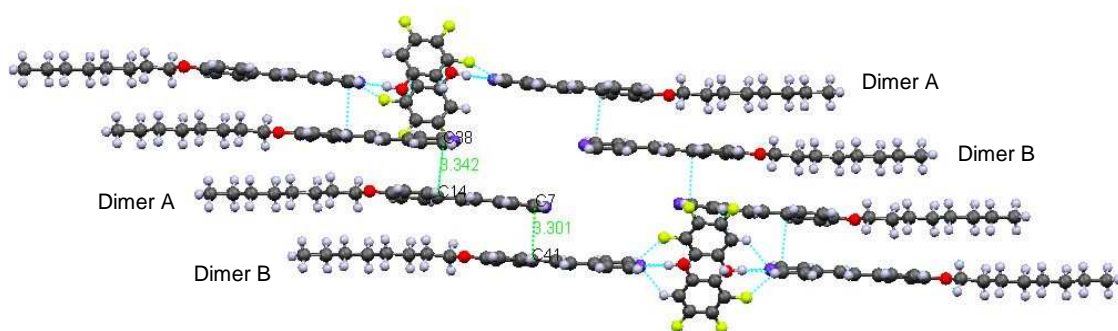
Figure 3.12: Slipped stacking of the two different sheets. Only one dimerized pair is shown per layer and some fluorophenols have been omitted for clarity.

An additional interesting feature found in the crystal packing of **2-6e** is how the dimerised fluorophenol ring pairs alternate orientation by 90° rotations along the *x*-axis in stacking, as shown in Figure 3.13.
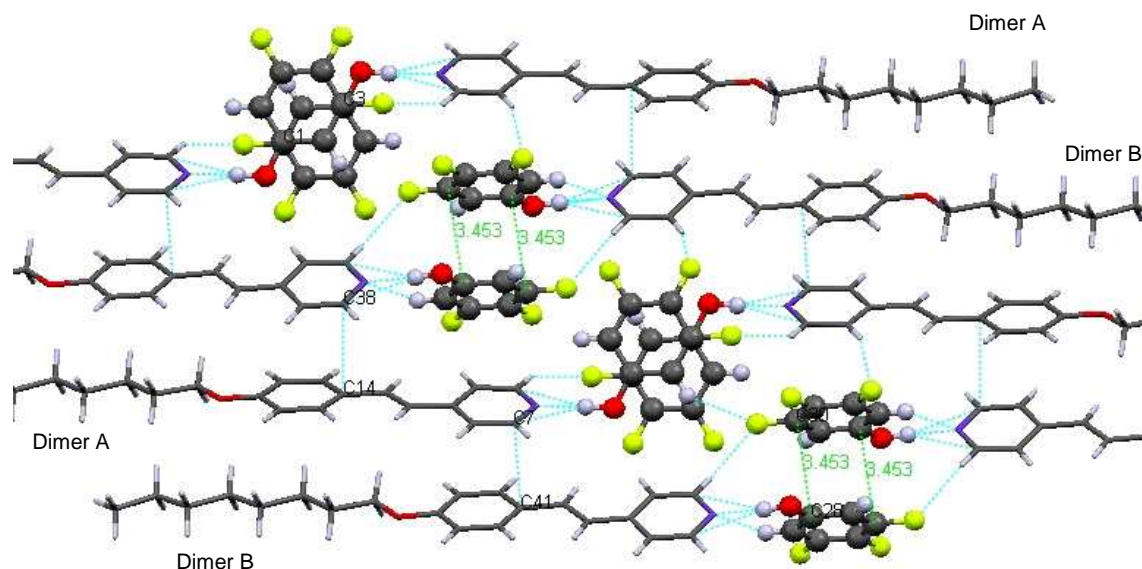
Figure 3.13: The pairing of fluorophenol rings and their alternating orientation as a function of the stacking direction along the *x*-axis.

3.2.3 Description of the Crystal Structures of Complexes 2-5a, 2-5d, 2-5f, 2-4a and 2-4b

The following crystal structures make up the largest group which share comparable unit cell dimensions and angles (Table 3.1), as well as in terms of molecule and dimer structure and crystal packing. All five complexes crystallised in the $P\bar{1}$ space group.

3.2.3.1 Complex 2-5a

The hydrogen bond is 1.667 Å long, 63.1% of the sum of the VdW radii, while the N···H–O angle is again close to linear at 173.20°. The fluorophenol ring is twisted out of the plane of the pyridine ring by 65.41°, while the angle between the aromatic planes of the stilbazole moiety is 16.11°; both such angles are ranked the largest among all the crystal structures obtained. The ligands are further linked by close contacts between H1 and two carbons (C7 and C11) on the pyridine ring, 2.580 Å (92.5% sum of vdW radii) and 2.673 Å (95.8% sum of vdW radii) in length respectively (Figure 3.14).

61
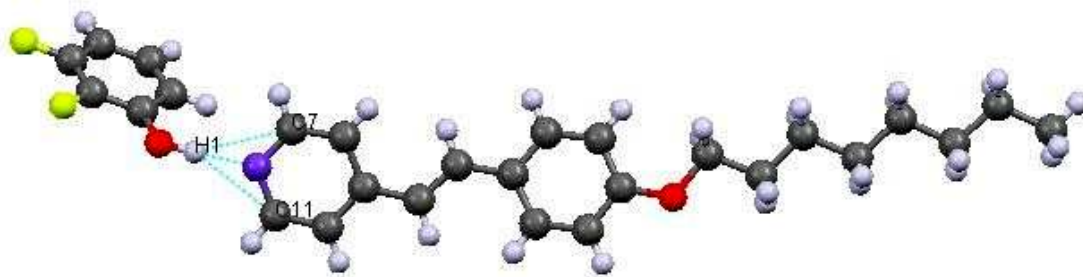
Figure 3.14: A single hydrogen-bonded molecule of **2-5a** and its intramolecular short contact interactions.

Dimers of this complex formed with a back-to-back, antiparallel motif supported by two F1A⋯F2A close contacts (2.833 Å, 96.4% sum of vdW radii) between the fluorophenols as seen in Figure 3.15(a). There is also a F2A⋯F2A short contact interaction, not seen due to the short contact definition adopted, which is 2.929 Å in length and 99.6% of the sum of the vdW radii, not shown in Figure 3.15. Within the dimer, the fluorophenols do not occupy the same plane but are instead stacked in a stepped fashion without overlapping. This gives the overall dimer a stepped motif, depicted in Figure 3.15(b).

(a)

(b)
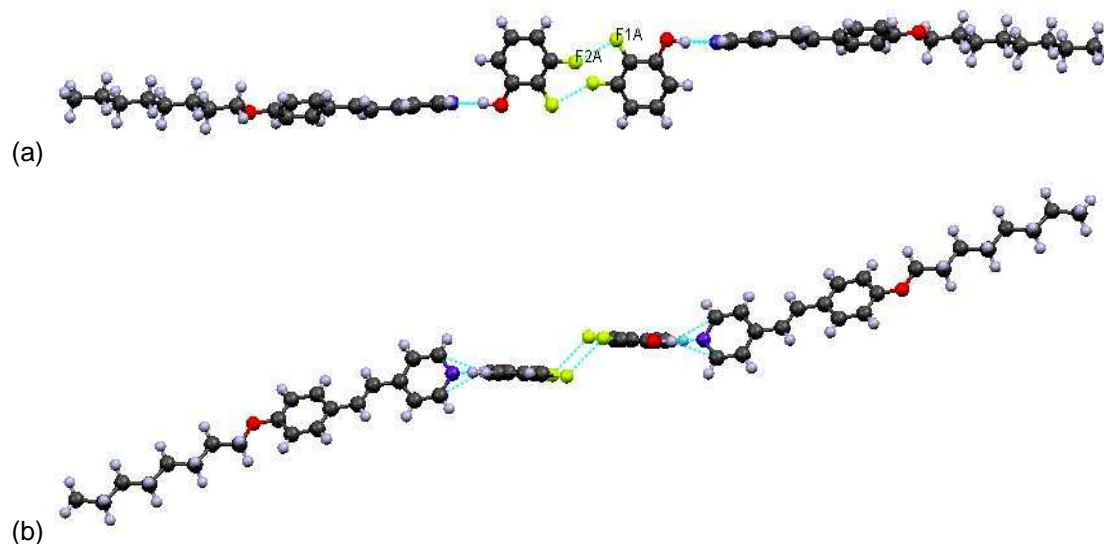
Figure 3.15: A dimer of complex **2-5a**. (a) The fluorophenol rings are back-to-back and there are two F1A–F2A short contacts interactions supporting dimerization. The stilbazoles are stepped-stacked within the dimer. (b) Another view of the same dimer to show its stepped motif.

The dimers then arrange into a slipped layer or sheet as shown in Figure 3.16, with two H18···H26B short contacts (2.198 Å, 100.8% sum of vdW) between aromatic and alkoxy protons linking antiparallel and interdigitated molecules into chains.
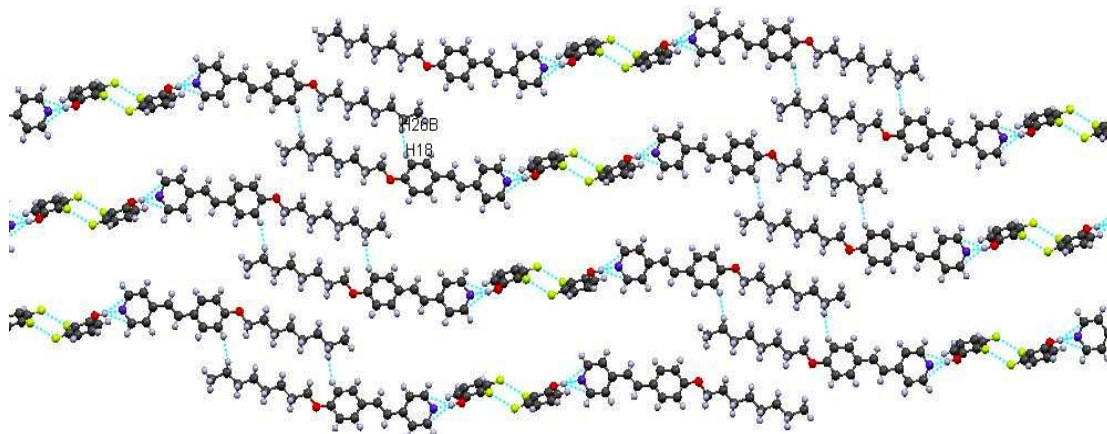
Figure 3.16: The dimer pairs arranged into an interdigitated layer.

In stacking (Figure 3.17(a)), the stepped dimers interact *via* two weak π–π short contact interactions at C9···C11 (3.276 Å, 96.4% sum of vdW radii). The stacked dimers are slipped and do not completely overlap as seen in Figure 3.17(b).

(a)

(b)
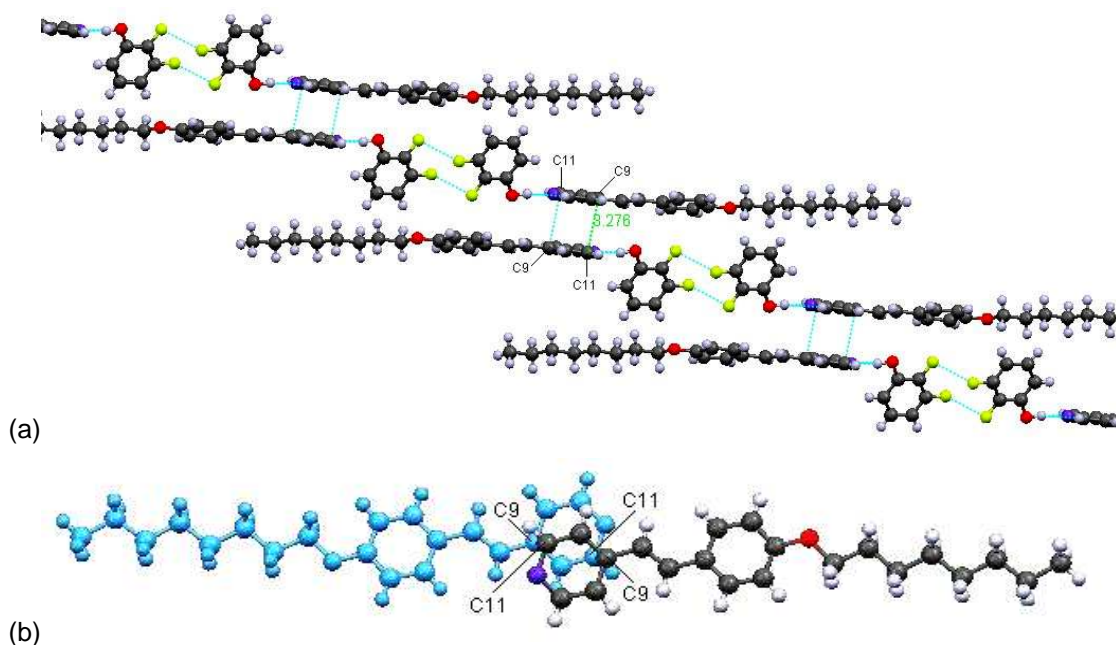
Figure 3.17: (a) The stacking of four dimer-pairs in the direction perpendicular to the stilbazole aromatic rings. (b) Top view of the stilbazole stacking shows how the pyridine rings do not strictly overlap. The stilbazole in blue is the bottom molecule in stacking.

3.2.3.2 Complex 2-5d

The crystal structure of **2-5d** shows the hydrogen bond length to be 1.580 Å (59.8% sum of vdW radii), while the N···H–O angle was found to be slightly bent at 167.99°. The angle between the planes of the pyridine and fluorophenol rings was 64.81°, while the two stilbazole aromatic rings made an angle of 13.29°. Four intramolecular short contacts were present in the complex between H1···C7 (2.627 Å, 94.2% sum of vdW radii), H1···C11 (2.476 Å, 88.7% sum of vdW radii), F1···N1 (2.895 Å, 95.9% sum of vdW radii) and F1···C11 (3.023 Å, 95.4% sum of vdW radii), as found in Figure 3.18.
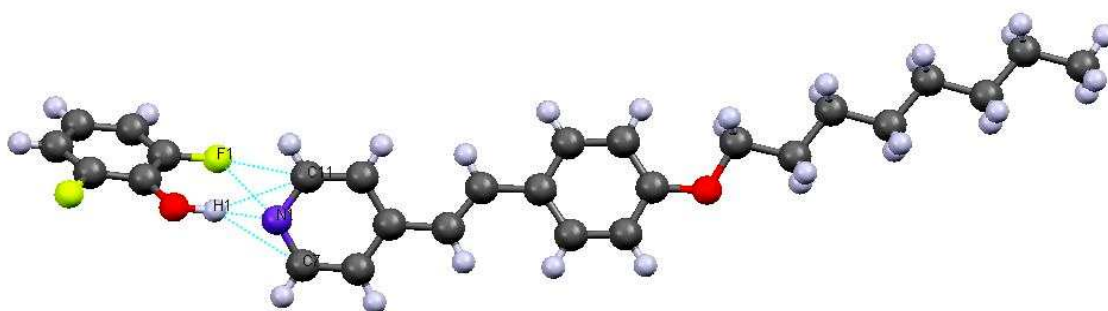
Figure 3.18: The hydrogen bonded complex of **2-5d** and the intramolecular close contacts present.

The dimer of complex **2-5d** bears much resemblance to that of **2-5a**, being antiparallel and back-to-back. The fluorophenols in the dimer interact *via* two H5···F2 short contacts which are greater than the sum of the vdW radii in length (2.627 Å, 102.6% sum of vdW radii). The dimer also takes on the same stepped character as the dimer in **2-5a** (refer to Figure 3.15(b)), shown here in Figure 3.19.

(a)
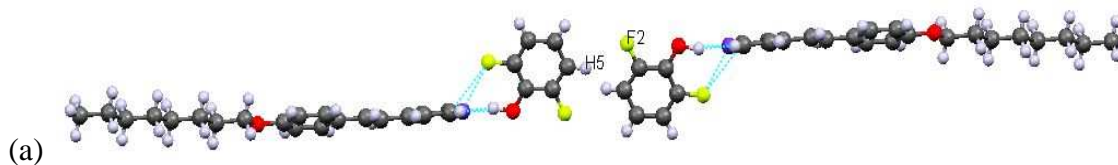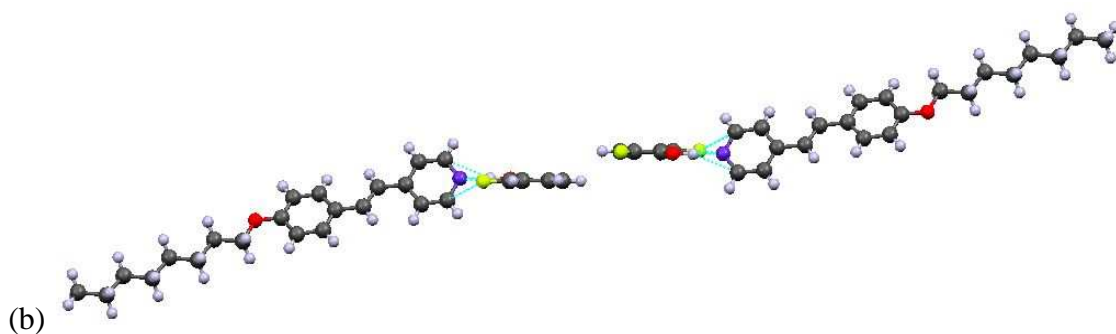
(b)

Figure 3.19: (a) The antiparallel, back-to-back dimer of the complex **2-5d**, connected by two F1 – H5 short contacts greater than the sum of the vdW radii. (b) The dimer takes on the same stepped shape as the dimer of **2-5a**.

Likewise, the crystal packing of **2-5d** is analogous to **2-5a**. The H18⋯H26B short contacts (2.264 Å, 103.9% of the sum of the vdW radii) link up the molecules into chains which then go on to arrange as an interdigitated, antiparallel sheet depicted in Figure 3.20.
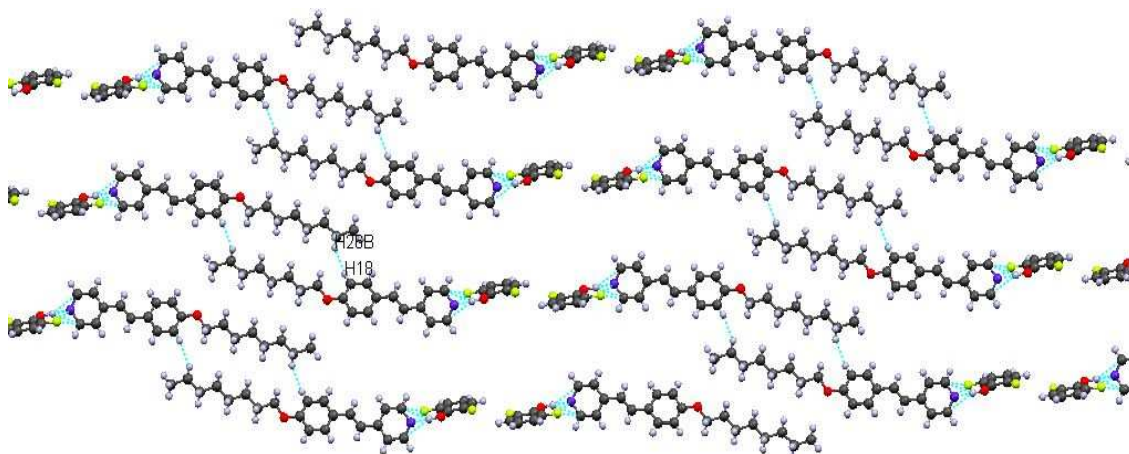
Figure 3.20: Expansion of the complex into a one dimensional sheet linked by H18⋯H26B short contacts.

The sheets also layer on top of each other in a stepped stacking, and in which the pyridine rings of two stilbazole units overlap in an antiparallel manner. These rings interact *via* two short contacts between C7 and C9 (3.278 Å, 96.4% sum of vdW radii), represented in Figure 3.21. The overlap of the stilbazole units in stacking is analogous to that in **2-5a**, as seen in Figure 3.17(b). Additionally, there is a H4⋯O2 short contact interaction, 2.612 Å in length and 100.1% of the sum of the vdW radii, which occurs between a fluorophenol in one dimer and a stilbazole in the dimer below.

65
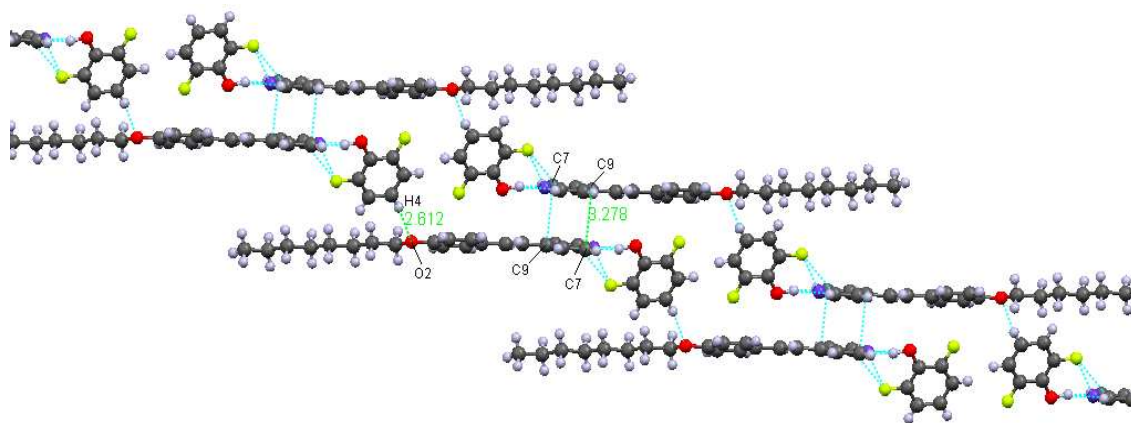
Figure 3.21: Stacking of **2-5d** complex in the crystal structure with the layers linked by C7···C9 short contacts. The fluorophenol units have been omitted for clarity.

3.2.3.3 Complex 2-5f

The hydrogen bond between H1 and N1 is 1.707 Å in length and 64.7% of the sum of the vdW radii value, while $\theta_{N \cdots H-O}$ is almost linear at 176.82° (Figure 3.22). The fluorophenol is twisted out of the pyridine plane by 62.76° while the aromatic rings in the stilbazole are reasonably co-planar with 15.46° between the two planes. The short contacts supporting complexation are between H1···C11 (2.687 Å, 96.3% sum of vdW radii), H1···C7 (2.637 Å, 94.5% sum of vdW radii) and H2···N1 (2.639 Å, 100.0% sum of vdW radii).
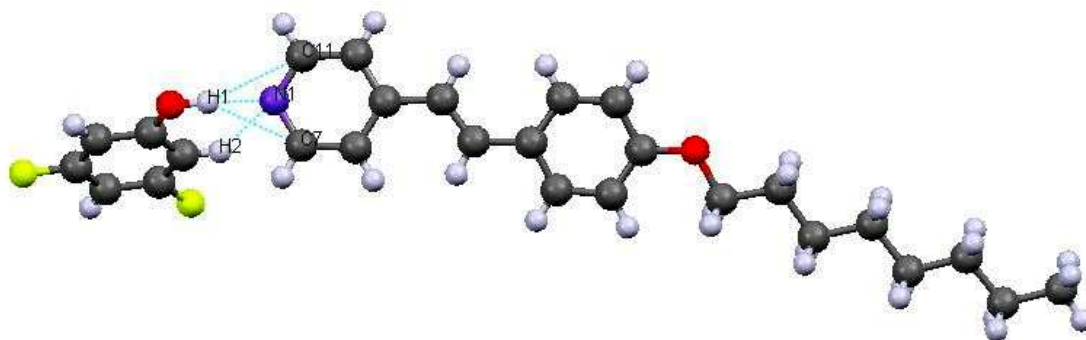
Figure 3.22: A single hydrogen bonded molecule of complex **2-5f** and its intramolecular short contacts.

Like the **2-5a** and **2-5d** complexes, dimers are formed between two **2-5f** molecules arranging back-to-back and joined by an F2···F2 interaction (2.938 Å, 99.9% sum of vdW radii), seen in Figure 3.23. The F2···H6 distance at 2.619 Å is greater than the sum

of the van der Waals radii. Also akin to the **2-5a** complex, the dimer adopts a stepped structure (refer to Figure 3.15(b)).
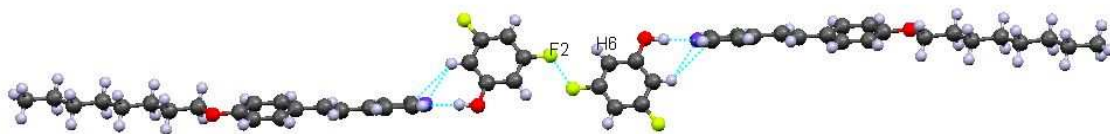
Figure 3.23: A back-to-back dimer formed between two molecules of **2-5f** linked by a F2···F2 interaction.

The familiar sheet or layer is formed from the expansion of the complex molecules in the *xy*-plane as shown in Figure 3.24. The complex molecules are linked into chains by interactions between interdigitated stilbazoles at the ring and alkoxy protons (H18···H26B, 2.185 Å, 100.2% sum of vdW radii).
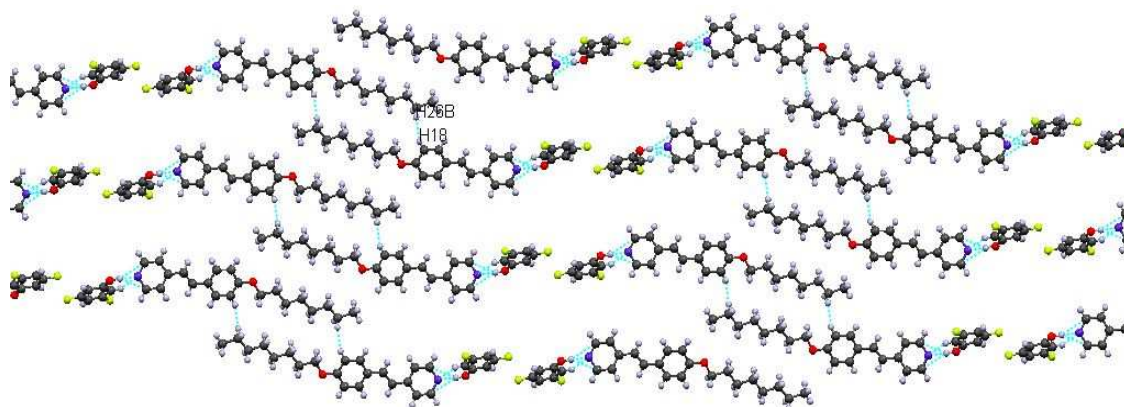
Figure 3.24: Expansion of the complex into a one-dimensional sheet linked by H18···H26B short contacts.

Once again, the complex packs into stepped layers of the dimers. The layers interconnect through two weak π–π C9···C11 short contacts (3.277 Å, 96.4% sum of vdW radii) where two pyridine rings overlap in an antiparallel fashion as well as between H4 and O2 (2.662 Å, 102.0% sum of vdW radii), seen in Figure 3.25. The pyridine overlap is again analogous to that seen in Figure 3.17(b).
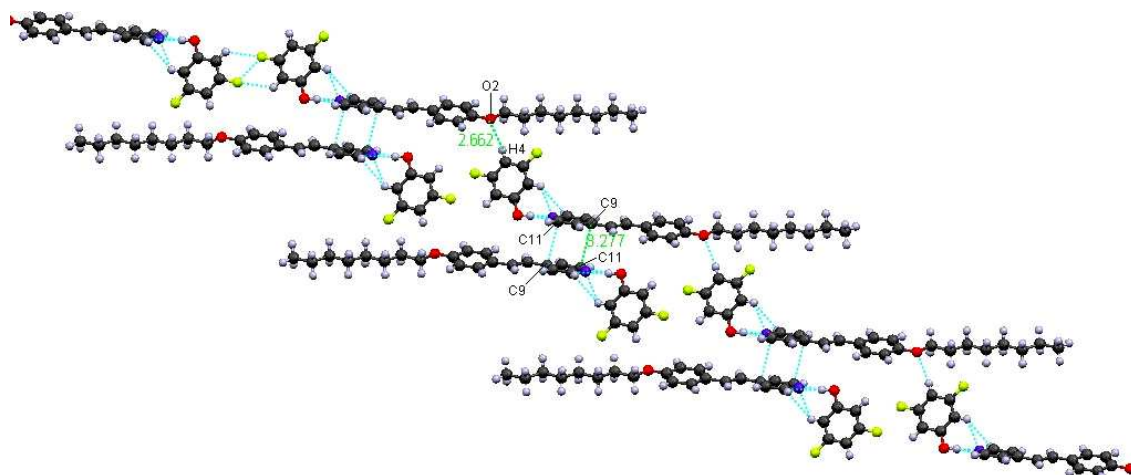
Figure 3.25: Stacking of **2-2f** complex in crystal structure. Layers are linked by π–π short contacts. Only one antiparallel dimer pair is shown per layer for clarity. For the overlapping of the pyridine rings, refer to Figure 2.22(b).

3.2.3.4 Complex 2-4a

The 4-octyloxy-4'-stilbazole and 2-fluorophenol ligands complex through a H1–N1 hydrogen bond 1.714Å long (64.9 % of the sum of VdW radii), which is supported by two other short contacts between H1···C7 (2.702 Å, 96.8% sum of vdW radii) and H1···C11 (2.635 Å, 94.4% sum of vdW radii). The N···H–O angle is very nearly linear at 175.86°, and the two stilbazole aromatic rings are almost co-planar with an angle of 14.69° between the two planes. The fluorophenol ring is however non co-planar with the stilbazole, being twisted 64.40° out of the plane of the pyridine ring (Figure 3.26).
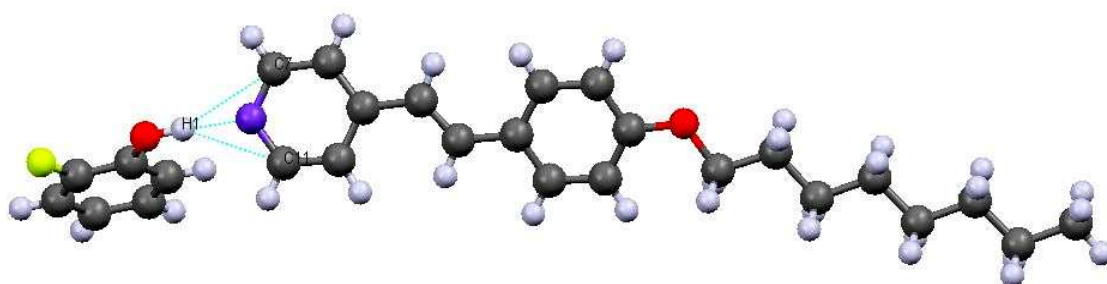
Figure 3.26: Crystal structure of a single molecule of the complex **2-4a**. The hydrogen bond is supported by two short contacts, H1···C7 and H1···C11.

The primary building block in the crystal structure of **2-4a** is the familiar antiparallel dimer (Figure 3.27) formed with the fluorophenol moieties positioned back-to-back, and connected by two F1···H3 short contacts (2.549 Å, 99.6% sum of vdW radii). Once

again the dimer adopts a stepped structure identical to those described before (refer to dimer of **2-5d**).

Figure 3.27: The familiar back-to-back, antiparallel dimer motif made up of two **2-4a** complexes.

The dimers go on to link in to the customary chains through short contact interactions between H18···H26B (2.202 Å, 101.0% sum of vdW radii), which in turn arrange into the same sheet or layer seen previously (refer to Figure 2.36). The sheet of back-to-back dimers stack up into slipped layers, just like those described before. Interactions between layers are only through two weak π–π short contacts at C7···C9 (3.272 Å, 96.2% sum of vdW radii), pictured in Figure 3.28 below.
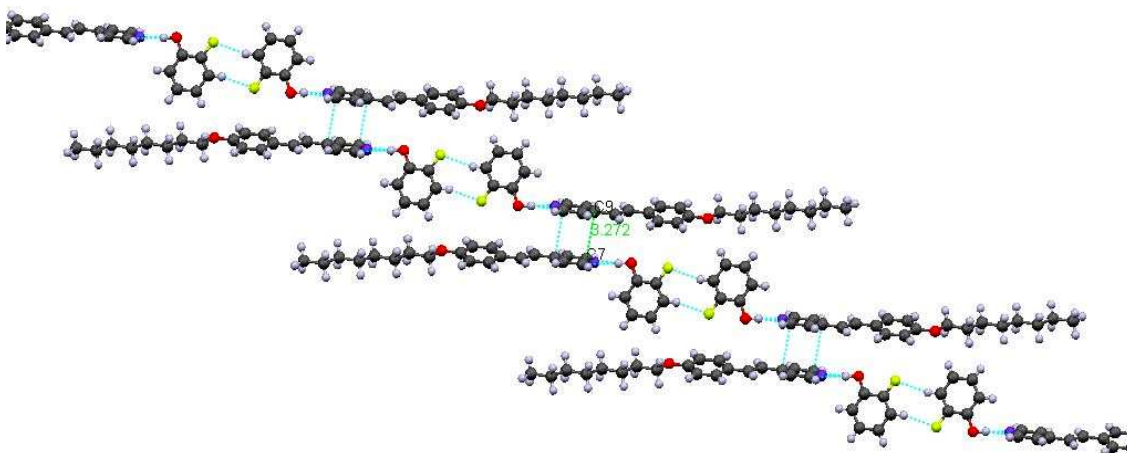
Figure 3.28: The sheets of back-to-back dimers stack up into slipped layers. Interactions between layers occur at C7···C9.

3.2.3.5   Complex 2-4b

The molecules of complex **2-4b** has a hydrogen bond that is 1.716 Å long (65.0% sum of VdW radii) backed by close contacts between H1 and the carbon atoms adjacent to the pyridine nitrogen atom (C7 and C11), as seen in Figure 3.29. The hydrogen bond forms as an almost linear extension of the alcohol O–H bond, with the angle between the two bonds, $\theta_{N···H–O}$, being 175.53°. There is a difference of 63.31° and 14.58°

69

between the planes of the fluorophenol and pyridine rings, and the two stilbazole rings, respectively.

Figure 3.29: A single hydrogen bonded molecule of the **2-4b** complex supported by short contacts between H1⋯C7 (2.632 Å, 94.3% sum of vdW radii) and H1⋯C11 (2.708 Å, 97.1% sum of vdW radii).

The antiparallel, back-to-back dimers of the complex (Figure 3.30) are connected by a short contact interaction between two fluorine atoms (F1⋯F1, 2.903 Å, 98.7% sum of vdW radii), and two F1⋯H2 contacts (2.614 Å, 102.1% sum of vdW radii) of the variety of greater length than the sum of the vdW radii.

Figure 3.30: Stepped, back-to-back dimer of complex **2-4b**.

In common with the rest of the complexes in this packing type, the **2-4b** back-to-back dimer duly arranges into a sheet of interdigitated complexes (refer to Figure 3.24). The stilbazole units of the dimers interacted *via* H18⋯H26B short contacts (2.212 Å, 101.5% sum of vdW radii) connecting them into chains. The stacking of the dimer layers also conformed to that previously seen, forming a stepped stack-up in which two dimers were connected by a partial overlap of antiparallel pyridine rings (refer to Figure 3.25). The two short contacts present were weak C7⋯C11 π–π interactions, 3.273 Å long and 96.3% of the sum of the vdW radii value.

3.2.4   Description of the Crystal Structure of Complex 2-4c

Complex **2-4c** was unique among those studied in crystallising in the Pbca space group and in its large unit cell dimensions. The two components of the **2-4c** complex are bound through a hydrogen bond, which was 1.828 Å (69.2 % sum of vdW radii) in length. There was also a single intramolecular interaction between the same hydrogen, H1, and C7 (2.593 Å, 92.9 % sum of vdW radii) in the stilbazole, as shown in Figure 3.31, showing the interaction to be unsymmetric. The N···H–O angle is slightly bent at 169.59°, while the aromatic rings in the stilbazole are nearly co-planar with an angle of 7.50° between their planes. On the other hand, the fluorophenol ring is twisted by 23.17° out of the plane of the pyridine ring.
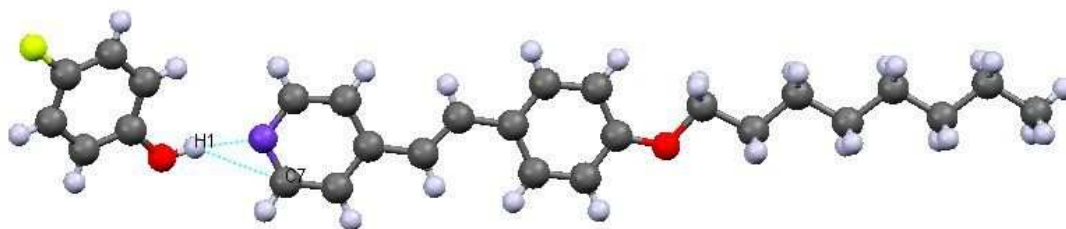
Figure 3.31: A single hydrogen-bonded complex molecule of **2-1c** and its intramolecular short contact interaction.

The crystal packing of the **2-4c** complex is made up of a repeating unit which comprises four different layers stacked upon each other. These repeating units then layer upon each other in turn. The next section looks at this repeating unit of four layers in detail.

The first layer forms from the complexes arranging into chains that zig-zag and are linked between the fluorophenol of one complex to the end of the alkoxy chain on the stilbazole in another (F1···H27B, 2.599 Å, 101.5% sum of vdW radii). The chains then align side-by-side, extending into a layer in the crystallographic *bc*-plane (Figure 3.32(a)). A C18···H20A close contact interaction (2.790 Å, 100.0% sum of vdW radii) interlinks the chains (Figure 3.32(a)). The stilbazoles propagate within the layer (along the *b*-axis) making an angle of 29.73° with the layer plane (Figure 3.32(b)), while the fluorophenol moiety angles at 24.23° to the layer plane.

(a)

(b)
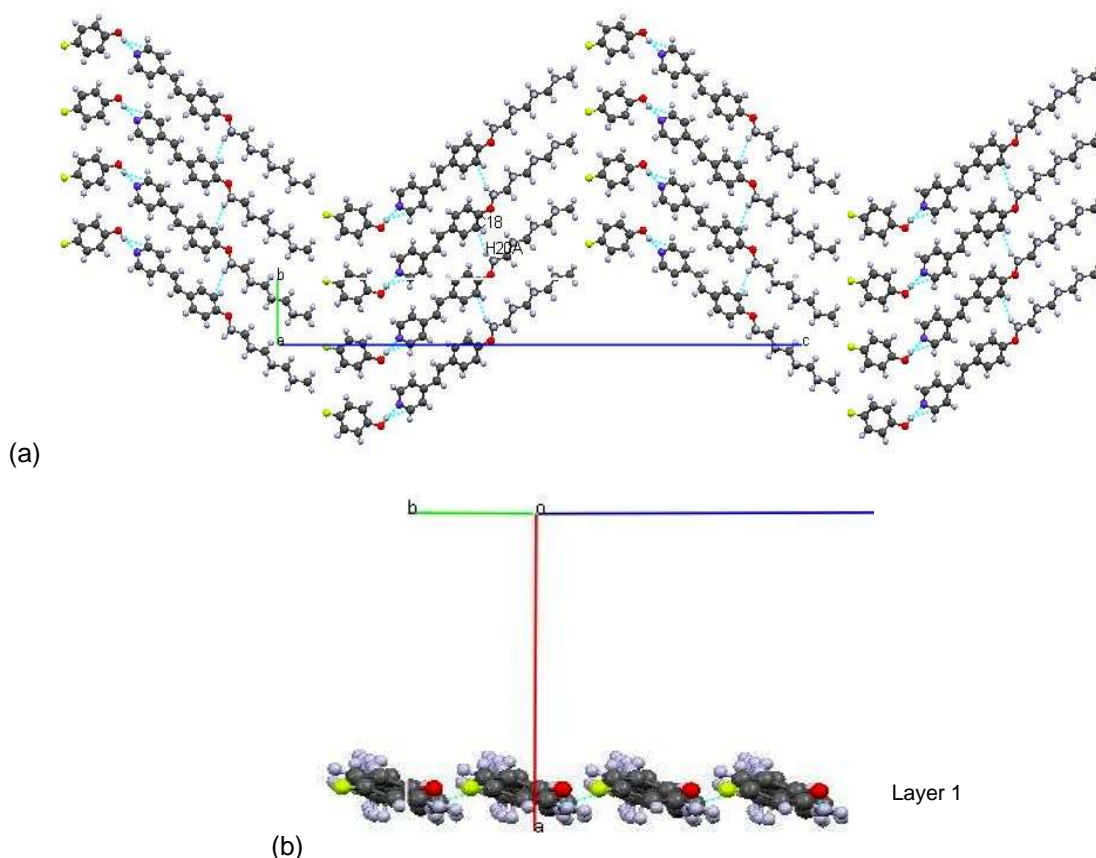
Layer 1

Figure 3.32: Packing of the complex into a sheet: (a) the view along the crystallographic *a*-axis gives an aerial view of the layer; the infinite sheet lies in the *bc*-plane and is made up of zig-zag chains connected by C18···H20A short contacts. (b) Looking down the molecule length the molecules are tilted with respect to the layer plane.

A second sheet similar to that described above, stacks above the first layer so that fluorophenol and stilbazole units line up and the zig-zag pattern is preserved (Figure 3.33(a)). The two layers interact *via* H···π short contacts between C13 and H15 (2.670 Å, 95.7% sum of vdW radii) which can be seen when viewed from Q (refer to Figure 3.33(a)). This view at Q is shown in Figure 3.33(b). The view at P in Figure 3.33(c) shows how the molecules angle or tilt in the opposite direction to the plane when compared to the lower layer. Also shown is the alternated spacing of the molecules, which means a complex in the second layer lies above the space in between two complexes in the first layer.

(a)

Q:

(b)

P:

(c)
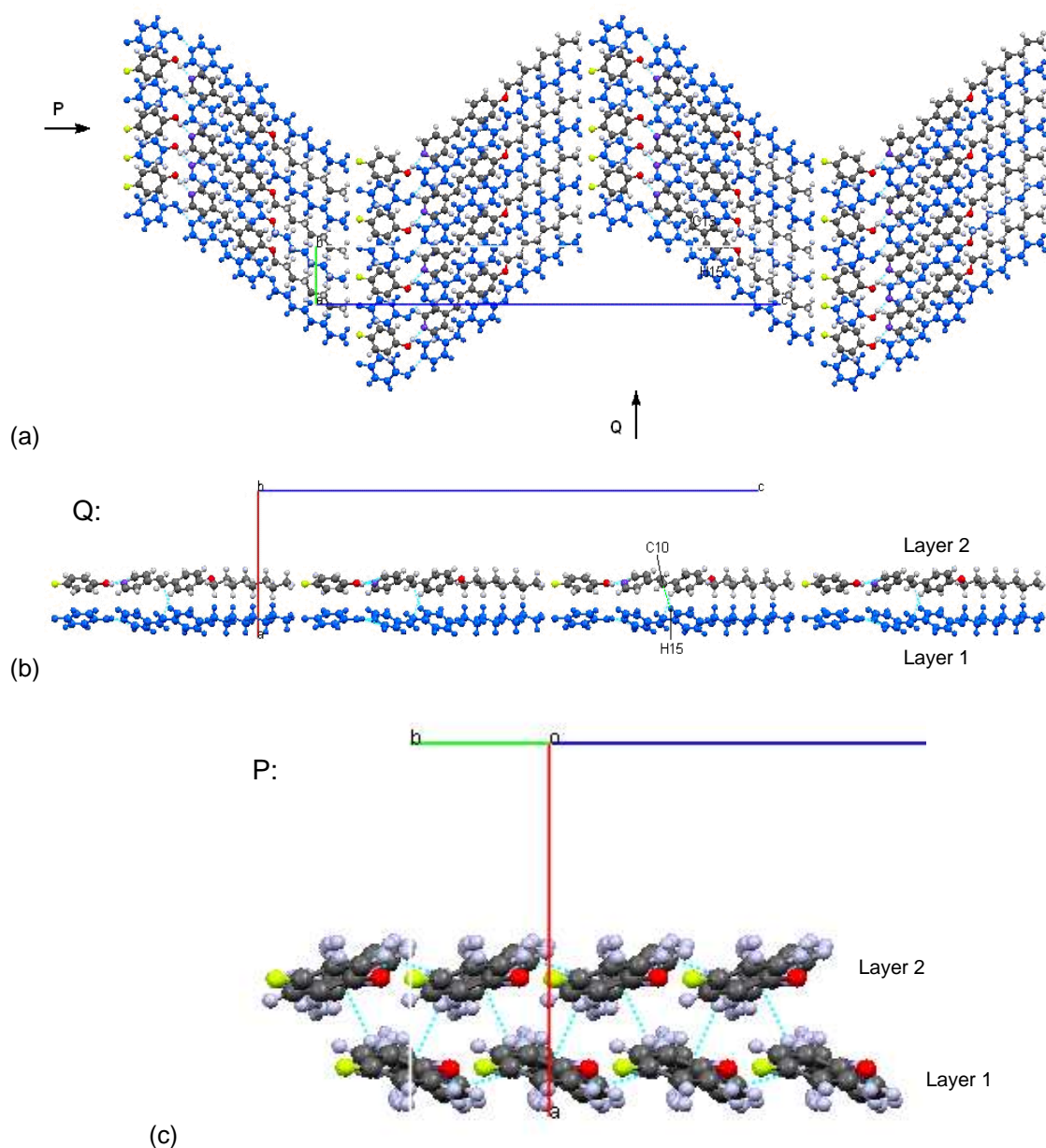
Figure 3.33: Stacking of the second layer. (a) The two stacked sheets viewed from above. The molecules in the new layer lie above the blue molecules of Layer 1, preserving the zig-zag pattern. (b) View from Q: the stilbazole and fluorophenol units stack above each other; the first layer is in blue for clarity. (c) View from P: the view down the molecular length shows the opposite direction angling of the molecules in different layers and how they are spaced alternately.

The next two layers which stack up above the first two described are slipped, causing the zig-zag pattern to be lost between layers (Figure 3.34(a) and (b)). The complexes in layers 3 and 4 are also antiparallel to those in layers 1 and 2, as seen in Figure 3.34(b). Figure 3.34(c) depicts how the tilt of the complexes is different in each layer as well as the C18···H20A short contacts present within a layer and the C13···H15 interactions between layers.

(a)

(b)

(b)
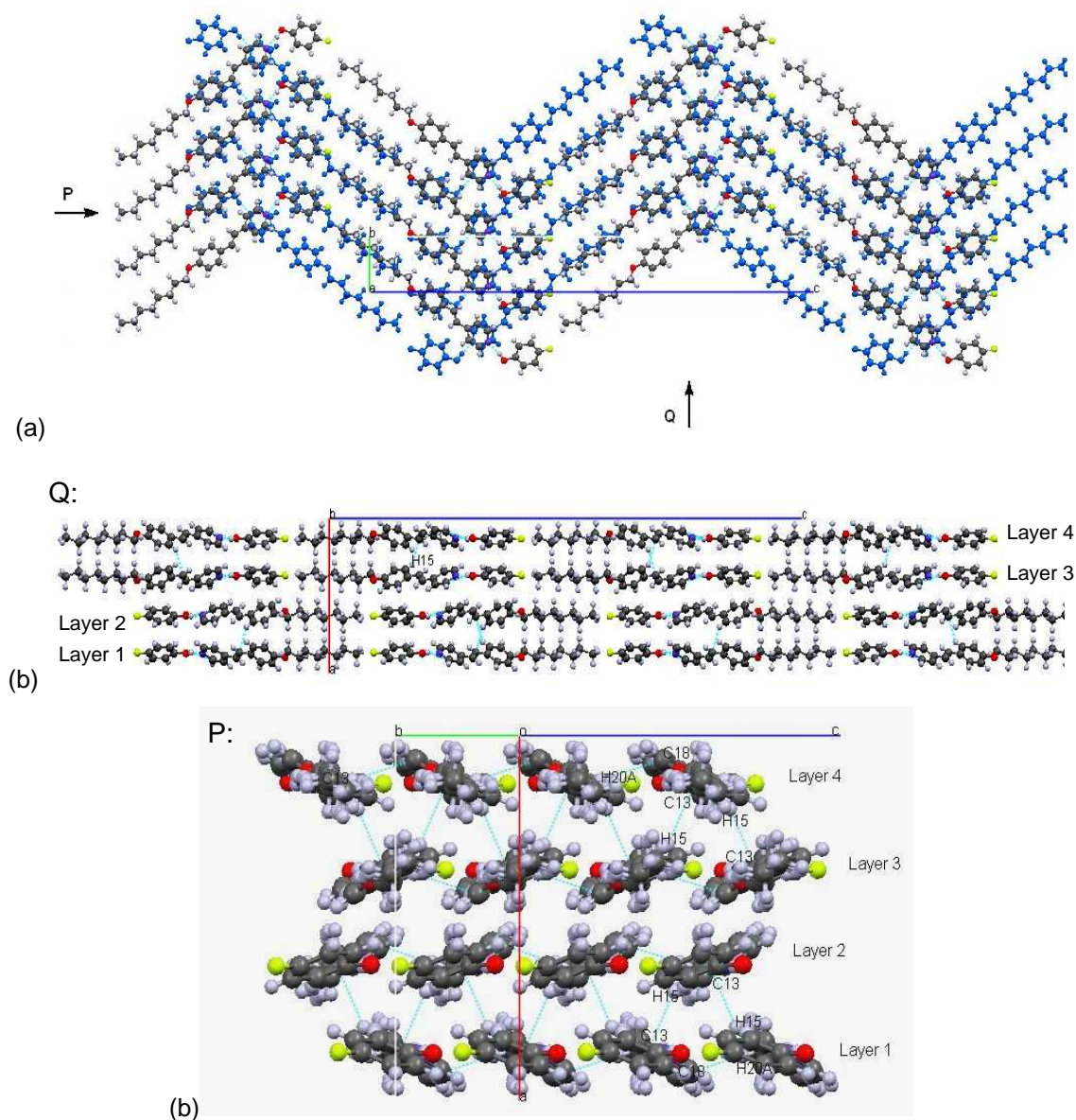
Figure 3.34: The four layers in the repeating unit. (a) Layer 3 slip stacks above layer 1 (in blue) resulting in a loss of the zig-zagged pattern. (b) View from Q, down the crystallographic *b-axis*: the complexes in layer 3 and 4 are antiparallel to those in layer 1 and 2. (c) A view of the packing of the molecules in the crystal structure down the molecular length showing the different complex tilts within each layer. The layers are interconnected *via* H···π C13···H15 short contacts.

Table 3.2 summarises the key crystallographic properties of the complexes which have been highlighted above.

Table 3.2: Selected properties of the complexes.

	2-7	2-6b	2-6e	2-4c
F-substitution	2,3,5,6-	2,3,6-	3,4,5-	4-
Fluorophenol pK_a	5.91	6.49	8.60	9.89
d(N⋯H)/Å	1.507	1.729	1.685	1.828
$\theta_{N⋯H⋯O}$/°	165.11	158.01	177.08	169.59
Space group	P$\overline{1}$	P$\overline{1}$	P$\overline{1}$	Pbca
Short contacts	H⋯F F⋯H (intra) F⋯C (intra) H⋯C (intra)	H⋯F O⋯H O⋯C (intra) H⋯C (intra)	H⋯F π⋯π O⋯H H⋯C (intra)	H⋯C (intra) H⋯F H⋯C

	2-5a	2-5d	2-5f	2-4a	2-4b
F-substitution	2,3-	2,6-	3,5-	2-	3-
Fluorophenol pK_a	8.65	7.07	8.66	8.73	9.29
d(N⋯H)/Å	1.667	1.580	1.707	1.714	1.716
$\theta_{N⋯H⋯O}$/°	173.20	167.99	176.82	175.86	175.53
Space group	P$\overline{1}$	P$\overline{1}$	P$\overline{1}$	P$\overline{1}$	P$\overline{1}$
Short contacts	F⋯F π⋯π H⋯C (intra) H⋯H	H⋯F F⋯C (intra) F⋯N (intra) H⋯C (intra) π⋯π H⋯H	H⋯F F⋯F H⋯C (intra) H⋯N (intra) π⋯π H⋯H	H⋯F H⋯C (intra) π⋯π H⋯H	H⋯F F⋯F H⋯C (intra) π⋯π H⋯H

3.3   Discussion

As fluorine is very electronegative, fluoro substituents on phenol withdraw electron density from the ring and so stabilise the conjugate base of the phenol (Figure 3.35).[4]
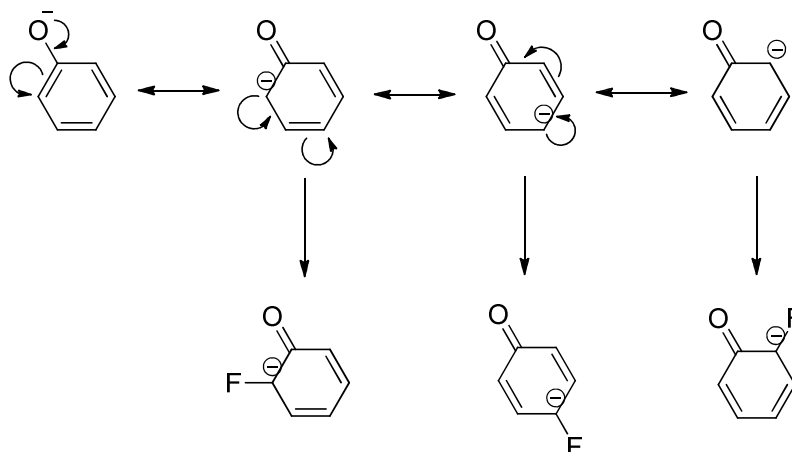
Figure 3.35: An electronegative fluoro substituent stabilises the conjugate base of phenol when located *ortho-* or *para-* to the oxygen by reducing the negative charge.

A more stable phenoxide ion drives the proton dissociation equilibrium in Figure 3.36 to the right, making for a stronger acid (measured by its pK_a value).[5]
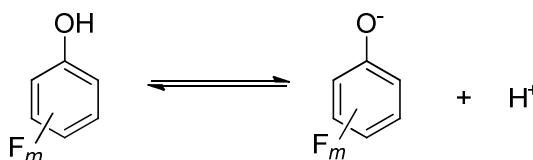
Figure 3.36: Acid dissociation equilibrium of the fluorophenol

More acidic protons can interact more strongly with the pyridine lone pair on the stilbazole, leading to a shorter hydrogen bond. As such, a correlation would be expected between the hydrogen bond length and the pK_a of the phenol. To study this effect, a plot of the N···H distance against the calculated pK_a values of the fluorophenols used was made (Figure 3.37). The calculated pK_a values were obtained by Han and Tao,[6] which also included experimental pK_a values for the fluorophenols. However, as the data for the calculated pK_a values formed a more complete set and as not all experimental pK_a values were available, the calculated pK_a values were chosen over the experimental ones to be used in this comparison (Table 3.2).[7]
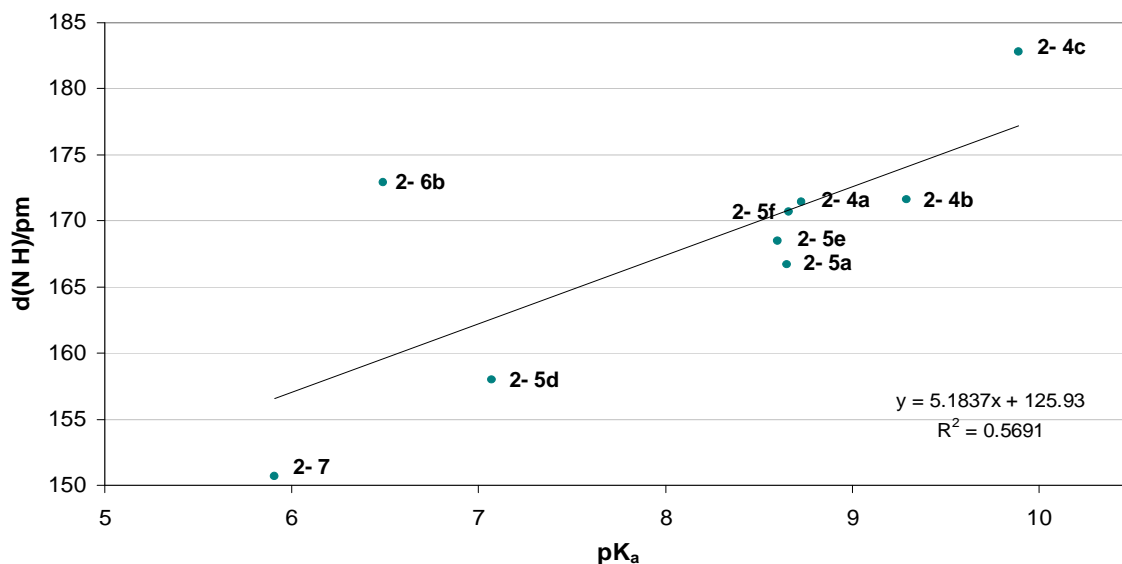
Figure 3.37: Plot of the N⋯H distance against the calculated pK_a value of the related fluorophenol in the hydrogen bonded complex.

The plot did not give the hydrogen bond distance to pK_a relation expected, as evident by the linear regression R-squared value of only 0.57. However, removing the outlier, complex **2-6b** ($pKa = 6.49$), gave a vast improvement, shown in Figure 3.38, where the linear correlation between the two values is now 0.94. Unfortunately, an explanation for the anomalously weak hydrogen bond formed in complex **2-6b**, despite **6b** being a relatively strong acid, is not obvious. As seen earlier, its crystal structure and packing are very similar to complex **2-7**, and neither are its short contact interactions particularly different from any of the other complexes. It may be that the hydrogen bond in the **3-6b** complex is longer than expected to accommodate better crystal packing, as the complex has the least linear hydrogen bond of all the complexes at 158.01 °C (Table 3.2). Nevertheless, complex **2-6b** aside, the plot in Figure 3.38 does show that the strength of the fluorophenol acid corresponds to the strength of the resulting hydrogen bonded complex.
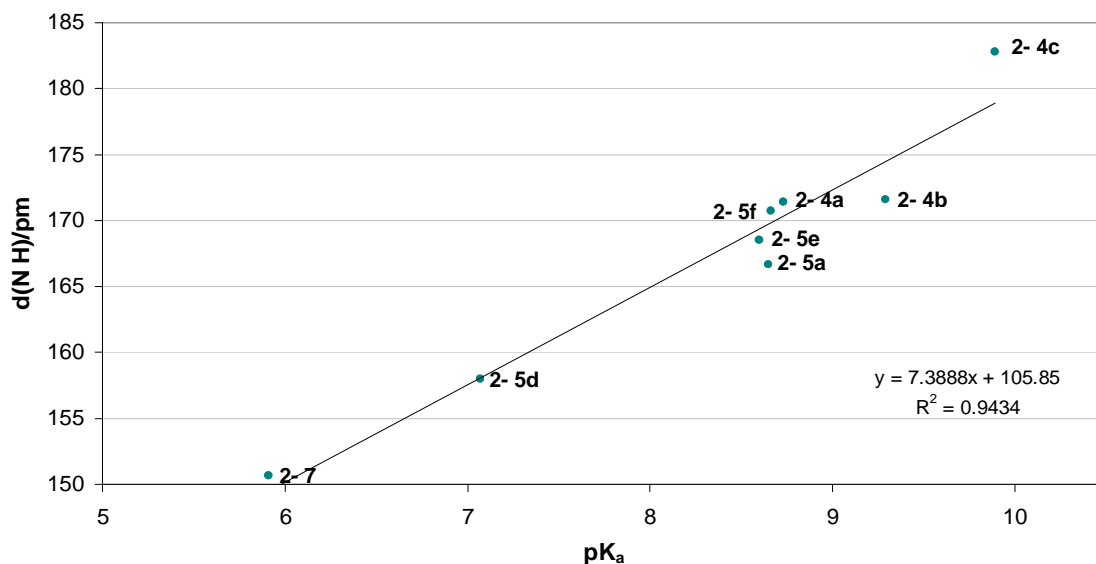
Figure 3.38: Plot of the N⋯H distance against pK_a, with complex **2-6b** ($pK_a = 6.49$) omitted.

Präsang *et al.* reported halogen-bonded complexes formed between 4-(*N,N*-dimethyl-amino)pyridine (DMAP) and iodobenzene with different degrees of fluorination (Figure 3.39).[7] While crystals of the complexes with 2-fluoroiodobenzene, 2,3,4-trifluoroiodobenzene and 2,3,5,6-tetrafluoroiodobenzene were reported in the paper analogous to complexes **2-4a**, **2-6b** and **2-7** in this project, the iodobenzene complexes did not, regrettably, crystallise in the $P\bar{1}$ space group.
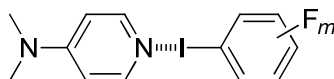
Figure 3.39: Structure of the halogen bonded complexes formed between 4-(*N,N*-dimethyl-amino)pyridine (DMAP) and iodobenzene with different degrees of fluorination.

The authors did note a good correlation between the halogen bond N⋯I distance with the degree of fluorination in the iodobenzene as well as with the calculated pK_a values of the analogous fluorophenols. While the plot of pK_a versus N⋯H distance is analogous to the pKa versus N⋯I plot, the similarity between the hydrogen-bonded and halogen-bonded systems ends there. For example, the N⋯I–C bond in the halogen-bonded complexes are very nearly linear, while the N⋯HO–C bond is bent, ranging from 117 °C to 131 °C.

The halogen-bonded complexes which did crystallise in the $P\bar{1}$ space group were with 4-fluoroiodobenzene, 2,4-difluoroiodobenzene and 2,3,4-trifluorobenzene. The crystals of the complexes showed one-dimensional chains supported by halogen bonding between the pyridine nitrogen and iodine as well as short contacts between the *para*-position fluorine and two hydrogen atoms, one hydrogen from each methyl group in the dimethylamino substituent of DMAP. No back-to-back dimer motifs were observed.[7]

The crystal structures of 3-fluorophenol,[8] 4-fluorophenol,[9] and pentafluorophenol[10] showed packing driven by intermolecular hydrogen bonding. Both the 3-fluorophenol and pentafluorophenol arranged into OH···OH hydrogen-bonded chains as shown in Figure 3.40(a) and (b), respectively, in the P2$_1$/c space group. The single crystals of 3-fluorophenol were obtained at 150 K, while pentafluorophenol was recrystallised at room temperature.[8,10]

(a)   (b)
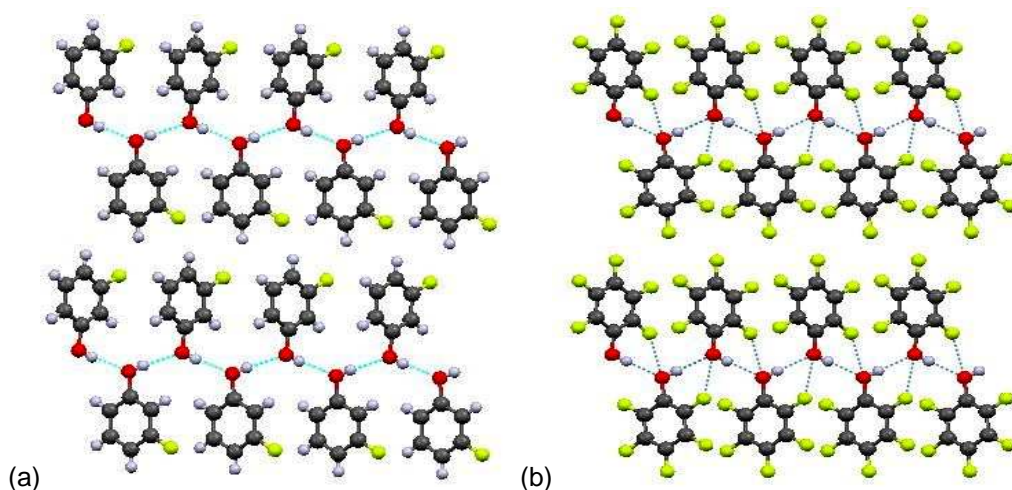
Figure 3.40: The crystal structures of (a) 3-fluorophenol and (b) pentafluorophenol.

Oswald *et al.* reported attaining two crystal structures for 4-fluorophenol, the first at 150 K, in the $R\bar{3}$ space group (Figure 3.41(a)), and the second at higher pressure (0.28 GPa), in the P2$_1$/c space group (Figure 3.41(b)). In the polymorph obtained at 150 K, six molecules arranged into a ring motif connected by OH···OH hydrogen bonds, while increasing the pressure saw the molecules arrange into the hydrogen-bonded chain motif, comparable to 3-fluorophenol and pentafluorophenol.[9]

(a)

(b)
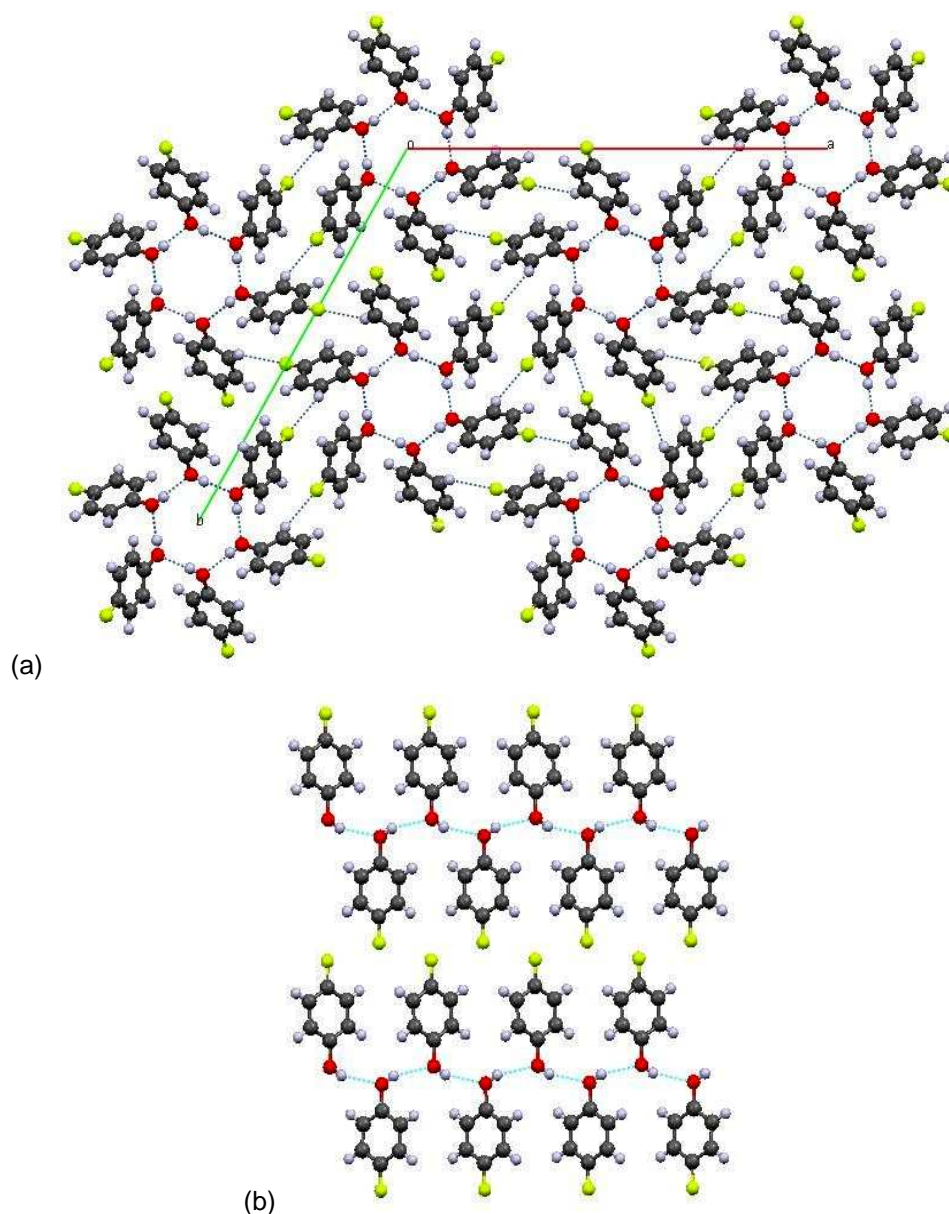
Figure 3.41: The crystal structure of 4-fluorophenol at (a) 150 K, and (b) 0.28 GPa viewed down the *c*-axis.

The pure fluorophenol crystals had weaker hydrogen bonds than when complexed to 4-octyloxy-4'-stilbazole. The hydrogen bonds in 3-fluorophenol and 4-fluorophenol crystals at 150 K were 2.044 Å (77.4% sum of vdW) and 1.906 Å (72.2% sum of vdW), respectively,[8,9] while the hydrogen-bond lengths in **2-4b** and **2-4c** were 1.716 Å long (65.0% sum of VdW radii) and 1.828 Å (69.2 % sum of vdW), respectively. In the complex, the hydrogen bond between fluorophenols is replaced by the stronger hydrogen bond between the nitrogen atom in the alkoxystilbazole and the fluorophenol. Thus, the hydrogen-bonded chain motif which drove the crystal packing in the fluorophenol crystals can not form, and instead the crystal packing of the new complex takes on a back-to-back dimer motif.

3.4   Conclusion

The complexes between alkoxystilbazole and fluorophenol were successfully prepared with good yield. The series of complexes consisting of **1** were mainly nematic, while those of **2** exhibited both nematic and smectic A mesophases. Increasing the alkoxy chain length to twelve carbons in **3**, saw all sixteen complexes in the series exhibit the smectic A phase, due to an increased balance in molecular rigidity and flexibility. A nematic phase was also observed in addition to the smectic A phase for some of these homologues. The stability of the mesophases as a function of fluorine substitution was found to have been preserved in each series when the complexes were arranged in order of decreasing clearing temperature, indicating a consistent influence of fluorine substitution on liquid crystallinity. The most stable complexes are those formed with **6c**, as the position-2 fluorine is able to form an intramolecular hydrogen bond and the position-4 and -5 fluoro substituents increase the complexes anisotropy.

Of the fourty-eight complexes prepared, single crystal structures of nine complexes with **2** were obtained. Out of these nine, eight crystallised in the $P\bar{1}$ space group, while **2-4c** was found to be in the Pbca space group. The complexes all formed the back-to-back dimer motif with some variation, in packing, except for complex **2-4c** in which the molecules arranged head-to-tail in zig-zagged chains. The plot of N···H distance versus the fluorophenol pK_a revealed a linear correlation between the strength of the hydrogen bond formed and the degree of fluorine substitution. This was analogous to the relationship reported for halogen-bonded complexes between 4-(*N,N*-dimethyl-amino)pyridine (DMAP) and iodobenzene with different degrees of fluorination.[7]

References

1. G. Rhodes, *Crystallography Made Crystal Clear: A Guide for Users of Macromolecular Models, 2nd Ed.,* Academic Press, San Diego, 2000.
2. W. Clegg, *Crystal Structure Determination,* Oxford University Press, Oxford, 1998.
3. W. C. Phillips, Y. Li, M. Stanton, J. Xie and D. O'Mara, *Nuc. Instrument. Method. Phys. Res. A.,* 1993, **334**, 621.
4. J. McMurry, *Fundamentals of Organic Chemistry, 5th Ed.,* Thompson, Brookes and Cole, Pacific Grove, 2003.
5. M. S. Silberberg, *Chemistry: The Molecular Nature of Matter and Change, 4th Ed.,* McGraw-Hill, New York, 2006.
6. J. Han and F. M. Tao, *J. Phys. Chem. A,* 2006, **257**, 110.
7. C. Präsang, A. Whitwood, and D.W. Bruce, *Cryst. Growth Des.,* 2009, **9(12)**, 5319.
8. I. D. H. Oswald, D. R. Allan, W. D. S. Motherwell and S. Parson, *Acta Cryst.,* 2005, **B61**, 69.
9. I. D. H. Oswald, D. R. Allan, G. M. Day, W. D. S. Motherwell and S. Parson, *Cryst. Growth Des.,* 2005, **5(3)**, 1055.
10. D. Das, R. Banerjee, R. Mondal, J. A. K. Howard, R. Boese and G. R. Desiraju, *Chem. Commun.,* 2006, 555.

CHAPTER 4

EXPERIMENTAL

All the fluorophenols were used as received from Fluorochem. Solvents for stilbazole synthesis and crystallisation were HPLC-grade and used as received.

4.1   Spectroscopic Techniques

Nuclear Magnetic Resonance. Samples were run on a Jeol ECX 270 with a field strength of 200 MHz, equipped with an auto-charger. Delta NMR software was used to process the spectra obtained.

Polarised Optical Microscopy. Mesomorphic studies were performed using an Olympus BX50 Optical Microscope equipped with a Linkam Scientific LTS350 heating stage, Linkam LNP2 cooling pump and Linkam TMS92 controller.

Differential Scanning Calorimetry. Calorimetry scans were run on a Mettler Toledo DSC822e, equipped with a TSO801R0 Sample Robot and calibrated using pure indium. Samples were run at heating cooling rates of $10°C \ min^{-1}$.

CHN Elemental Analysis. Analysis was carried out on an Exeter Analytical Inc CE 440 Elemental Analyser and a Sartorius SE2 analytical balance by Dr. Phil Helliwell at The University of York.

Small Molecule X-ray Crystallography. Analysis was run on a Bruker Smart Apex X-ray diffractometer using a Mo-K_α source equipped with an Oxford cryostream cooling system by Dr. Adrian C. Whitwood at The Unviersity of York

4.2 Synthesis of the 4-Alkyloxystilbazoles

All homologues were prepared in the same manner as described for 4-octyloxy-4'-stilbazole, as described by Huck et al.[1]

A summary of the general synthetic route used to prepare the stilbazole is shown in the repeat of Scheme 2.1 below.
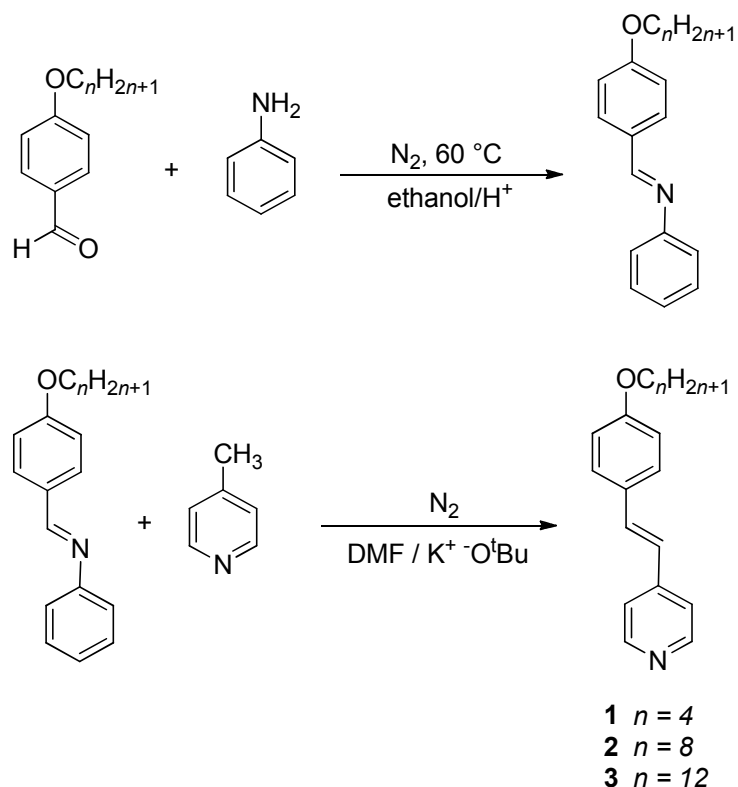
Scheme 2.1: Synthetic route for the component 4-alkoxy-4'-stilbazole

4.2.1 4-Octyloxy-4'-benzylideneaniline

The benzylideneaniline prepared by dissolving 4-octyloxy-4'-benzaldehyde (9.14 g, 39.0 mmol) and aniline (3.63 g, 39.0 mmol) in a 1:1 ratio in ethanol (50 cm^3), together with a few drops of acetic acid. The reaction mixture was kept at 60 °C for 20 h under nitrogen and with stirring. Subsequently, the solution was allowed to cool to 0 °C and the white, shiny flakes formed were filtered off, washed with cold ethanol (25 cm^3) and left to air-dry.[2] The product obtained was used for the next reaction without further purification (11.35 g, 94.1%).

4.2.2   4-Octyloxy-4'-stilbazole

A round-bottom flask was charged with 4-octyloxy-4'-benzylideneaniline (10.99 g, 35.5 mmol) dissolved in DMF (125 cm^3) and one molar equivalent of 4-picoline (3.31 g, 35.5 mmol) under nitrogen, and was then heated to 60 °C. Five equivalents of potassium tert-butoxide (19.92 g, 177.5 mmol) was added within 2 min following which the temperature of the reaction mixture was raised to 80 °C and kept so for 3 h.[3,4] Once cooled to room temperature, the deep violet solution was poured into ice-cold water (250 cm^3) and the resulting pale orange slurry neutralized with hydrochloric acid (2M) to a pH of 7-8. The solid was then filtered off and washed thoroughly with water (3 x 125 cm^3), stirring the solid into a slurry with each washing. The crude product was then dissolved in CH_2Cl_2, and the remaining water removed by separation. The resulting yellow solution was dried over $MgSO_4$ and filtered. Dichloromethane was then removed completely *in vacuo* and the crude product recrystallized three times from hot hexane at 0 °C (7.78 g, 70.7%).
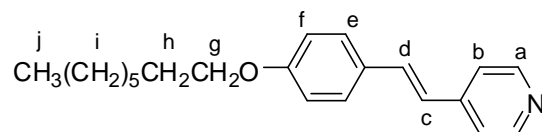
^{1}H NMR δ_H (270 MHz, CD_2Cl_2): 8.45 (2H, d, H$_a$, J = 6.2 Hz, AA'XX'), 7.43 (2H, d, H$_f$, J = 8.9 Hz, AA'XX'), 7.29 (2H, d, H$_b$, J = 6.2 Hz, AA'XX'), 7.22 (1H, d, H$_d$, J_{AB} = 16.4 Hz), 6.84 (2H, d, H$_e$, J = 8.9 Hz, AA'XX'), 6.84 = (1H, d, H$_c$, J_{AB} = 16.5 Hz), 3.92 = (2H, t, H$_g$, OCH$_2$), 1.72 (2H, m, H$_h$, CH$_2$), 1.26 (10H, broad m, H$_i$, CH$_2$), 0.83 (3H, t, H$_j$, CH$_3$). Experimental analysis found (required): C 81.5 (81.5), H 8.8 (8.8), N 4.6 (4.5).

4.3 Stilbazole-Fluorophenol Complex Formation

$C_nH_{2n+1}O$ — [stilbazole-fluorophenol structure] — $N^{''''''}H-O$ — F_m

where n = 4, 8, and 12
m = 5, 4, 3, 2 and 1
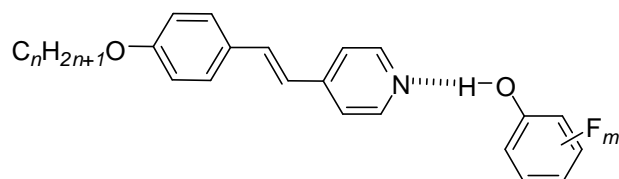
The preparation of the 4-octyloxy-4'-stilbazole-tetrafluorophenol complex is described. The respective penta-, tri-, di- and mono-substituted fluorophenol homologues were prepared in the same way. The butyloxy homologues were also made in the same way, however the dodecyloxy homologues were prepared using hexane as solvent.

4-Octyloxy-4'-stilbazole (99.0 mg, 0.32 mmol) and pentafluorophenol (58.9 mg, 0.32 mmol) were dissolved separately in just enough pentane and the solutions then combined in a round-bottom flask. The reaction mixture was stirred for 1½ h at room temperature, after which the stirrer was removed, the flask sealed with a septum and left at room temperature for the complex to crystallise. Alternatively the reaction mixture can also be diluted with pentane, sealed and placed in the fridge to crystallise. The fine, pale yellow crystals were then collected by decantation (153.0 mg, 95.3%). The purity of the sample was confirmed by the absence of biphasic behaviour under optical miscroscopy studies, CHN analysis and X-ray Crystallography.

4.4   Characterization

Table 4.1: CHN Analysis results for all the stilbazole-fluorophenol complexes produced.

Complex	Experimental Analysis Found (Required) / %					
	C		H		N	
1-8	63.179	(63.16)	4.605	(4.61)	3.472	(3.20)
1-7	65.801	(65.87)	4.982	(5.05)	3.353	(3.34)
1-6a	68.794	(68.82)	5.547	(5.52)	3.494	(3.49)
1-6b	68.935	(68.82)	5.561	(5.52)	3.466	(3.49)
1-6c	68.954	(68.82)	5.575	(5.52)	3.497	(3.49)
1-6d	68.823	(68.82)	5.513	(5.52)	3.466	(3.49)
1-6e	68.793	(68.82)	5.571	(5.52)	3.491	(3.49)
1-5a	72.183	(72.05)	6.048	(6.05)	3.664	(3.65)
1-5b	72.033	(72.05)	6.091	(6.05)	3.675	(3.65)
1-5c	72.252	(72.05)	6.069	(6.05)	3.674	(3.65)
1-5d	72.157	(72.05)	6.076	(6.05)	3.643	(3.65)
1-5e	72.101	(72.05)	6.044	(6.05)	3.669	(3.65)
1-5f	72.013	(72.05)	6.064	(6.05)	3.611	(3.65)
1-4a	75.769	(75.59)	6.673	(6.62)	3.935	(3.83)
1-4b	75.558	(75.59)	6.654	(6.62)	3.804	(3.83)
1-4c	75.503	(75.59)	6.603	(6.62)	3.849	(3.83)
2-8	65.615	(65.71)	5.804	(5.72)	3.280	(2.84)
2-7	68.367	(68.20)	6.217	(6.15)	2.912	(2.95)
2-6a	70.923	(70.88)	6.628	(6.61)	3.034	(3.06)
2-6b	70.898	(70.88)	6.612	(6.61)	3.074	(3.06)
2-6c	70.890	(70.88)	6.612	(6.61)	3.067	(3.06)
2-6d	70.909	(70.88)	6.612	(6.61)	3.041	(3.06)
2-6f	70.927	(70.88)	6.636	(6.61)	3.009	(3.06)
2-5a	73.903	(73.78)	7.194	(7.11)	3.225	(3.19)
2-5b	73.728	(73.78)	7.170	(7.11)	3.205	(3.19)
2-5c	73.850	(73.78)	7.107	(7.11)	3.191	(3.19)
2-5d	73.843	(73.78)	7.364	(7.11)	3.311	(3.19)
2-5e	73.762	(73.78)	7.129	(7.11)	3.159	(3.19)
2-5f	73.852	(73.78)	7.140	(7.11)	3.160	(3.19)
2-4a	77.190	(76.93)	7.696	(7.65)	3.328	(3.32)
2-4b	76.679	(76.93)	7.755	(7.65)	3.236	(3.32)
2-4c	77.064	(76.93)	7.730	(7.65)	3.363	(3.32)
3-8	67.778	(67.74)	6.622	(6.60)	2.795	(2.55)
3-7	70.154	(70.04)	7.082	(7.02)	2.644	(2.63)
3-6a	72.684	(72.49)	7.478	(7.46)	2.727	(2.73)
3-6b	72.771	(72.49)	7.492	(7.46)	2.815	(2.73)
3-6c	72.873	(72.49)	7.560	(7.46)	2.805	(2.73)
3-6d	72.309	(72.49)	7.465	(7.46)	2.763	(2.73)
3-6f	72.632	(72.49)	7.496	(7.46)	2.771	(2.73)
3-5a	75.318	(75.12)	7.977	(7.93)	2.845	(2.83)
3-5b	75.386	(75.12)	8.023	(7.93)	2.882	(2.83)
3-5c	75.268	(75.12)	7.952	(7.93)	2.810	(2.83)
3-5d	75.309	(75.12)	7.970	(7.93)	2.857	(2.83)
3-5e	75.127	(75.12)	7.905	(7.93)	2.817	(2.83)
3-5f	74.833	(75.12)	8.082	(7.93)	2.832	(2.83)
3-4a	77.863	(77.95)	8.451	(8.44)	2.954	(2.93)
3-4b	77.665	(77.95)	8.488	(8.44)	2.931	(2.93)
3-4c	77.979	(77.95)	8.412	(8.44)	2.904	(2.93)

References

1. D. M. Huck, H. L. Nguyen, P. N. Horton, M. B. Hursthouse, D. Guillon, B. Donnio and D. W. Bruce, *Polyhedron*, 2006, **25**, 307.
2. D. M. Huck, H. L. Nguyen, B. Donnio and D.W. Bruce, *Liq. Cryst.*, 2004, **31**, 503.
3. A. E. Siegrist, *Helv. Chim. Acta*, 1967, **50**, 906.
4. H. Meier, *Angew. Chem. Int. Ed. Eng.,* 1992, **31**, 1399.

Appendix